2011-05-27

Inflammation Alters Histone Methylation in the Central Nervous System: Implications for Neuropsychiatric Disease: A Dissertation

Caroline M. Connor
University of Massachusetts Medical School

INFLAMMATION ALTERS HISTONE METHYLATION IN CENTRAL NERVOUS SYSTEM: IMPLICATIONS FOR NEUROPSYCHIATRIC DISEASE

A Dissertation Presented

By

Caroline Martine Connor

Submitted to the Faculty of the

University of Massachusetts Graduate School of Biomedical Sciences

Worcester, Massachusetts

in partial fulfillment for the requirements for the degree of

DOCTOR OF PHILOSOPHY

May 27, 2011

Program in Neuroscience

INFLAMMATION ALTERS HISTONE METHYLATION IN
CENTRAL NERVOUS SYSTEM:
IMPLICATIONS FOR NEUROPSYCHIATRIC DISEASE

A Dissertation Presented
By

Caroline Martine Connor

The signatures of the Dissertation Defense Committee signifies completion and approval as to style and content of the Dissertation

_____
Schahram Akbarian, MD/PhD, Thesis Advisor

_____
Charles Sagerstrom, PhD, Member of Committee

_____
David Paydarfar, MD/PhD, Member of Committee

_____
David Weaver, PhD, Member of Committee

_____
Thomas Kemper, MD, Member of Committee

The signature of the Chair of the Committee signifies that the written dissertation meets the requirements of the Dissertation Committee

_____
Job Dekker, PhD, Chair of Committee

The signature of the Dean of the Graduate School of Biomedical Sciences signifies that the student has met all graduation requirements of the school.

_____
Anthony Carruthers, PhD,
Dean of the Graduate School of Biomedical Sciences

Program in Neuroscience
May 27, 2011

ABSTRACT

Maternal infection during pregnancy is associated with increased risk of both schizophrenia and autism in offspring. Based on this observation, the maternal immune activation mouse model was developed, in which pregnant rodents are treated with immune-activating agents and the brains and behavior of the adult offspring studied. This model has been found to recapitulate a variety of molecular, cellular, and behavioral abnormalities observed in both schizophrenia and autism. However, despite the abundant evidence provided by these studies that prenatal exposure to inflammation alters brain development and function later in life, the molecular mechanisms by which inflammation mediates these effects remains unclear.

It has been suggested that other prenatal risk factors for neuropsychiatric disease may alter brain development, in part, via epigenetic mechanisms such as DNA methylation and histone modification. However, a link between inflammation and epigenetic modification in brain has not been established. Therefore, the focus of my thesis was to examine the effect of inflammation on the histone modification, trimethylated histone H3 lysine 4 (H3K4me3), which has been implicated in both normal brain development and in schizophrenia.

In Chapter II, I describe experiments examining the effect of a specific, cytokine, interleukin-6 (IL-6), on H3K4me3 in rat forebrain culture. I show that IL-6 treatment results in altered levels of H3K4me3 at multiple gene

promoters, frequently in conjunction with altered mRNA expression levels, and demonstrate that a subset of these alterations appear to be dependent on signaling via the signal transducer and activator of transcription 3 (Stat3) pathway. Furthermore, some of the genes affected by IL-6 also showed altered H3K4me3 levels in autism postmortem brain. Though a direct link still remains to be established, this observation suggests that epigenetic changes observed in neuropsychiatric disease may have been induced by prenatal exposure to inflammation. In Chapter III, I describe *in vivo* experiments employing the maternal immune activation (MIA) mouse model to examine the effects of prenatal inflammation on H3K4me3 in the brain of the offspring, at both fetal and adult stages. I found that immune activation resulted in increased levels of IL-6 protein in fetal brain, working memory deficits in the adult offspring, and subtle changes in H3K4me3 levels in fetal and adult brain.

Taken together, these findings demonstrate that an environmental risk factor for schizophrenia and autism—namely, inflammation—is capable of inducing robust and widespread histone modifications in a model of the central nervous system and smaller changes *in vivo*. This suggests that prenatal exposure to inflammation in human populations may lead to increased susceptibility for neuropsychiatric disorders, in part, by altering chromatin modifications in developing brain.

TABLE OF CONTENTS

LIST OF FIGURES

COPYRIGHT

CHAPTER I: Introduction

Schizophrenia and Autism: An Overview

Schizophrenia and autism are both complex psychiatric disorders classified as neurodevelopmental in nature. Schizophrenia is characterized by positive symptoms, including hallucinations and delusions, negative symptoms, such as flat affect and social withdrawal, and cognitive symptoms, which include deficits in working memory, attention, and language. Due to the debilitating nature of this disease, there is a high rate of both homelessness and suicide in this patient population. The term “autism” was first used by Eugen Bleuler to describe the social withdrawal observed in schizophrenia patients [1]. Since this time autism, or autism spectrum disorder (ASD), has been classified as a distinct neuropsychiatric disorder, characterized by impaired social interaction, verbal and nonverbal communication skills, and repetitive or stereotyped behaviors [2]. Neither schizophrenia nor autism demonstrates a defining neuropathology or genetic risk architecture, and there is very little definitive evidence regarding specific mechanisms underlying their pathogenesis.

A role for genetics in the pathoetiology of schizophrenia and autism is well-established, based on twin studies which demonstrated that the risk for these disorders is positively correlated with degree of relatedness [3]. However, the concordance rate in monozygotic twins is less than 100% for

both disorders—approximately 50% for schizophrenia and 60% for autism—indicating that environmental factors must also be involved in disease pathogenesis [4, 5]. Moreover, it has been shown that the concordance rate of schizophrenia in monozygotic twins who share a placenta is higher than that for twins with separate placentas, who have rates similar to dizygotic twins [6]. These findings highlight the importance of the intrauterine environment in the development of neuropsychiatric disease.

Disease with onset in adulthood induced by prenatal and early postnatal exposure to environmental factors is referred to as "fetal reprogramming." This concept was first developed by studies demonstrating that prenatal malnutrition was associated with an increased risk for a variety of medical complications in adulthood, including cardiovascular disease, metabolic syndrome, and endocrine disturbances [7, 8]. A number of environmental factors have been associated with schizophrenia and autism, including maternal diet and stress, advanced paternal age, birth in later winter/early spring, and urban environment [9].

It has been proposed that such early environmental factors induce disease phenotypes via epigenetic mechanisms, such as DNA methylation and histone modifications. In the next section, I will provide an overview of the field of epigenetics. Then, I will provide specific examples of how environmental factors have been shown to alter epigenetic modifications and impact physiology in both animal models and humans, with an emphasis on

the brain. Subsequently, I will focus on one environmental factor associated with increased risk of both schizophrenia and autism: maternal infection during pregnancy. I hypothesize that this particular environmental factor alters brain development, in part, by inducing changes in the fetal epigenome and precipitates neuropsychiatric disease later in life.

Epigenetics:

The literal translation of the term epigenetics is “over” or “above genetics” and is typically defined as a heritable modification that impacts gene expression without alteration of the DNA sequence. Epigenetic information is encoded in chemical modifications of both DNA, in the form of DNA methylation, as well as modification of its associated histone proteins; together, this complex of DNA and protein is known as chromatin. The fundamental unit of chromatin is the nucleosome, which consists of 146 base-pairs (bp) of DNA wrapped around an octamer of the four core histones: H2A, H2B, H3, and H4 [10].

The amino-terminal tails of these histones are subject to a variety of post-translational modifications, including acetylation, methylation, phosphorylation, ubiquination, and SUMOylation, and these modifications—individually or in concert—recruit effector proteins, through which they exert their effects on chromatin structure and function, namely, transcription [10]. Though the relationship can be complex, specific histone modifications have

been associated with either increases or decreases in transcription. For example, levels of trimethylated histone H3 lysine 4 (H3K4me3) and acetylation of H3K9 and H3K14 tend to be positively correlated with transcription, while trimethylatation of H3K9 and H3K27 tends to be associated with decreased transcription. Multiple histone modifications acting together to bring about a particular effect is referred to as the "histone code" [11]. With the advent of next generation sequencing, it has become possible to generate of genome-wide histone modification maps through the use of chromatin immunoprecipitation following by deep-sequencing (ChIP-Seq) [12].

Epigenetics in Neuropsychiatric Disease

Evidence suggests that epigenetic marks are altered in adult brain in neuropsychiatric disorders such as schizophrenia. For example, H3K4me3 and DNA methylation are altered at the glutamate decarboxylase 1 (*GAD1*) and reelin (*RELN*) promoters, respectively, and these variations are associated with corresponding decreases in mRNA [13-15]. Altered expression of two chromatin-modifying enzymes—histone deacetylase 1 (*HDAC1*) and DNA methyltransferase 1 (*DNMT1*)—has also been reported in schizophrenia [16, 17]. These findings suggest that changes in histone modifications and DNA methylation in mature brain in patients with schizophrenia—and other complex neuropsychiatric disorders—can result in

ongoing changes in gene expression that may underlie some of the cognitive deficits and mood symptoms observed in these disorders. While the timing and origin of these aberrant marks is unclear, evidence from animal models (described below) suggests that they may occur during fetal and postnatal development.

A role for epigenetics in autism has also been described, though the evidence is derived primarily from genetic studies rather than identification of altered chromatin modifications in postmortem brain. Specifically, mutations in chromatin-modifying enzymes—including methyl CpG binding protein 2 (*MECP2*), histone acetyltransferase 4 (*HDAC4*), and the H3K4 demethylase *JARID1C/KDM5C/SMCX*—have all been identified in ASD patients [18-20].

Environment and Epigenetics

Gene expression programs in the developing fetus are under exquisite control by epigenetic machinery, including in the brain. The brain—arguably the most complex organ in mammals—requires highly regulated control of gene expression in a timing-, region-, and cell-specific manner in order to coordinate the myriad processes required to produce a fully-functioning central nervous system, capable of higher cognitive processes. Changes to the epigenome *in utero* have the potential to impact early neurodevelopmental processes, including differentiation of neurons and glial cells, neuronal migration, axon pathfinding, and dendritic arborization;

disruption of any of these processes is expected to negatively impact brain function throughout life.

Data from animal models provides evidence that exposure to environmental factors during prenatal and early postnatal life impact chromatin modifications in the brain. In a seminal study, maternal care in rats was found to alter DNA methylation and H3K9 acetylation of the glucocorticoid receptor gene (*Nr3c1*) in hippocampus as well as anxiety-like behavior in offspring [21]. Further studies demonstrated that reversal of these chromatin modifications with the histone deacetylase (HDAC) inhibitor, trichostatin A, or the methyl donor, L-methionine, also reversed the effects of early maternal on the stress response in adult offspring [22, 23]. Maternal care has also been shown to modulate DNA methylation and H3K9 acetylation of the *Gad1* gene in rodent brain [24]. A study by Murgatroyd *et. al.* (2009) revealed that early life stress in mice resulted in sustained hypomethylation of the arginine vasopressin (*Avp*) promoter accompanied by increased mRNA, hyperactivity of the hypothalamic-pituitary-adrenal (HPA)-axis, and a depressive-like phenotype in adult animals [25]. Exposure to early enrichment, in the form of communal nesting, was found to increase levels of histone H3 acetylation at the brain-derived neurotrophic factor (*Bdnf*) promoter in hippocampus in mouse [26]. Interestingly, adult mice exposed to early enrichment only displayed elevated Bdnf protein following a stressor, indicating the histone modification did not affect basal levels.

Animal models have also demonstrated that exposure to environmental stimuli *in utero* can induce alterations in epigenetic modifications detectable in brain postnatally. Cocaine administration to pregnant rats on embryonic days 18 and 19 resulted in global hypomethylation, as well as both hyper- and hypomethylation at specific gene loci, in hippocampal neurons of neonatal and adolescent offspring [27]. Intrauterine growth retardation in rats led to increased levels of H3K4me3 and H3K9ac at the glucocorticoid receptor gene (*Nr3c1*), in conjunction with increased mRNA, in hippocampus that was detectable during early postnatal and adolescent time points [28].

While there is some evidence that early environment influences chromatin modifications in human brain as well, most studies conducted in human populations utilize blood samples for epigenetic analyses. One study of suicide victims with a history of childhood abuse were found to have increased DNA methylation in the promoter region of a neuron-specific glucocorticoid receptor (*NR3C1*) in hippocampus [29]. The same gene demonstrated increased DNA methylation in cord blood mononuclear cells from infants born to mothers with depression; while this study did not examine the methylation status of this gene in brain, these infants were found to have increased salivary cortisol following exposure to a stressor, indicating altered HPA-axis function [30].

Maternal Infection, Schizophrenia, and Autism

A variety of environmental factors have been linked to increased risk of schizophrenia and autism, including maternal diet and stress, advanced paternal age, birth in later winter/early spring, and urban environment [9]. Perhaps one of the most well-replicated environmental factors associated with increased risk of schizophrenia and autism is maternal infection during pregnancy. This link was first established by a study which found that individuals who were in their 2nd trimester *in utero* during the 1957 influenza epidemic were more likely to be diagnosed with schizophrenia [31]. This finding was further substantiated by more recent work showing elevated levels of influenza antibody and interleukin-8 (IL-8) in banked serum from mothers of schizophrenia patients [32]. It has since been reported that an estimated 30% of schizophrenia cases could be eliminated through the prevention of viral (influenza, rubella, herpes simplex virus), bacterial, and parasitic (toxoplasma) infection in pregnant women [33]. Maternal infection during pregnancy has been associated with increased risk of autism in offspring as well. Early studies in the 1960's linked rubella epidemics with increased rates of autism and a recent study of over 10,000 autism cases from the Danish Medical Registrar found an association with maternal viral infection [34-36].

It has been suggested that prenatal exposure to infection may only increase risk of psychosis in genetically susceptible individuals. For example,

a recent study found that fetal exposure to maternal pyelonephritis was only associated with increased incidence of schizophrenia in individuals with a family history of a psychotic disorder [37]. Additionally, it was found that seropositivity for herpes simplex virus 1 (HSV1) and the rs1051788 SNP of the MHC Class I polypeptide-related sequence B (*MICB*) gene exerted a significant joint effect on gray matter volume reduction in prefrontal cortex, and this effect was more pronounced in the schizophrenia group compared to controls [38].

That a variety of viral and bacterial infections have been linked to increased risk of schizophrenia suggests that it is the maternal immune response—rather than the infectious agent itself—that precipitates development of psychiatric disease. In further support of this theory, other conditions that give rise to inflammation have also been associated with increased rates of schizophrenia in the offspring, including diabetes mellitus—offspring of diabetic mothers have an estimated 7 times greater risk of developing schizophrenia [39]. In obese women, the placenta produces significantly more pro-inflammatory cytokines [40]. Maternal immune activation in the absence of a pathogen has been modeled in rodents through the administration of inflammation-inducing agents, including poly(I:C), LPS, and turpentine, to pregnant females. The offspring of these animals display a number of behavioral, histological, and molecular alterations in brain

reminiscent of symptoms and neuropathology observed in schizophrenia and autism. This animal model will be further reviewed in Chapter III.

Immune Dysregulation in Schizophrenia and Autism

Several lines of evidence suggest that ongoing inflammation or immune dyregulation may be present in schizophrenia and autism. For example, there exists a large body of literature on altered cytokine levels in schizophrenia patients, in both serum and cerebral spinal fluid (CSF). Increased levels of IL-6, interleukin 1 receptor (IL-1R), and IL-2R have been reported in serum in schizophrenia, while altered IL-6, IL-2, and tumor necrosis factor α (TNFα), have been reported in CSF or brain [41-44]. Cytokines, including IL-6, TNFα, granulocyte macrophage colony-stimulating factor (GM-CSF), IL-8, and interferon γ (IFNγ), have also been reported to be elevated in autism brain [45, 46]. IL-1β, IL-6, IL-8, and IL-12 were found to be elevated in serum of children between 2 and 5 years of age [47].

Some studies have shown that cytokine profiles are affected by the phase of the illness. For example, increased levels of cytokines in CSF have been reported to precede psychotic episodes [48]. Another study demonstrated that the cyclooxygenase (COX) byproducts, 15d-prostaglandin J(2) and prostaglandin E(2), were found to be increased and decreased, respectively, in serum of schizophrenia patients experiencing an acute exacerbation of their illness [49].

Altered immune cell profiles have also been reported in schizophrenia and autism patients. For example, mitogen-induced upregulation of IL-6 and TNFα, and downregulation of IL-2, IL-4, and IFNγ, by peripheral blood monocytes from schizophrenia patients has been reported [50]. T cells from ASD children were also found to have aberrant cytokine responses to stimulation *in vitro*—T cells treated with phytohemagglutinin (PHA) produced significantly higher levels of GM-CSF, TNFα, and IL-13 [47]. Peripheral blood monocytes from ASD children stimulated various toll-like receptor agonists produced significantly more cytokines, including IL-1β, IL-6, and TNFα [51].

Studies on schizophrenia and autism postmortem brain have also yielded evidence for immune activation in central nervous system in these disorders. For example, increased microglial activation has been observed in postmortem autism brain [46, 52]. Additionally, microarray studies of schizophrenia and autism postmortem brain have revealed altered expression of a wide variety of immune transcripts, including upregulation of heat shock protein genes *HSPA6*, *HSPB8*, *HSBP1*, and *HSPA1B* as well as two interferon-induced transmembrane proteins, *IFITM3* and *IFITM1* [53-56].

Genetic studies demonstrating the presence of single nucleotide polymorphisms (SNPs) in a variety of immune molecule genes in schizophrenia suggests that there may be an underlying immune system deficit in this psychiatric disorder. SNPs within the IL-1 gene complex have been associated with schizophrenia; the same group later found that

schizophrenia risk was 10 times higher in individuals with the IL-1β 2.2 allele who also possessed the neuregulin 1 (*NRG1*) CC genotype [57, 58]. A recent meta analysis also found significant association of the rs16944 SNP in the IL-1β with schizophrenia [38]. And one study reported an association between the integrin-β 3 gene (*ITGB3*) and autism [59].

Of note, several clinical trials have explored the efficacy of anti-inflammatory medications as an adjuvant therapy in schizophrenia. Akhondzadeh *et. al.* (2007) found that the cyclooxygenase-2 (COX-2) inhibitor, celecoxib, when administered in combination with the antipsychotic medication, risperidone, significantly improved psychotic symptoms in schizophrenia over the group given risperidone alone [60]. Additionally, it has been reported that chronic use of steroidal anti-inflammatory drugs decrease risk of schizophrenia [61]. Anti-inflammatory medications have also shown promise in the treatment of autism—a pilot study in 25 children diagnosed with an ASD found improvement of symptoms following treatment with the PPARγ agonist pioglitazone [62]. Also of note, antipsychotic medications appear to possess anti-inflammatory properties. For example, haloperidol was found to inhibit lipopolysaccharide (LPS)-induced release of IL-1β and TNFα by whole blood cultures and the promonocyte cell line, THP-1 [63]. Additionally, antipsychotics have been shown to inhibit microglial activation and release of cytokines *in vitro* [64, 65].

Taken together, these data provide strong evidence for immune activation in both the precipitation—and maintenance—of symptoms in schizophrenia and autism. Immune molecules—including cytokines, chemokines, complement cascades, and MHC—play a critical role during development of the central nervous system. Such molecules have been implicated in a diverse array of developmental processes, including cellular differentiation, neuronal migration, axonal pathfinding, and dendritic arborization [66-68]. Given the essential role of the immune system in normal CNS development, it is not surprising that alteration of these molecules during critical periods can profoundly impact brain function. However, the precise molecular mechanisms by which prenatal exposure to inflammation alters brain development remain unclear. As has been suggested for fetal reprogramming by other environmental factors, it is possible that inflammation alters neurodevelopment via epigenetic mechanisms.

Inflammation and epigenetics

A direct role for inflammation in the regulation of epigenetic mechanisms during brain development and in neuropsychiatric disease has not been established. Inflammation has long been linked to other diseases, including cancer and atherosclerosis; more recently, it has been discovered that chronic inflammation may be involved in the “reprogramming” of the epigenome. Data from other cell types provides clues as to how immune

molecules—pro-inflammatory cytokines in particular—induce chromatin modifications. For example, LPS-induced pro-inflammatory cytokines were found to upregulate the H3K27-specific demethylase, Jumonji C (JmjC) domain-containing protein, Jmjd3, in macrophages [69]. And treatment of mouse embryonic stem (ES) cells with the IL-6 family cytokine member, leukemia inhibitory factor (LIF), resulted in phosphorylation of histone H3 at tyrosine 41 via JAK2 [70]. Finally, there is a single report that a cytokine, IL-1β, alters H3K9me3 at the *NeuroD* promoter in mouse neural stem cells [71].

In this thesis, I sought to determine whether immune activation was capable of inducing chromatin modifications, and accompanying gene expression changes, in the central nervous system. In Chapter II, I describe experiments in which I examine the effect of a specific cytokine, IL-6, on levels of H3K4me3 in a rat forebrain culture system. In Chapter III, I describe experiments in which I explored the impact of prenatal exposure to inflammation on H3K4me3 in brain *in vivo*, employing the maternal immune activation (MIA) mouse model of schizophrenia and autism. Finally, in Chapter IV, I discuss the outlook for the future of epigenetic research in neuropsychiatric disease.

Chapter II:

Interleukin-6 Alters Histone H3 Lysine 4 Trimethylation in Rat Forebrain Culture: Implications for Neuropsychiatric Disease

H3K4me3 ChIP-Seq on autism postmortem brain was performed by Iris Cheung and the data analyzed by Hennady Shulha and Zhiping Weng.

Introduction

Maternal infection during pregnancy has been shown to increase risk of both schizophrenia and autism in offspring [72]. Because multiple infectious agents have been linked to the development of these disorders, it is believed that it is the maternal response to infection—rather than the pathogen itself—that alters fetal brain development and precipitates the onset of neuropsychiatric disease later in life. Several lines of evidence have implicated the pro-inflammatory cytokine, interleukin-6 (IL-6), in the pathoetiology of both schizophrenia and autism. Prior to discussing these studies, I will provide a brief overview of this cytokine.

IL-6 is a pro-inflammatory cytokine first identified as a B-cell maturation factor [73]. It has since been implicated in a wide variety of normal physiological processes, including hematopoiesis, the acute phase response, liver regeneration, and gliogenesis and it is dysregulated in multiple diseases, such as atherosclerosis, autoimmune disease, neoplasm, stroke, and neurological disorders, including multiple sclerosis, Alzheimer's disease, and Parkinson's disease [74]. The IL-6 cytokine family, which includes IL-11, IL-27, IL-31, ciliary neurotrophic factor (CNTF), leukemia inhibitory factor (LIF), oncostatin M (OSM), cardiotrophin-1 (CT-1), and cardiotrophin-like cytokine (CLC), are grouped together because they all signal via glycoprotein 130 (gp130) [75]. When IL-6 binds to its cognate receptor, IL-6R, homodimerization with two gp130 subunits is induced. Associated janus

kinase (JAK) proteins phosphorylate gp130 tyrosine residues, leading to the activation of several signaling pathways: signal transducer and activator of transcription (STAT), ras-raf-MAPK (ERK1/2), and PI3K/Akt [76]. The specific pathways activated depend upon the particular cell type.

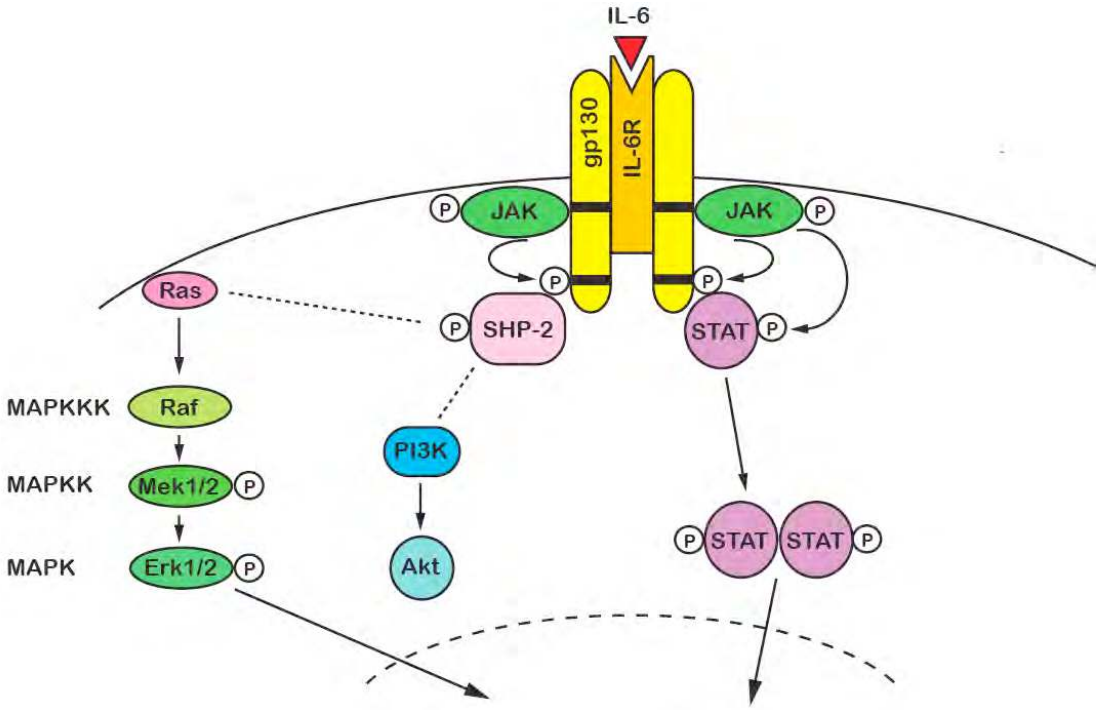

Figure 1: Signaling pathways activated by IL-6 binding to IL-6R. IL-6 binds to IL-6R and induces homodimerization of the signal-transducing subunit, gp130. Subsequently, levels of phosphorylated Stat (pStat), pErk1/2, and pAkt are elevated and have downstream effects on gene expression.

IL-6, IL-6R, and soluble IL-6R (sIL-6R) are expressed in both rodent and human brain. Transcripts of genes were noted to increase during postnatal development in rat and have been detected in neurons of the hippocampus, cortex, striatum, and cerebellum in mature rat [77-79]. In human brain, IL-6R immunoreactivity has been reported in both undifferentiated neurons during earlier stages of pregnancy as well as in cortical pyramidal neurons at later stages of pregnancy and in the adult [80]. Additionally, gp130 protein is expressed in both neurons and glia in rat brain; mRNA has been demonstrated in human cortex [81, 82]. In addition to its more well-known role in the orchestration of neuroinflammation and fever in response to trauma or infection, IL-6 is involved in a number of normal physiological processes in brain, including neurogenesis, astrogliogenesis, and oligodendrogenesis; neurotransmitter release; neuronal survival following insult; and maintenance of the blood-brain barrier [74].

Recently, it has been suggested that IL-6 plays a role in the pathogenesis of both schizophrenia and autism. IL-6 is reportedly increased in schizophrenia and autism patients, in both serum and CSF [42, 46]. Additionally, data from preclinical animal models suggest that prenatal exposure to IL-6 alters brain development and function in the offspring. An elegant study conducted by Smith *et. al.* (2007) [83] demonstrated that blockade of IL-6 with a neutralizing antibody prevented the effects of maternal immune activation (MIA) with the viral mimic, poly(I:C), on the offspring.

Likewise, poly(I:C) had no effects on IL-6 knockout mice. Furthermore, treatment with IL-6 alone recapitulated the behavioral deficits in adult offspring caused by poly(I:C). Importantly, blockade of other cytokines upregulated by poly(I:C)— IL-1α, TNFα, and IFNγ—did not prevent the effects of MIA on behavior. Another group demonstrated that IL-6 administration to pregnant rodents resulted in increased levels of phosphorylated Stat3 in brain of neonatal and adult offspring and, furthermore, that co-administration of Stat3 inhibitors with [84].

However, it remains unclear how, precisely, IL-6 might be altering brain development in the fetus. Cytokines, in addition to other immune molecules, are known to play critical roles in a variety of neurodevelopmental processes, including neuro- and gliogenesis, neuronal migration, axon pathfinding, and dendritic aborization; therefore, exposure to abnormal levels of these substances is expected to have a deleterious effect on proper brain development. Indeed, this has been shown by multiple transgenic and knockout mouse models reviewed in [66]. However, the molecular mechanisms by which IL-6 regulates these neurodevelopmental processes is currently unclear.

I hypothesize that exposure to IL-6 during fetal brain development may result in both transient and long-lasting chromatin modifications, which result in aberrant gene expression and, ultimately, neuropsychiatric disease. Though this cytokine could potentially impact a wide range of chromatin

modifications, I chose to focus on the histone mark, trimethylated histone H3 lysine 4 (H3K4me3), because it is well-characterized, in terms of function and genomic localization, is important for brain development, and appears to be altered in schizophrenia [12, 85-87]. To examine whether IL-6 was capable of modulating H3K4me3 on an acute time-scale in a model of the central nervous system, I exposed primary culture of rat forebrain to IL-6 (and its cognate receptor, IL-6R) and measured levels of H3K4me3 genome-wide employing ChIP-Seq.

Materials and Methods

Cell culture: Cells were prepared from forebrain of embryonic day 14.5 (E14.5) SASCO SD rat embryos (Charles River Laboratories; Wilmington, MA). Live cells were plated at $1.2 – 1.4 \times 10^6$ cells per 100 mm polystyrene Petri dish (VWR; West Chester, PA) coated with poly-L-lysine (Sigma; St. Louis, MO), 15 μg/ml poly-L-ornithine (Sigma), and 1 μg/ml fibronectin (R&D Systems; Minneapolis, MN), and treated daily with 1 μg/ml fibroblast growth factor 2 (FGF2) (R&D Systems). At 6 days *in vitro* (DIV), cells were passaged and stored in dimethyl sulfoxide (DMSO) in liquid nitrogen.

For experiments intended for RNA and protein extraction, cells were removed from liquid nitrogen, re-suspended in media with D-MEM/F-12 (Invitrogen; San Diego, CA) with 2 μg/mL FGF2, plated on pre-coated

polystyrene 6-well plates (BD Biosciences; Franklin Lakes, NJ) at 0.27 – 0.28 $\times 10^6$ cells per well, and grown until approximately 95% confluent (for experiments with undifferentiated cultures). Alternatively, for experiments with differentiated cultures, cells were plated more densely (0.69 – 1.0 $\times 10^6$ cells per well) and expanded for 1-3 days, at which point FGF2 was withdrawn and the cells were allowed to differentiate for 3 days before treatment with IL-6 and IL-6R. For immunofluorescence experiments, cells were plated on pre-coated polystyrene 2-chamber slides (Thermo Fisher Scientific; Rochester, NY) at 0.24 $\times 10^6$ cells per 4 cm^2 well, FGF2 withdrawn after 1 DIV, and allowed to differentiate for 3 days prior to treatment.

IL-6 / IL-6R treatment: For dose-response experiments, the six wells of each 6-well plate were treated with 0, 5, 10, 50, 100, or 150 ng/ml of recombinant human interleukin-6 (IL-6; Peprotech; Rocky Hill, NJ) and recombinant human soluble interleukin-6 receptor (IL-6R; Peprotech) for 12 hours. As an additional control, some plates were co-treated with the above doses of IL-6 and IL-6R plus 1.5 μg of IL-6 neutralizing antibody (#CBL2117; Millipore). Cells intended for RNA extraction were harvested as follows. Following IL-6 / IL-6R treatment, cells were rinsed with PBS, incubated in 1× Hank's Balanced Salt Solution (HBSS; Invitrogen) for 5 min at 37°C, and detached by forcefully pipetting the HBSS over the cells with a fine-tipped pipette. The cell suspension was transferred to a 1.5 ml tube, centrifuged for 10 min at 8000

rpm, and the cell pellet frozen at -80°C. Plates containing cells for protein extraction were rinsed with PBS and stored at -80°C.

For time-course experiments for protein extraction, four 6-well plates of differentiated cultures were treated with 100 ng/ml IL-6 and IL-6R for 5, 10, 15, or 30 min; a fifth plate was treated with media only as control. Each time-point was conducted in triplicate, with cells derived from fetal rats of 3 independent litters. For time-course experiments for immunofluorescence, each well of 2-chamber slides containing differentiated cultures was treated with either 100 ng/ml IL-6 and IL-6R or media only for 5, 10, 15, 60, 90, or 120 min. Subsequently, the cells were rinsed with PBS, fixed in ice-cold methanol for 10 min at -20°C, rinsed with PBS, and stored at 4°C.

RT-PCR:

To determine which doses of IL-6 and IL-6R had an effect on transcription in this cell culture system, the mRNA of a gene known to be affected by IL-6—glial fibrillary acidic protein (*Gfap*)—was examined following treatment with 5-150 ng/ml IL-6 and IL-6R for 12 hours. RNA was extracted from cell pellets with the RNaqueous kit (Ambion). *Gfap* mRNA levels were measured using the One-Step RT-PCR kit (Applied Biosystems; Foster City, CA) with intron-spanning primers designed to target the *Gfap* gene (forward: cagcggctctgagagagatt; reverse: ggaagcaacgtctgtgaggt). Amplification reactions were performed in triplicate on an ABI PRISM 7500 Real Time

Polymerase Chain Reaction (PCR) System (Applied Biosystems). Data were analyzed using the $\Delta\Delta C_t$ method; values were normalized to 18S ribosomal RNA (rRNA) levels.

Western blots:

Protein was extracted by adding 200 µl 1x Laemmli Buffer to each well and scraping the cells from the plate with the back of a pipette tip. The cell solution was transferred to a 1.5 ml tube and DNA digested by incubating with 2 µl of DNase I (Roche Diagnostics) at 37°C for 1 hour. Samples were then centrifuged 10 min at 13,000 rpm at 4°C, denatured at 95°C for 5 min, and stored at -80°C.

To determine if an IL-6-responsive gene was also affected at the protein level, Gfap protein was measured by Western blot. Proteins from differentiated cells treated with 5-150 ng/ml IL-6 and IL-6R were electrophoresed on a 10-20% linear gradient Tris-HCl polyacrylamide gel (Bio-Rad Laboratories; Hercules, CA) and transferred to a polyvinylidene difluoride (PVDF) membrane. Membranes were incubated in rabbit anti-Gfap antibody (#AB5804; Millipore) diluted 1:2000 in tris-buffered saline with Tween 20 (TBS-T) with 5% milk overnight at 4°C and rabbit anti-panH3 (Millipore) diluted 1:100,000 for 4 hours as loading control. Immunoreactivity was developed by the sequential addition of peroxidase-conjugated secondary antibody (Amersham Bioscience; Piscataway, NJ) and Super

Signal West Dura Extend Reagent (Pierce; Rockford, IL) and signal was detected with chemiluminescence-based film autoradiography.

To determine which of the IL-6 signaling pathways were upregulated by IL-6 and IL-6R treatment in this cell culture system, the phosphorylated (active) forms of Stat3 (pStat3), Akt, and Erk1/2 proteins were measured in differentiated cultures treated for 5, 10, 15, or 30 min with 100 ng/ml IL-6 and IL-6R. Proteins were electrophoresed and transferred to PVDF membrane, as described above, and the membrane was incubated in rabbit anti-pStat3 (#9131; Cell Signaling Technology; Danvers, MA) diluted 1:1000, rabbit anti-pAkt (#4058; Cell Signaling Technology) diluted 1:5000, and rabbit anti-pErk1/2 (#4370; Cell Signaling Technology) diluted 1:5000 overnight at 4°C. H4 (1:5000; 06-760; Millipore) was used as a loading control.

Immunofluorescence:

To examine the cellular expression pattern of pStat3 following IL-6 and IL-6R treatment, double-immunofluorescence experiments were performed on differentiated cultures treated for 15, 30, 60, 90, and 120 min with 100 ng/ml IL-6 and IL-6R, or media only as control. Methanol-fixed cells were permeabilized by incubating in 0.1 M PBS with 0.2% Triton-X100 for 10 min at room temperature, blocked in 10% normal goat serum (NGS; Vector Laboratories) and 0.2% Triton-X100 in PBS for 20 min, and incubated in rabbit anti-pStat3 antibody (1:100) and mouse anti-neuron-specific class III β-

tubulin (Tuj1) (#MMS-435P; Covance; Princeton, NJ) diluted 1:500 in PBS with 0.2% Triton-X100 overnight at 4°C. The next day, cells were rinsed in PBS 3× 5 min and incubated in anti-mouse AlexaFluor 488 (Invitrogen) diluted 1:5000 and anti-rabbit AlexaFluor 594 (Invitrogen) diluted 1:10,000 in PBS with 0.2% Triton-X100 for 20 min at room temperature. Subsequently, cells were again washed in PBS, the plastic chambers removed, and the slides coverslipped with DAPI (Vector Laboratories). Additionally, pStat3 protein levels were examined in astrocytes following 15 min IL-6 and IL-6R treatment by double-labeling with pStat3 and mouse anti-Gfap antibody (#MAB3402; Millipore) diluted 1:1000.

Microarray:

Differentiated cultures were treated for 1 or 12 hrs with 100 ng/mL IL-6 / IL-6R (n = 3 per time point) or media only (n = 3) and harvested with 1× HBSS as described above. RNA extracted with the RNaqueous kit (Ambion) and RNA integrity (RIN) assessed with a 2100 Bioanalyzer (Agilent; Santa Clara, CA). cDNA was prepared from RNA employing the Whole Transcript Expression kit (Ambion; Austin, TX). Briefly, 200 ng RNA was mixed with 2 μl poly-A spike control RNA from the GeneChip Whole Transcript Terminal Labeling and Controls kit (Affymetrix; Santa Clara, CA) and first strand cDNA synthesized. Subsequently, second strand cDNA was prepared and used for cRNA synthesis. cRNA was purified with Nucleic Acid Binding Beads and

Wash Solution and then second cycle cDNA synthesized. Second cycle cDNA was hydrolyzed with RNase H and purified. The purified, single-stranded cDNA was fragmented and labeled with the GeneChip Whole Transcript Terminal Labeling and Controls kit, and then submitted to the Genomics Core Facility at University of Massachusetts Medical School for hybridization to Affymetrix GeneChIP Rat Gene 1.0 ST arrays, washing, and scanning with an Affymetrix GeneChip Scanner 3000 7G.

Microarray data analysis: Quality of microarray data was assessed employing the Bioconductor package, arrayQualityMetrics [88]. Microarray data was then uploaded to MicroArray Computational Environment 2.0 (MACE), which employs Robust Multiarray Average (RMA) to preprocess raw oligonucleotide microarray data. The preprocessed data were stored as base 2 log transformed real signal numbers and used for fold-change calculations and statistical tests. Mean signal values and standard deviations were first computed for each gene across samples and the fold-change of expression of a gene between treatment groups was calculated by taking the ratio of these mean signal values. To determine differential expression of genes, MACE internally conducts a Student t-test with the expression signal values of the two hybridizations for all genes in the set.

H3K4me3 ChIP and deep sequencing: Differentiated cultures were treated for 1 or 12 hrs with 100 ng/mL IL-6 and IL-6R (n = 3 per time point) or saline (n = 4) and harvested with 1× HBSS as described above.

Nuclei extraction: in 5 ml Lysis Buffer (0.32 M sucrose, 10 mM Tris-HCl, 5 mM $CaCl_2$, 3 mM $Mg(Ace)_2$, 0.1 mM EDTA, 1 mM DTT, and 0.1% Triton-X100; pH 8.0) for 1 min on ice. The solution was transferred to a 15 ml ultracentrifuge tube and 9 ml of Sucrose Solution (1.8 M sucrose, 10 mM Tris-HCl, 3 mM $Mg(Ace)_2$, and 1 mM DTT; pH 8.0) was pipetted beneath the lysate. Samples were ultracentrifuged for 2.5 hours at 24,400 rpm at 4°C, the buffers and debris discarded, and the pelleted nuclei re-suspended in 200 µl Dounce Buffer for Native ChIP (10 mM Tris-base, 4 mM $MgCl_2$, and 1 mM $CaCl_2$; pH 7.5). Nuclei were freeze-thawed 2× prior to beginning chromatin immunoprecipitation.

Chromatin immunoprecipitation (ChIP): Chromatin was digested with micrococcal nuclease (4 U/ml) for 5 min at 37°C and the reaction was stopped by the addition of 0.5 M EDTA, pH 8 (1:10). Subsequently, 350 µl of Hypotonic Solution (0.2 mM EDTA, PMSF 1:1000, DTT 1:3000, and benzamidin 1:2000; pH 8.0) was added to each sample, and samples were pre-cleared by rotating for 30 minutes with 45 µl of protein G agarose beads (Millipore; Billerica, MA) re-suspended in 1× Frozen Storage Buffer (FSB; 20

mM Tris-base; 5 mM EDTA, and 50 mM NaCl; pH 7.5). Samples were then centrifuged for 5 min at 3000 rpm at 4°C and the supernatant transferred to a new tube; 500 µl of H3K4me3 antibody solution (4 µg rabbit anti-H3K4me3 antibody [#07-473; Millipore] and 15 µg H3K4me2 peptide [Abcam; Cambridge, MA] pre-incubated for 1 hour in 1× FSB with 0.2 mM EDTA, pH 8) and 50 µl of 10× FSB were added and samples were rotated overnight at 4°C. The next day, samples were incubated with 90 µl protein G agarose beads re-suspended in 1× FSB for 1 hour at 4 °C and then centrifuged for 1 min at 3000 rpm and the supernatant discarded. Beads were rotated for 3 min with 1 ml Low Salt Buffer (20 mM Tris-base, 150 mM NaCl, 2 mM EDTA, 1% Triton-X100, and 0.1% SDS; pH 8.0), centrifuged for 1 min at 3000 rpm, and the supernatant discarded; beads were then sequentially washed with 1 ml each High Salt Buffer (20 mM Tris-base, 500 mM NaCl, 2 mM EDTA, 1% Triton-X100, and 0.1% SDS; pH 8.0), Lithium Chloride Buffer (250 mM LiCl, 10 mM Tris-base, 1 mM EDTA, 1% Igepal CA-630, and 1% deoxycholic acid; pH 8.0), and TE Buffer (10 mM Tris-base and 1 mM EDTA; pH 8.0). Chromatin was eluted from beads by rotating for 15 min in 250 µl Elution Buffer (100 mM $NaHCO_3$ and 1% SDS) and then centrifuging for 1 min at 3000 rpm; the supernatant was transferred to a separate tube and set aside. An additional 250 µl Elution Buffer was added to the beads and vortexed for 15 min; samples were centrifuged for 5 min at 13,000 rpm and the supernatant combined with the first 250 µl. Proteins were digested by

incubating samples with 2.5 μl proteinase K (10 μg/ml), 10 μl of 0.5 M EDTA (pH 8.0), and 25 μl Tris-HCl (pH 6.5) for 3 hours at 52°C. After protein digestion, 500 μl of phenol-chloroform (pH 8.0) was added, the samples vortexed, and centrifuged for 5 min at 13,000 rpm; the aqueous phase (approximately 500 μl) was transferred to a new tube and DNA precipitated by the addition of 50 μl 3M sodium acetate (1:10; pH 5.2), 1.375 ml 100% ethanol (2.75× volume), and 2 μl glycogen, and incubated at -80°C overnight. The next day samples were centrifuged at 13,000 rpm for 10 min at 4°C, the supernatant discarded, and the DNA pellets gently washed with ice-cold 75% ethanol. Subsequently, samples were centrifuged for 5 min at 14,000 rpm, the supernatant discarded, and the DNA pellets air-dried. DNA was re-suspended in 36 μl 4 mM Tris-HCl (pH 8.0) and 2 μl used for measuring DNA concentration; the remaining 34 μl was used for preparation of libraries for deep sequencing.

Deep sequencing: Immunoprecipitated DNA was processed for deep sequencing as follows. The ends of the DNA fragments were blunted using the End-it DNA Repair kit (Epicentre; Madison, WI), the reaction cleaned with the QIAquick Gel Extraction kit (Qiagen; Valencia, CA), and the fragments A-tailed by incubating with 0.2 mM dATP and 0.8 U/μl Exo-minus Klenow DNA polymerase in 1× Klenow Buffer for 1 hour at room temperature. Subsequently, the reaction was again cleaned with the QIAquick Gel

Extraction kit and the Genomic Adaptor Oligo Mix (Illumina; San Diego, CA) was ligated to fragments overnight at 16°C employing the Fast Link kit (Epicentre). The next day, fragments were PCR-amplified with Illumina single-read primers, the reaction cleaned with the QIAquick kit, and fragments around 250 base pairs gel-purified. The H3K4me3 ChIP libraries were deep sequenced by an Illumina Genome Analyzer (GA II).

ChIP-Seq Data analysis: Raw sequence reads were aligned to the rat reference genome (version rn4) using Bowtie [89] to determine the total number of reads per library, as well as the number of uniquely-mappable, multi-mappable, and non-mappable reads. Only uniquely aligned reads with up to 1 mismatch were considered in this analysis and reads mapping to forward and reverse strands were pooled. The aligned sequence data was converted to ELAND format and, concurrently, normalized for sequencing depth by randomly sampling the same number of reads from each library (the lowest number of uniquely-mappable reads). Genomic regions significantly enriched for reads—called peaks—were detected with the model-based analysis for ChIP-Seq (MACS) program [90] and the percentage of proximal (< 2 kb from a transcription start site, or TSS), medial (2-10 kb from TSS), and distal (> 10 kb from TSS) peaks were determined. Data from normalized libraries was uploaded to the University of California Santa Cruz (UCSC)

Genome Browser, which allows visualization of H3K4me3 levels in each sample genome-wide.

After confirming that each library was of good quality (i.e., possessing both a high percent of uniquely-mappable reads and proximal peaks), group differences in H3K4me3 levels within TSS (0 bp) and +500 bp were measured employing the DESeq Bioconductor package [91, 92]. Read counts per gene region were calculated using the Genominator package [93] from Bioconductor 2.7, the count tables annotated, and differential H3K4me3 was inferred using the DESeq. Comparing treatment groups with DESeq offers an advantage over MACS, because it measures all reads within defined genomic intervals. Thus, it is possible to detect regions with H3K4me3 levels significantly altered by treatment that do not necessarily contain a statistically significant peak as called by MACS.

Stat3 inhibitor treatment: To determine the role of the Stat3 pathway in mediating the effects of IL-6 on both gene expression and H3K4me3 in rat forebrain culture, cells were pre-incubated with 100 μM S31-201, a small molecule pStat3-specific inhibitor [94] and then treated with the standard dose of 100 ng/mL IL-6 / IL-6R for 1 hour in the presence of inhibitor. The 100 μM dose was selected based on a dose-response experiment in which cells were pre-incubated with 50, 100, or 200 μM S31-201 for 2 hrs and then stimulated with IL-6 / IL-6R for 15 min. Protein was extracted, electrophoresed,

transferred to a PVDF membrane, and immunoblotted with pStat3 antibody as described above. Additionally, pAkt and pErk1/2 immunoblots were performed to confirm that S31-201 was indeed pStat3-specific. Following S31-201 + IL-6 / IL-6R co-treatment, cells were prepared for microarray or H3K4me3 ChIP-Seq, as described above.

Comparison of IL-6 microarray and ChIP-Seq data sets with autism

H3K4me3 ChIP-Seq:

To examine whether an *in vitro* "model" of autism reproduces alterations in H3K4me3 observed in postmortem brain in this disorder, the 12 hr IL-6 forebrain culture ChIP-Seq and microarray data sets were compared to data from human disease. H3K4me3 ChIP-Seq was performed on neuronal nuclei isolated from cortex of 16 autism subjects and 14 controls. The autism H3K4me3 ChIP-Seq experiment reported 480 human genes as differentially expressed (DE) from all annotated genes in the Ensembl database (53630). In the 12 hr microarray experiment of IL-6 treated rat forebrain culture, 604 rat genes were found to be DE out of the total number assayed on the rat Affymetrix GeneChip (28826). Seventeen genes were altered in both data sets. This experimental number of overlapping genes was compared with the number of genes that are in common when 480 genes are randomly selected from the Ensembl gene set and 604 genes randomly selected from the microarray set. Random sampling without replacement was

repeated 10,000 times. The random rat gene sets were converted to human genes using the Homologene database (http://www.ncbi.nlm.nih.gov/) and the number of genes occurring in rat and human samples determined for all 10,000 sampling events.

Results

IL-6 / IL-6R treatment exerts a concentration-dependent effect on *Gfap* mRNA and protein:

To establish the dose range of IL-6 and IL-6R that has an effect on transcription in the rat forebrain culture system, cells were treated with 5, 10, 50, 100, or 150 ng/mL IL-6 and IL-6R for 12 hours and the mRNA of a positive control gene—*Gfap*—measured with qRT-PCR. Transcript levels demonstrated a concentration-dependent increase in both undifferentiated (**Figure 2A**) and differentiated cells (**Figure 2B**) compared to control. Fold-changes of *Gfap* mRNA in undifferentiated cells ranged from 6 to 245-fold and from 0.49 to 8-fold in differentiated cells. Co-treatment with a constant dose of IL-6 neutralizing antibody completely blocked the IL-6/IL-6R-induced increase of *Gfap* mRNA levels at lower doses and partially blocked the increase at the higher doses. Additionally, Gfap protein also demonstrated a concentration-dependent increase, with protein first visible by Western blot at 50 ng/mL (**Figure 2C**). The 12 hr treatment had no discernable effect on cell

viability at any dose. Based on these findings, the 100 ng/mL dose was selected for use in further experiments.

IL-6 / IL-6R treatment exerts a time-dependent effect on pStat3, pAkt, and pErk1/2 protein:

In order to determine which signaling pathways known to be activated by IL-6 in other cell types are induced in the rat forebrain culture system, differentiated cultures were treated with 100 ng/mL IL-6 / IL-6R for 5, 10, 15, or 30 minutes and the phosphorylated forms of Stat3, Akt, and Erk1/2 protein measured by Western blot. All three phospho-proteins demonstrated a time-dependent increase relative to control, with the highest levels apparent at the 30 min time point (**Figure 3**).

Next, in order to determine which cell types are activated by IL-6 / IL-6R in this system, cultures were treated for 5, 10, 15, 30, 60, or 90 minutes and then processed for Gfap/pStat3, pAkt, or Erk1/2 (astrocytes) or Tuj1/ pStat3, pAkt, or Erk1/2 double-immunofluorescence (neurons). As shown by Western blot, pStat3 immunoreactivity increased in a time-dependent manner, with immunoreative nuclei first visible at 5 min and lasting approximately 60 min (**Figure 4A**). However, as shown in **Figure 4A**, none of the pStat3-IR nuclei colocalized with the Tuj1-IR neurons. The majority of pStat3-IR nuclei were observed in the Gfap-IR astrocytes (**Figure 4B**) and a smaller proportion did not overlap with either neurons or astrocytes.

Immunoreactivity for pAkt and pErk1/2 was not observed in control or IL-6 / IL-6R treated cultures, despite detection by Western blot (data not shown), and may represent limited utility of the particular antibodies employed.

IL-6 / IL-6R treatment alters gene expression in rat forebrain culture:

In order to obtain a global overview of the effects of IL-6 on the transcriptome in rat forebrain culture, microarrays were employed to measure mRNA changes in cells treated for either 1 or 12 hrs with 100 ng/mL IL-6 / IL-6R (**Figures 5 and 6**). Additionally, a set of cultures at the 1 hr time-point were treated with IL-6 / IL-6R in combination with the Stat3 inhibitor, S31-201, to determine the proportion of IL-6-responsive genes regulated by this pathway.

Pre-treatment of cell culture with 50, 100, and 200 μM S31-201 for 2 hrs prior to the addition of IL-6 / IL-6R for 15 min resulted in a concentration-dependent attenuation of pStat3 protein (**Fig. 5A**); based on this experiment, the 100 μM dose was selected for microarray and ChIP-Seq experiments. Treatment with IL-6 / IL-6R for 1 hr resulted upregulation of 1386 genes ≥ 1.5-fold and downregulation of 792 genes ≤ -1.5-fold. As expected, a wide variety of genes with immune function were altered by cytokine stimulation, including suppressor of cytokine signaling (*Socs3*), leukemia inhibitory factor receptor alpha (*Lifr*), heat shock protein 1 (*Hspb1*), interleukin 1 receptor type I (*Il1r1*), and interferon induced transmembrane protein 3 (*Ifitm3*). Interestingly, some

of these genes—including *Ifitm3*, *Hspb1*, and growth arrest and DNA-damage inducible beta (*Gadd45b*)—show altered expression levels in schizophrenia and autism postmortem brain [53, 54, 56]. Additionally, a number of non-immune genes implicated in schizophrenia and autism were also altered by IL-6 exposure, including glutamate decarboxylase 1 (*Gad1*), metabotropic glutamate receptor 5 (*Grm5*), neuropeptide Y (*Npy*), and gamma-aminobutyric acid (GABA) A receptor alpha 3 (*Gabra3*) [95-97].

Due to the large numbers of transcripts altered by IL-6 / IL-6R treatment, only those genes showing maximal blockade by Stat3 inhibitor treatment are shown in the heatmap in **Fig. 5C**. When the groups were analyzed by non-hierarchical clustering for this set of genes, the saline and Stat3 inhibitor groups clustered together and their similarity in signal intensity can be observed. Of the 1386 genes increased ≥ 1.5-fold by IL-6 / IL-6R relative to saline, 98 (7.1%) were also increased by IL-6 / IL-6R relative to IL-6 / IL-6R + S31-201 (also ≥ 1.5-fold), indicating that the effect of IL-6 was attenuated for these genes by Stat3 inhibition. If all genes increased ≥ 1.2-fold by IL-6 / IL-6R relative to IL-6 / IL-6R + S31-201 are included, 383 genes (29.8%) were blocked by Stat3 inhibitor treatment. Of the 792 genes decreased ≤ -1.5-fold, 43 (5.4%) were attenuated by S31-201 at the -1.5-fold level and 136 (17.2%) were attenuated at the -1.2-fold level.

Consistent with the knowledge that the Jak2/Stat3 pathway plays a central role in inflammatory signaling—including in the central nervous

system—many of the genes blocked by the Stat3 inhibitor have immune function, including the above-mentioned *Ifitm1*, *Ifitm3*, *Hspb1*, *Il1r1*, *Socs3*, in addition to oncostatin M receptor (*Osm*), tumor necrosis factor receptor superfamily 21 (*Tnfrsf21*), and chemokine (C-C) motif ligand 2 (*Ccl2*).

Additionally, there were several non-immune genes with potential relevance for schizophrenia and autism whose IL-6-induced upregulation was attenuated by Stat3 inhibition. For example, growth associated protein 43 (*GAP43*) was recently identified as an autism susceptibility gene and *Gap43+/-* mice display an autism-like phenotype in several behavioral tests, including decreased social interaction and stress-induced anxiety [98, 99]. The glutamate receptor-like protein 1a (*GRIN1A*) is located on chromosome 15q22.1, an autism susceptibility locus [100]. Multiple glutathione-S-transferase genes have been associated with schizophrenia and autism; the alpha 4 variant (*Gsta4*) was upregulated by IL-6 in this study [101-105]. Thus, it is possible that Parker-Athill and colleagues observed that administration of Stat3 inhibitors in pregnant mice ameliorated the behavioral effects of maternal IL-6 treatment on offspring, in part, by preventing the expression changes in these genes.

Treatment with IL-6 / IL-6R for 12 hr resulted in markedly fewer changes in mRNA levels than at the 1 hr time-point: 77 genes were upregulated ≥ 1.5-fold, while 37 genes were downregulated ≤ -1.5-fold. These changes are illustrated in heatmap in **Fig. 6A**. Of the 77 genes

increased ≥ 1.5-fold, 47 (61%) were also increased ≥ 1.5-fold at the 1 hr time point (**Fig. 6B**). Of the 37 genes decreased ≤ -1.5-fold, 9 (24.3%) were decreased at 1 hr. It should be noted that some of the genes showing smaller fold-changes (1.2 to 1.5) at 12 hrs had robust fold-changes at 1 hr, such as *Ifitm1*, *Anxa5*, and *Trib1*, all of which were increased ≥ 3-fold at the earlier time point. Conversely, several genes upregulated ≥ 3-fold at 12 hrs—*Il17rb*, *A2m*, and *Chdh*—were not altered at 1 hr. In total, 22 genes increased ≥ 1.5-fold at 12 hrs were not altered at 1 hr (230 ≥ 1.2-fold), while 27 genes decreased ≤ -1.5-fold were not changed at the earlier time point (133 ≤ -1.2-fold).

IL-6 / IL-6R treatment alters H3K4me3 levels in rat forebrain culture:

Alignment of each deep-sequenced H3K4me3 library with rat genome revealed library sizes ranging from 2.1×10^6 to 19.5×10^6 total reads (**Fig. 7**). Importantly, a high percent of these total reads (72-78%) were uniquely mappable to rat genome, indicating good library quality. A smaller percentage (13-17%) of reads mapped to multiple locations and 9-11% of reads were not mappable. Neither multi-mappable nor non-mappable reads were included in subsequent analyses. Following normalization of all rat H3K4me3 libraries to the lowest number of unique reads obtained (2.1×10^6), MACS software was used to identify peaks, or regions of the genome significantly enriched for H3K4me3. This analysis revealed a high percent

(68-69%) of proximal peaks—peaks within 2 kb of a gene TSS—for all groups, which is consistent with studies showing that H3K4me3 is primarily enriched at the 5' end of genes [12]. A smaller percentage of peaks (6%) were medial (2-10 kb from TSS) and 24-27% were distal (> 10 kb). Medial and distal peaks could represent enhancer elements or transcription start sites of currently unidentified genes.

Treatment for 1 hr with IL-6 / IL-6R resulted in increased H3K4me3 levels at 235 genes ≥ 1.5-fold and decreased levels at 259 genes ≤ -1.5-fold (**Fig. 8**). The heatmap in **Fig. 8A** represents all genes with ≥ 2-fold change in H3K4me3 in either direction for IL-6 / IL-6R treated cultures relative to saline. The heatmap in **Fig. 8B** represents the genes whose IL-6-induced H3K4me3 alterations were maximally attenuated by the Stat3 inhibitor, S31-201. In total, Stat3 inhibition resulted in attenuation of IL-6-induced H3K4me3 changes at 25 of the 235 genes increased ≥ 1.5-fold and 5/259 genes ≤ -1.5-fold. Thus, while Stat3 signaling appears to play a critical role in the modulation of H3K4me3 at specific gene promoters, it is clear from the number of H3K4me3 changes *not* affected by S31-201 treatment that IL-6 regulates this histone modification via multiple pathways in this CNS model system. Of note, of 21 genes whose increased in H3K4me3 appears Stat3-dependent, 13 also had their mRNA changes blocked by S31-201, suggesting that the H3K4me3 alterations at these gene promoters are important for transcription.

A subset of genes with altered H3K4me3 levels exhibited corresponding changes in mRNA levels. Of the 235 genes with increased H3K4me3 ≥ 1.5-fold, 67 also had increased mRNA (≥ 1.5-fold); of the 259 genes with decreased H3K4me3 ≤ -1.5-fold, 9 genes had decreased mRNA (**Fig. 8C**).

Treatment for 12 hrs with IL-6 / IL-6R resulted in increased H3K4me3 levels at 33 genes ≥ 1.5-fold (149 genes ≥ 1.2-fold), while 38 genes had decreased H3K4me3 ≤ -1.5-fold (60 genes ≤ -1.2-fold) (**Fig. 9**). The heatmap in **Fig. 9A** depicts all genes with fold-changes of 1.5 or greater in either direction. The H3K4me3 profile from the UCSC Genome Browser is shown for the suppressor of cytokine signaling 3 (*Socs3*) gene in **Fig. 9B**, which demonstrated the greatest increase in H3K4me3 at this time-point (3.2-fold; $p = 1.94^{-20}$). Interestingly, *Socs3*, and two other immediate-early genes, *Fos* and *Junb*, all exhibited a highly unusual histone methylation pattern—rather than being confined to the region immediately proximal to the TSS, as is typical for this mark, H3K4me3 was observed to encompass the entire gene and surrounding regions; this effect was more pronounced in the IL-6 / IL-6R-treated samples. This may represent an important feature of immediate-early genes, which must be capable of transcriptional activation within minutes.

As with the 1 hr time-point, there was some overlap between H3K4me3 and mRNA levels after 12 hrs treatment; however, the majority of genes demonstrate either altered histone methylation or mRNA, not both.

For the 33 genes increased ≥ 1.5-fold, 7 had corresponding increases in mRNA (also at the 1.5-fold level); for the 38 genes decreased ≤ -1.5-fold, 3 had corresponding decreases in mRNA (**Fig. 9C**).

The overlap between H3K4me3 changes at 1 and 12 hrs was smaller than that observed for gene expression changes: 5 of the 77 genes increased ≥ 1.5-fold at 12 hrs were also increased at 1 hr, while 3 of the 37 genes decreased at 12 hrs were also decreased at 1 hr (**Fig. 9D**). Another group of genes showed opposing changes at the two time-points. Four genes that were increased ≥ 1.5-fold at 1 hr (*Dlx2*, *Glrx1*, *Gsta4*, and *Hopx*) were decreased at 12 hrs; similarly, 21 genes decreased ≤ -1.5-fold at 1 hr were increased at 12 hrs (between 1.27 and 1.62-fold). Finally, some genes changed at only one time-point: 225 genes were increased ≥ 1.5-fold and 238 genes were decreased ≤ -1.5-fold at 1 hr but not at 12 hrs. Conversely, 22 genes were increased ≥ 1.5-fold and 32 were decreased ≤ -1.5-fold at 12 hrs but not at 1 hr.

Genes with altered H3K4me3 peaks in autism brain are affected by IL-6 / IL-6R treatment in rat forebrain culture:

Due to the observation that some of the genes affected by 12 hr IL-6 treatment—at either the mRNA or H3K4me3 levels, or both—also demonstrated altered H3K4me3 levels in autism postmortem brain in a study conducted by our laboratory, I sought to determine if this overlap was

significant employing random sampling. The number of experimentally determined overlapping genes (17) was significantly higher than 95% of overlaps derived from random sampling (mean = 2.7). Likewise, the overlap of 4 genes (*SOCS3, FOS, KCNJ10,* and *KCNT1*) altered in autism ChIP-Seq, rat culture microarray, and rat culture ChIP-Seq is also significant, as random sampling produces virtually no overlaps.

Interestingly, *Socs3* mRNA and H3K4me3 were significantly increased following IL-6 treatment in rat forebrain culture and also revealed a significantly higher H3K4me3 peak in two autism postmortem samples relative to controls. Also of note, the few autism samples with altered H3K4me3 appear to have many changes at other immune genes, including interferon, alpha-inducible 6 (*IFI6*), NFκB activating protein-like (*NKAPL*), interferon regulatory factor 9 (*IRF9*), heat shock 70kDa protein 2 (HSPA2), janus kinase 3 (*JAK3*), transforming growth factor family members *TGFB1* and *TGFBR1*, and multiple major histocompatibility complex loci, including *HLA-F*, *HLA-B*, *HLA-E,* and *HLA-F*. In a study by another group, two of these same postmortem samples revealed significant increases in microglial activation [52]. While prenatal exposure to maternal infection in these cases cannot be unequivocally proven, it is interesting that they show altered H3K4me3 methylation profiles at genes that have a central role in inflammatory signaling, some of which are affected by IL-6 treatment in cell culture.

Discussion

This is the first report that IL-6, a cytokine implicated in a variety of neuropsychiatric disorders, is capable of altering H3K4me3 in a model of the central nervous system. Very little is known regarding the regulation of specific chromatin modifications in developing and mature brain; what causes them to become altered in disorders like schizophrenia and autism is also not known. Clearly, such epigenetic modifications must be capable of responding to a diverse array of environmental stimuli in order to regulate cellular response; however, links between specific stimuli and specific histone modifications in brain remain enigmatic. In the current study, I sought to examine a specific environmental factor known to increase risk for schizophrenia and autism and investigate its role in the modulation of chromatin. Specifically, I demonstrated: (1) IL-6 alters H3K4me3 levels at multiple gene promoters in rat forebrain culture (2) many of these genes have corresponding mRNA changes and have been implicated in neuropsychiatric disease (3) a subset of H3K4me3 and mRNA changes are Stat3-dependent (4) pStat3 immunoreactivity is confined to astrocytes, suggesting that Stat3-dependent H3K4me3 and mRNA changes are driven by astrocyte activation, and (5) some genes affected by IL-6 also demonstrate altered H3K4me3 levels in postmortem autism brain.

Interestingly, there were many more genes demonstrating IL-6 induced H3K4me3 and mRNA changes at the 1 hr time point versus 12 hour. That

many alterations disappear at the later time point suggests that IL-6 signaling is under strict regulation in central nervous system and is reflective of the transient nature of the cytokine stimulus. Attenuation of IL-6 signaling over time can be explained, in part, by the increased expression of *Socs3* gene, which remained highly enriched for the H3K4me3 mark at 12 hours. However, this observation raises the question: if IL-6 signaling is under such tight control in brain, how might H3K4me3 changes that occur *in utero* escape regulation in a disorder such as schizophrenia or autism?

There has been recent interest in uncovering the specific signaling pathways through which IL-6 mediates its effects on neurodevelopment. This has been motivated by a report showing *complete* blockade of IL-6 resulted in maternal death of pregnant mice following infection with influenza virus [83]. This emphasizes the dual nature of IL-6 in both attenuating and propagating inflammation. Preventing the deleterious effects of IL-6 on fetal brain development, while preserving its beneficial effects, may require the blockade of one pathway while leaving other pathways intact. This knowledge will aid in the development of novel therapeutics for the treatment of infection during pregnancy to protect both the mother and her offspring. The need for such treatment is emphasized by the finding that an estimated 30% of schizophrenia cases could be eliminated through the prevention of maternal infection during pregnancy [106].

Recent work suggests that the Stat3 pathway plays a critical role in mediating the effects of maternal cytokines on fetal brain development and adult behavior in mice [84]. This study showed that injection of pregnant mice with IL-6 resulted in behavioral abnormalities in the adult offspring, and that Stat3 inhibition ameliorated these effects. Based on this study, I was interested to: (1) examine the role of the Stat3 pathway in regulating IL-6-induced H3K4me3 and gene expression changes in rat forebrain culture, and (2) identify genes that might explain the deleterious effects of IL-6-mediated Stat3 signaling.

I found that Stat3 inhibition resulted in the blockade of multiple gene expression changes induced by IL-6. As described in the Results section, many of these genes have immune function, and include cytokines and cytokine receptors, heat shock factors, chemokines, and interferon-induced proteins. Importantly, many of these genes have been reported to be altered in schizophrenia and autism postmortem brain [53, 54, 56]. Additionally, non-immune genes implicated in schizophrenia or autism also appear to be regulated by Stat3 including, *Gap43*, *Grinl1a*, and *Gsta4* [98-105].

However, in contrast to the large number of transcripts regulated by the Stat3 pathway, far fewer H3K4me3 changes appear to be Stat3-dependent in the forebrain culture system. The genes whose H3K4me3 levels were most affected by Stat3 inhibition are depicted in Figure 7B. Though few are established schizophrenia or autism susceptibility genes,

several have been implicated in neurodevelopment and brain function. For example, epithelial membrane protein 1 (*Emp1*) is highly expressed by young neurons in developing mouse brain and has been implicated in neurite extension [107]. Additionally, GS homeobox 2 (*Gsx2*) is a transcription factor expressed very early in development and is required for differentiation of interneurons fated for striatum and olfactory bulb [108, 109]. Finally, one gene—GTP binding protein overexpressed in skeletal muscle (*Gem*)—is reportedly increased in autism postmortem brain [56]. While a role for *Gem* in brain has not been established, this Ras-related GTP protein is known to be upregulated in T cells following cytokine stimulation, suggesting an immune function [110]. From these findings, I conclude that IL-6 regulates H3K4me3 at a number of gene promoters; however, these changes can only be partially attributed to Stat3 signaling. This highlights the importance of investigating the roles of other signaling pathways involved in IL-6-mediated H3K4me3 in brain.

It is of interest that a variety of genes affected by IL-6 at both the mRNA and H3K4me3 levels also have altered H3K4me3 peaks in neurons in a subset of autism cases. While it is not possible to prove that these aberrant methylation peaks in autism brain were caused by an early exposure to an immune stimulus, the fact that IL-6 was shown to alter this same histone modification in forebrain culture strengthens the link between inflammation, chromatin modification, and neuropsychiatric disease.

Medical records available from brain tissue banks are often lacking in basic information regarding course of illness and medication history, in addition to details such as maternal infection during pregnancy or other early environmental exposures. Prospective studies examining the link between maternal infection and the development of schizophrenia and autism have been conducted, and have confirmed that infection does indeed elevate risk for development of schizophrenia later in life [36, 72]. The brains from such study subjects would provide valuable resources for the field of neurobiology as specific molecular and cellular changes observed in the disease cohort could be correlated with environmental variables.

Important future experiments will include the clarification of cellular specificity of IL-6 on H3K4me3. Though the current study observed increased pStat3 protein primarily in astrocytes, two points must be kept in mind. First, not all H3K4me3 and mRNA changes were Stat3-dependent. Secondly, even for those changes that appear Stat3-dependent, a mechanism whereby astrocytes induce downstream modifications in neurons cannot be ruled out. Thus, from the current data, we can only conclude that some IL-6 induced alterations of H3K4me3 and mRNA are likely initiated by astrocytes, but not necessarily confined to this cell population. Pure astrocyte and neuron culture experiments could be employed to delineate which histone methylation changes are contributed by each cell type. However, it may be important to preserve neuron-astrocyte cross-talk during IL-6

stimulation in order to more closely recapitulate what is occurring in the mixed forebrain culture system and in the brain. To perform this experiment, fetal mice could be exposed to increased levels of IL-6 protein and the neurons and astrocytes then sorted using cell-specific antibodies and magnetic beads.

Additionally, it would be of interest to further explore the mechanisms by which pStat3 regulates H3K4me3 in brain. This could be examined by pStat3 immunoprecipitation following IL-6 stimulation and analysis of the protein complex via mass spectrometry to determine potential interacting proteins such as histone methyltransferases and demethylases. Indirect evidence for pStat3 interaction with a histone methyltransferase is derived from two independent immunoprecipitation studies. The first reported an IL-6 induced interaction of pStat3 with Ctr9, a component of the PAF transcription complex, in mouse liver; Ctr9 depletion resulted in decreased Stat3 promoter binding in conjunction with decreased H3K4me3 levels [111]. Importantly, Ctr9 knockdown only abrogated expression of IL-6-responsive genes and not those induced by INFβ, IL-1β, or TNFα, suggesting that different cytokines modulate chromatin via distinct mechanisms. The second study reported interaction of the human histone methyltransferase, mixed-lineage leukemia 1 (MLL1), with the PAF complex protein, PAF1, at the Hox9a locus in mouse embryonic fibroblasts [112]. Together, these studies suggest that Stat3 regulates H3K4me3, in part, via MLL1.

Recently, it was shown that IL-6 induces dimethylation of STAT3 at K140 via the H3K4 methyltransferase, SET9, in human A4 cells [113]. Mutation of K140 resulted in enhanced STAT3 phosphorylation, DNA binding activity, and transcription of the STAT3-target gene, *SOCS3*, suggesting that methylation of this lysine residue negatively regulates STAT3 activity. Moreover, STAT3 was also shown to directly interact with the histone demethylase, lysine-specific demethylase, LSD1. That STAT3 is capable of recruiting histone-modifying enzymes to specific gene promoters suggests another mechanism whereby IL-6 might regulate H3K4me3.

It must be noted that other signaling pathways activated by IL-6—namely, PI3K/Akt and Erk1/2—likely play a critical role in modulation of H3K4me3 and gene expression in the brain. This is highlighted by the observation in the current study that Stat3 inhibition only blocked a subset of IL-6 induced H3K4me3 and mRNA changes. Therefore, future studies examining H3K4me3 modulation by pAkt and pErk1/2 through the use of inhibitors is warranted.

Exposure to environmental factors during prenatal and early postnatal development is linked to increased risk of schizophrenia and autism. It has been suggested that these stimuli may alter neurodevelopment, in part, via epigenetic mechanisms. However, a direct link between inflammation and histone modifications in brain has not been established. My findings support a role for the pro-inflammatory cytokine, IL-6, in the regulation of the

chromatin modification, H3K4me3, in central nervous system. Moreover, a number of genes affected by IL-6 *in vitro* display altered H3K4me3 in autism postmortem brain. Though indirect, these data provide evidence suggesting that aberrant chromatin modifications observed in schizophrenia and autism postmortem brain may have been caused by early exposure to inflammation.

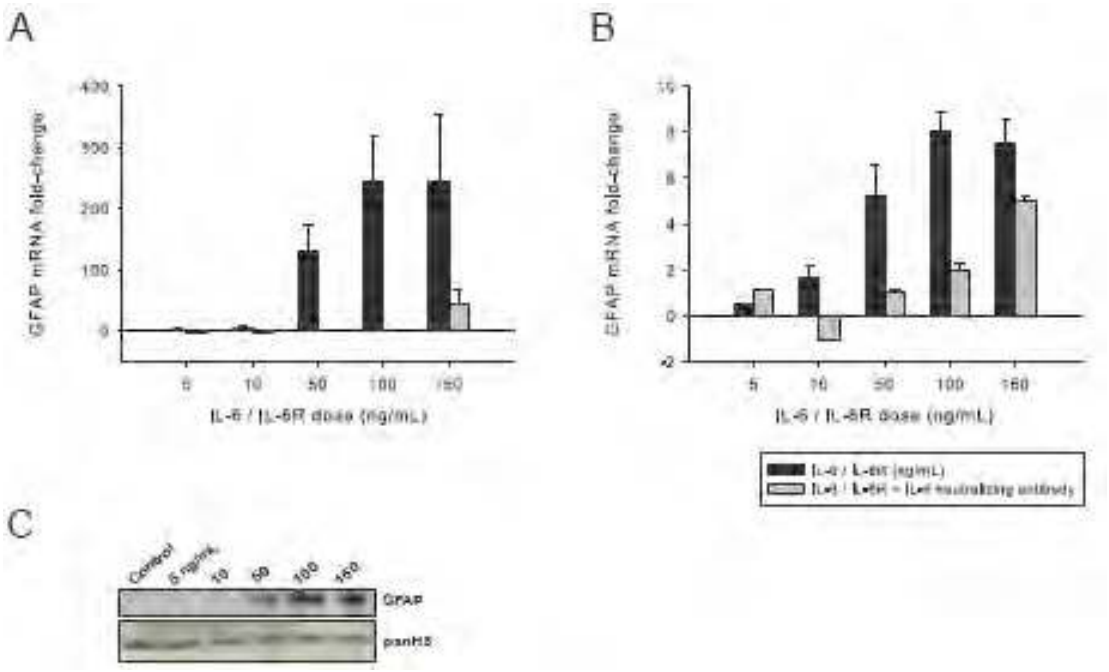

Figure 2: *Gfap* mRNA and protein demonstrate a dose-dependent upregulation in rat forebrain culture following IL-6 and IL-6R treatment. **(A)** *Gfap* mRNA increases in undifferentiated E14.5 forebrain culture following 12 hour treatment with 5, 10, 50, 100, and 150 ng/mL IL-6 and IL-6R compared to control culture (n = 3). This increase was prevented by the addition of 1.5 μg IL-6 neutralizing antibody. Data are expressed as mean ± standard error of the mean (SEM). **(B)** *Gfap* mRNA also increases in differentiated E14.5 forebrain culture (3 DIV following withdrawal of FGF) following 12 hr treatment with 5-150 ng/mL IL-6 and IL-6R (n = 3). **(C)** Gfap protein also increased in differentiated forebrain cultures following 12 hr treatment with IL-6 and IL-6R, with protein first detectable by Western blot at a dose of 50 ng/mL. Western blot is representative of 3 experiments.

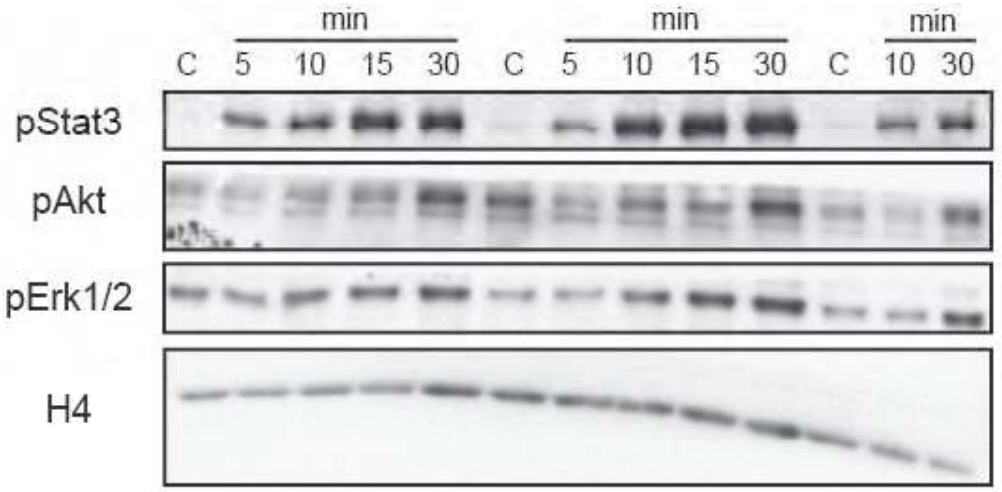

Figure 3: Phosphorylated Stat3 (pStat3), pAkt, and pErk1/2 protein demonstrate a time-dependent upregulation in rat forebrain culture following IL-6 and IL-6R treatment. Levels of phosphorylated Stat3, Akt, and Erk1/2 protein increase in differentiated rat forebrain culture following 5, 10, 15, and 30 minutes treatment with 100 ng/mL IL-6 and IL-6R relative to control culture (indicated as C in figure). Each time point was conducted in triplicate.

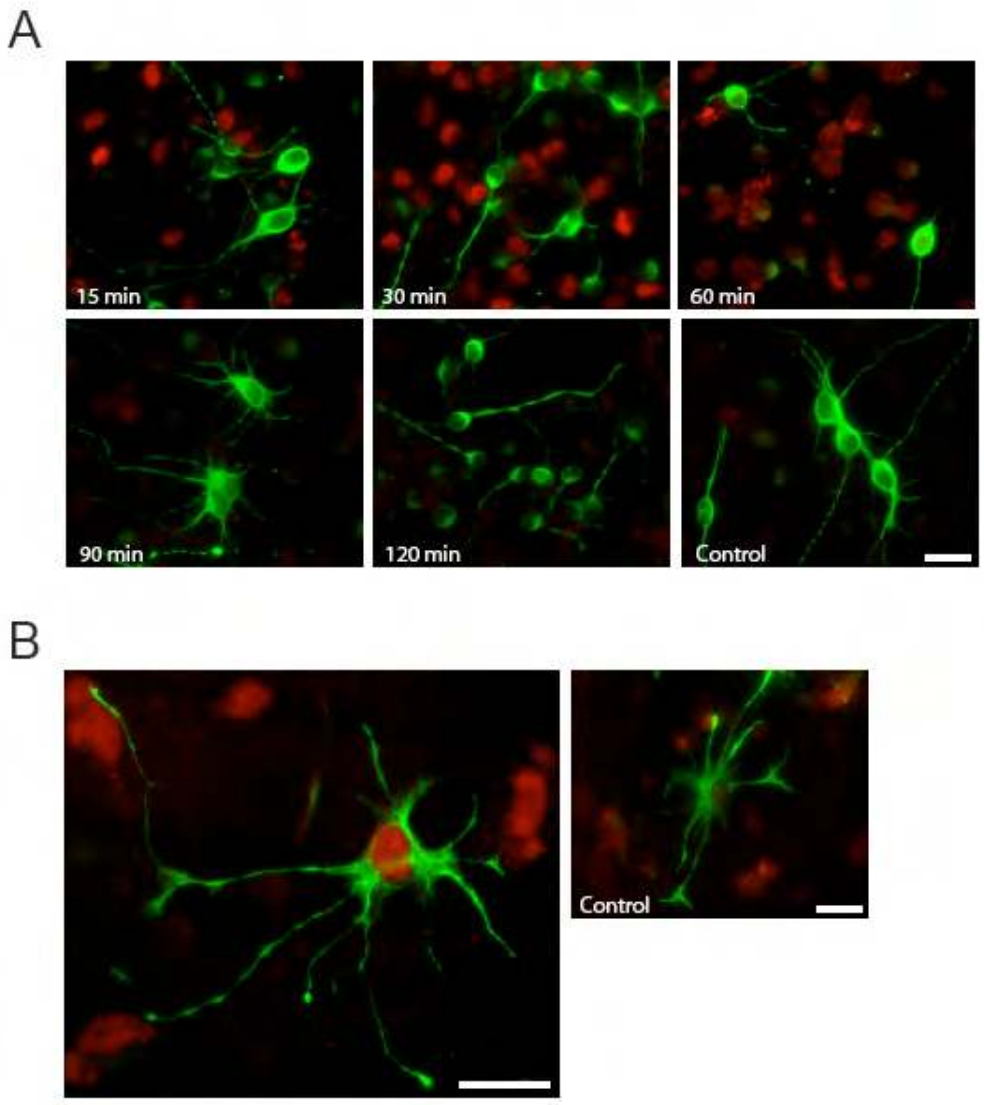

Figure 4: pStat3 protein is upregulated in astrocytes, but not in neurons, in rat forebrain culture following IL-6 and IL-6R treatment. (A) pStat3-immunoreactive nuclei (red) are visible in differentiated rat forebrain culture after 15, 30, and 60 minutes treatment with 100 ng/mL IL-6 and IL-6R. Immunoreactivity returns to control levels by 90 min. Note that none of the pStat3-immunoreactive nuclei overlap with Tuj1-immunoreactive cells (green). **(B)** An astrocyte labeled with anti-Gfap antibody (green) with a pStat3-immunoreactive nucleus. The majority of pStat3 protein appears to be localized to the nuclei of astrocytes.

A

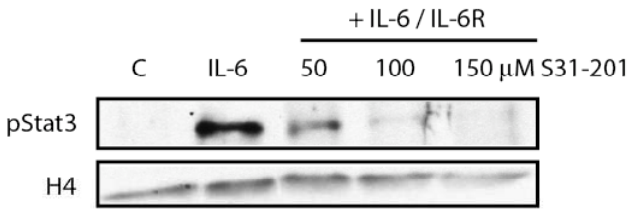
+ IL-6 / IL-6R
C
IL-6
50
100
150 μM S31-201
pStat3
H4

B

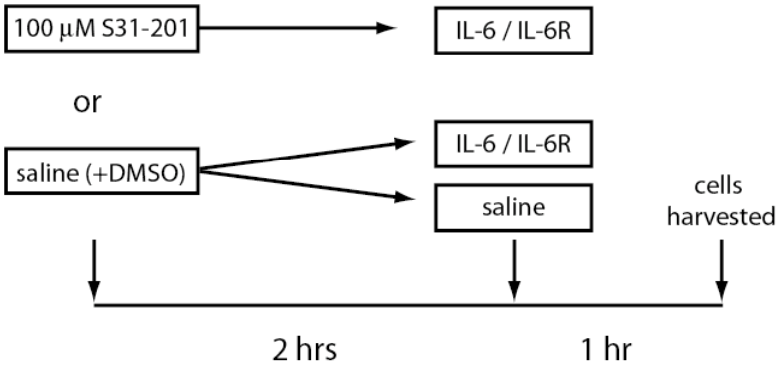
100 μM S31-201
IL-6 / IL-6R
or
saline (+DMSO)
IL-6 / IL-6R
saline
cells harvested
2 hrs
1 hr

C

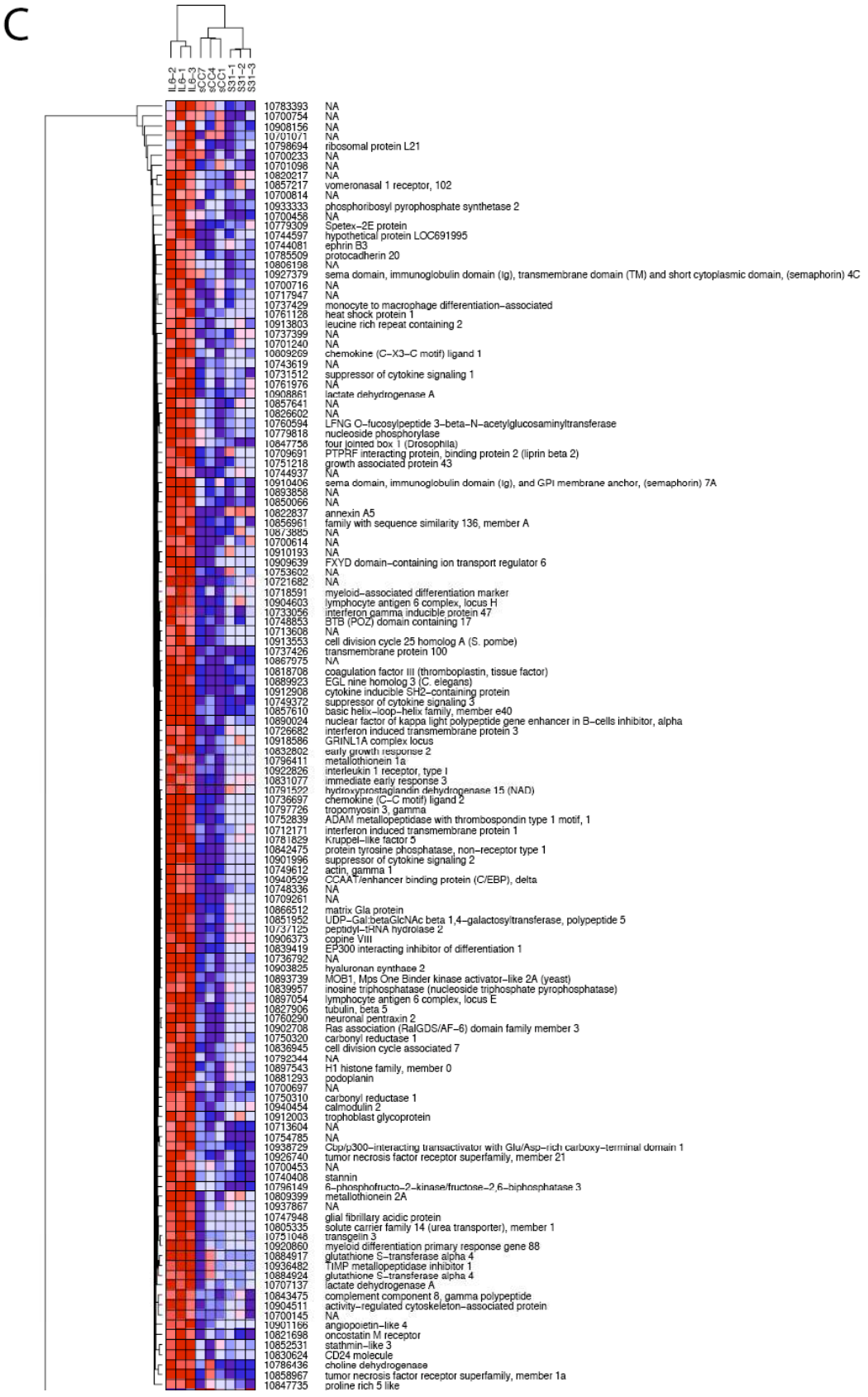
IL6−2
IL6−1
IL6−3
sCC7
sCC4
sCC1
S31−1
S31−2
S31−3
10783393 NA
10700754 NA
10908156 NA
10701071 NA
10798694 ribosomal protein L21
10700233 NA
10701098 NA
10820217 NA
10857217 vomeronasal 1 receptor, 102
10700814 NA
10933333 phosphoribosyl pyrophosphate synthetase 2
10700458 NA
10779309 Spetex−2E protein
10744597 hypothetical protein LOC691995
10744081 ephrin B3
10785509 protocadherin 20
10806198 NA
10927379 sema domain, immunoglobulin domain (Ig), transmembrane domain (TM) and short cytoplasmic domain, (semaphorin) 4C
10700716 NA
10717947 NA
10737429 monocyte to macrophage differentiation−associated
10761128 heat shock protein 1
10913803 leucine rich repeat containing 2
10737399 NA
10701240 NA
10809269 chemokine (C−X3−C motif) ligand 1
10743619 NA
10731512 suppressor of cytokine signaling 1
10761976 NA
10908861 lactate dehydrogenase A
10857641 NA
10826602 NA
10760594 LFNG O−fucosylpeptide 3−beta−N−acetylglucosaminyltransferase
10779818 nucleoside phosphorylase
10847736 four jointed box 1 (Drosophila)
10709691 PTPRF interacting protein, binding protein 2 (liprin beta 2)
10751218 growth associated protein 43
10744937 NA
10910406 sema domain, immunoglobulin domain (Ig), and GPI membrane anchor, (semaphorin) 7A
10893858 NA
10850066 NA
10822837 annexin A5
10856961 family with sequence similarity 136, member A
10873885 NA
10700614 NA
10910193 NA
10909639 FXYD domain−containing ion transport regulator 6
10753602 NA
10721682 NA
10718591 myeloid−associated differentiation marker
10904603 lymphocyte antigen 6 complex, locus H
10733056 interferon gamma inducible protein 47
10748853 BTB (POZ) domain containing 17
10713608 NA
10913553 cell division cycle 25 homolog A (S. pombe)
10737426 transmembrane protein 100
10867975 NA
10818708 coagulation factor III (thromboplastin, tissue factor)
10889923 EGL nine homolog 3 (C. elegans)
10912908 cytokine inducible SH2−containing protein
10749372 suppressor of cytokine signaling 3
10857610 basic helix−loop−helix family, member e40
10890024 nuclear factor of kappa light polypeptide gene enhancer in B−cells inhibitor, alpha
10726682 interferon induced transmembrane protein 3
10918586 GRINL1A complex locus
10832802 early growth response 2
10796411 metallothionein 1a
10922826 interleukin 1 receptor, type I
10831077 immediate early response 3
10791522 hydroxyprostaglandin dehydrogenase 15 (NAD)
10736697 chemokine (C−C motif) ligand 2
10797726 tropomyosin 3, gamma
10752839 ADAM metallopeptidase with thrombospondin type 1 motif, 1
10712171 interferon induced transmembrane protein 1
10781829 Kruppel−like factor 5
10842475 protein tyrosine phosphatase, non−receptor type 1
10901996 suppressor of cytokine signaling 2
10749612 actin, gamma 1
10940529 CCAAT/enhancer binding protein (C/EBP), delta
10748336 NA
10709261 NA
10866512 matrix Gla protein
10851952 UDP−Gal:betaGlcNAc beta 1,4−galactosyltransferase, polypeptide 5
10737129 peptidyl−tRNA hydrolase 2
10906373 copine VIII
10839419 EP300 interacting inhibitor of differentiation 1
10736792 NA
10903825 hyaluronan synthase 2
10893739 MOB1, Mps One Binder kinase activator−like 2A (yeast)
10839957 inosine triphosphatase (nucleoside triphosphate pyrophosphatase)
10897054 lymphocyte antigen 6 complex, locus E
10827906 tubulin, beta 5
10760290 neuronal pentraxin 2
10902708 Ras association (RalGDS/AF−6) domain family member 3
10750320 carbonyl reductase 1
10836945 cell division cycle associated 7
10792344 NA
10897543 H1 histone family, member 0
10881293 podoplanin
10700697 NA
10750310 carbonyl reductase 1
10940454 calmodulin 2
10912003 trophoblast glycoprotein
10713604 NA
10754785 NA
10938729 Cbp/p300−interacting transactivator with Glu/Asp−rich carboxy−terminal domain 1
10926740 tumor necrosis factor receptor superfamily, member 21
10700453 NA
10740408 stannin
10796149 6−phosphofructo−2−kinase/fructose−2,6−biphosphatase 3
10809399 metallothionein 2A
10937867 NA
10747948 glial fibrillary acidic protein
10805335 solute carrier family 14 (urea transporter), member 1
10751048 transgelin 3
10920860 myeloid differentiation primary response gene 88
10884917 glutathione S−transferase alpha 4
10936482 TIMP metallopeptidase inhibitor 1
10884924 glutathione S−transferase alpha 4
10707137 lactate dehydrogenase A
10843475 complement component 8, gamma polypeptide
10904511 activity−regulated cytoskeleton−associated protein
10700145 NA
10901166 angiopoietin−like 4
10821698 oncostatin M receptor
10852531 stathmin−like 3
10830624 CD24 molecule
10786436 choline dehydrogenase
10858967 tumor necrosis factor receptor superfamily, member 1a
10847735 proline rich 5 like

(***Figure 5C*** *continued.*)

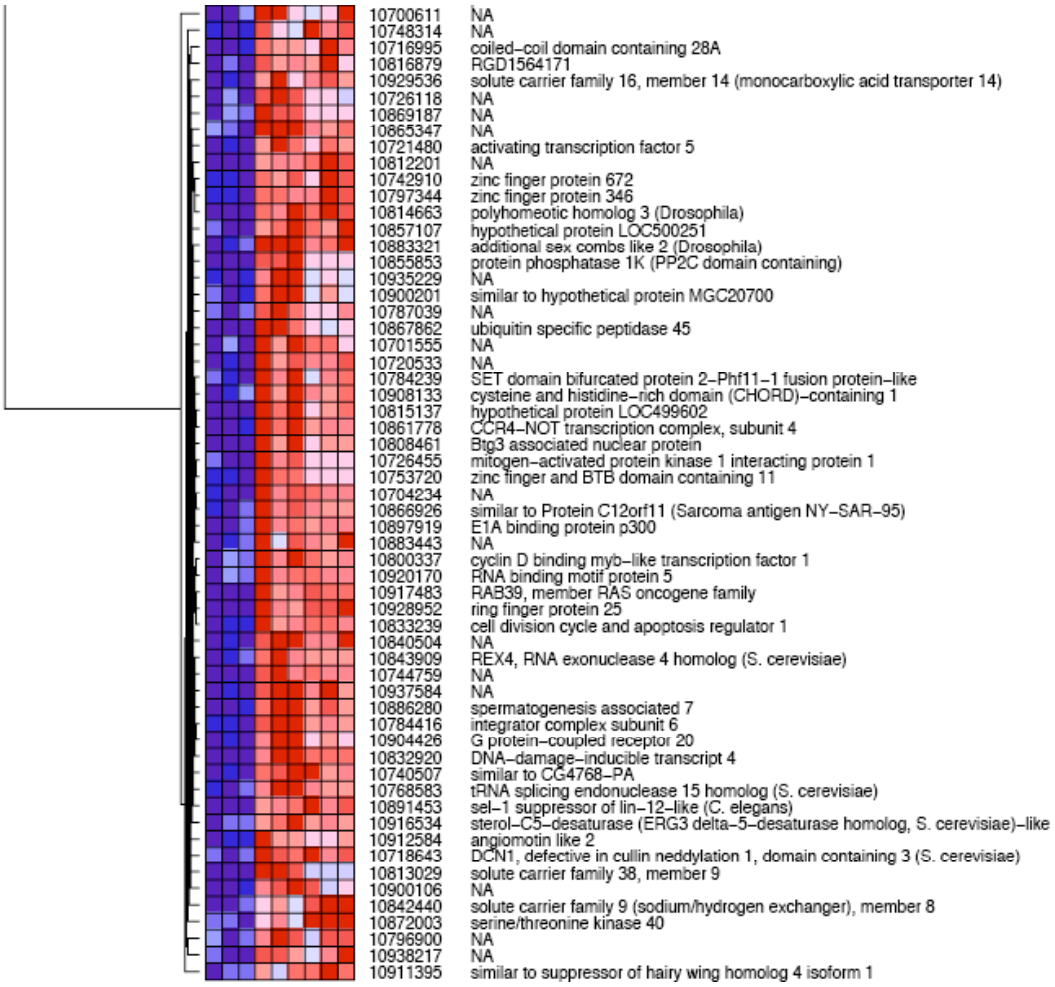

Figure 5: 1 hour IL-6 treatment alters gene expression in rat forebrain culture, in part via the pStat3 pathway. (A) Treatment with 50, 100, and 150 μM S31-201, a Stat3 inhibitor, results in a dose-dependent downregulation of pStat3 protein induced by 15 min exposure to IL-6 / IL-6R. **(B)** Cells were pre-treated with 100 μM S31-201 (or saline + DMSO) for 2 hrs; subsequently, 100 ng/mL IL-6 / IL-6R was added to media and cells were incubated for 1 hr prior to harvesting for microarray and ChIP-Seq studies. Control cultures were treated with saline + DMSO only. **(C)** Treatment with 100 ng/mL IL-6 and IL-6R for 1 hr upregulated 451 genes ≥ 2-fold (1386 genes ≥ 1.5-fold) and downregulated 104 genes ≤ -2-fold (792 genes ≤ -1.5-fold). The heatmap depicts the genes that were maximally blocked by Stat3 inhibitor treatment (red = increase relative to saline; blue = decrease). Of 1386 genes upregulated by IL-6 ≥ 1.5-fold, 98 genes (7.1%) were blocked by pStat3 inhibitor treatment at the 1.5-fold level. Of 792 genes downregulated ≤ -1.5-fold, 43 genes (5.43%) were blocked by pStat3 inhibitor treatment.

A

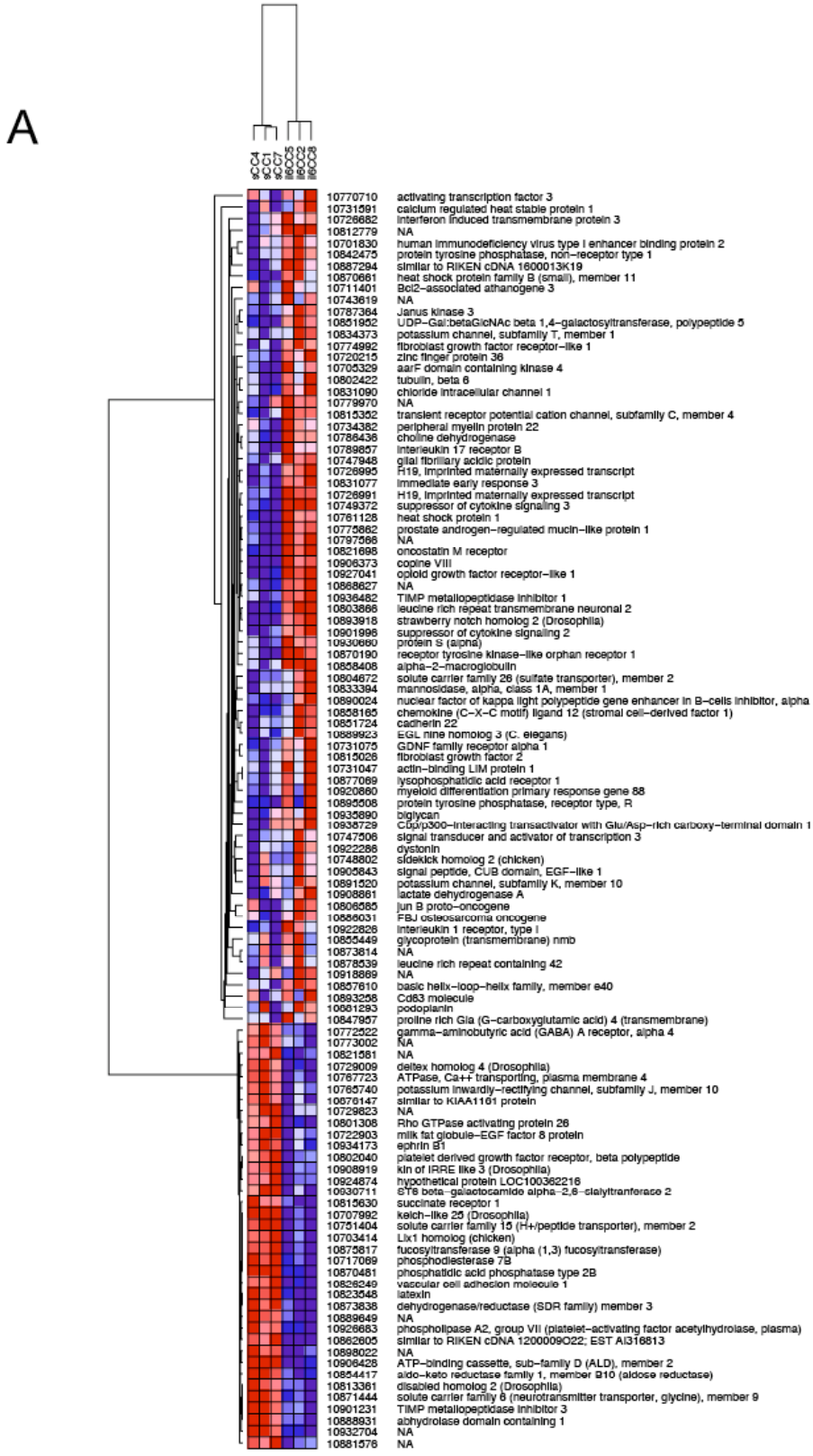
sCC4
sCC1
sCC7
sCC5
sCC2
sCC3
10770710 activating transcription factor 3
10731591 calcium regulated heat stable protein 1
10726682 interferon induced transmembrane protein 3
10812779 NA
10701830 human immunodeficiency virus type I enhancer binding protein 2
10842475 protein tyrosine phosphatase, non−receptor type 1
10887294 similar to RIKEN cDNA 1600013K19
10870661 heat shock protein family B (small), member 11
10711401 Bcl2−associated athanogene 3
10743619 NA
10787364 Janus kinase 3
10851952 UDP−Gal:betaGlcNAc beta 1,4−galactosyltransferase, polypeptide 5
10834373 potassium channel, subfamily T, member 1
10774992 fibroblast growth factor receptor−like 1
10720215 zinc finger protein 36
10705329 aarF domain containing kinase 4
10802422 tubulin, beta 6
10831090 chloride intracellular channel 1
10779970 NA
10815352 transient receptor potential cation channel, subfamily C, member 4
10734382 peripheral myelin protein 22
10786436 choline dehydrogenase
10789857 interleukin 17 receptor B
10747948 glial fibrillary acidic protein
10726995 H19, imprinted maternally expressed transcript
10831077 immediate early response 3
10726991 H19, imprinted maternally expressed transcript
10749372 suppressor of cytokine signaling 3
10761128 heat shock protein 1
10775862 prostate androgen−regulated mucin−like protein 1
10797586 NA
10821695 oncostatin M receptor
10906373 copine VIII
10927041 opioid growth factor receptor−like 1
10868627 NA
10936482 TIMP metallopeptidase inhibitor 1
10803866 leucine rich repeat transmembrane neuronal 2
10893918 strawberry notch homolog 2 (Drosophila)
10901996 suppressor of cytokine signaling 2
10930660 protein S (alpha)
10870190 receptor tyrosine kinase−like orphan receptor 1
10858406 alpha−2−macroglobulin
10804672 solute carrier family 26 (sulfate transporter), member 2
10833394 mannosidase, alpha, class 1A, member 1
10890024 nuclear factor of kappa light polypeptide gene enhancer in B−cells inhibitor, alpha
10858165 chemokine (C−X−C motif) ligand 12 (stromal cell−derived factor 1)
10851724 cadherin 22
10889923 EGL nine homolog 3 (C. elegans)
10731075 GDNF family receptor alpha 1
10815026 fibroblast growth factor 2
10731047 actin−binding LIM protein 1
10877089 lysophosphatidic acid receptor 1
10920860 myeloid differentiation primary response gene 88
10895508 protein tyrosine phosphatase, receptor type, R
10935890 biglycan
10938729 CBP/p300−interacting transactivator with Glu/Asp−rich carboxy−terminal domain 1
10747506 signal transducer and activator of transcription 3
10922286 dystonin
10748802 sidekick homolog 2 (chicken)
10905843 signal peptide, CUB domain, EGF−like 1
10891520 potassium channel, subfamily K, member 10
10908861 lactate dehydrogenase A
10806585 jun B proto−oncogene
10886031 FBJ osteosarcoma oncogene
10922826 interleukin 1 receptor, type I
10855449 glycoprotein (transmembrane) nmb
10873814 NA
10878539 leucine rich repeat containing 42
10918869 NA
10857610 basic helix−loop−helix family, member e40
10893258 Cd63 molecule
10661283 podoplanin
10847957 proline rich Gla (G−carboxyglutamic acid) 4 (transmembrane)
10772522 gamma−aminobutyric acid (GABA) A receptor, alpha 4
10773002 NA
10821581 NA
10729009 deltex homolog 4 (Drosophila)
10767723 ATPase, Ca++ transporting, plasma membrane 4
10765740 potassium inwardly−rectifying channel, subfamily J, member 10
10676147 similar to KIAA1161 protein
10729823 NA
10801308 Rho GTPase activating protein 26
10722903 milk fat globule−EGF factor 8 protein
10934173 ephrin B1
10802040 platelet derived growth factor receptor, beta polypeptide
10908919 kin of IRRE like 3 (Drosophila)
10924874 hypothetical protein LOC100362216
10930711 ST6 beta−galactosamide alpha−2,6−sialyltranferase 2
10815630 succinate receptor 1
10707992 kelch−like 25 (Drosophila)
10751404 solute carrier family 15 (H+/peptide transporter), member 2
10703414 Lix1 homolog (chicken)
10875817 fucosyltransferase 9 (alpha (1,3) fucosyltransferase)
10717069 phosphodiesterase 7B
10870481 phosphatidic acid phosphatase type 2B
10826249 vascular cell adhesion molecule 1
10823548 latexin
10873838 dehydrogenase/reductase (SDR family) member 3
10889649 NA
10926683 phospholipase A2, group VII (platelet−activating factor acetylhydrolase, plasma)
10862605 similar to RIKEN cDNA 1200009O22; EST AI316813
10898022 NA
10906428 ATP−binding cassette, sub−family D (ALD), member 2
10854417 aldo−keto reductase family 1, member B10 (aldose reductase)
10813361 disabled homolog 2 (Drosophila)
10871444 solute carrier family 6 (neurotransmitter transporter, glycine), member 9
10901231 TIMP metallopeptidase inhibitor 3
10888931 abhydrolase domain containing 1
10932704 NA
10881578 NA

B

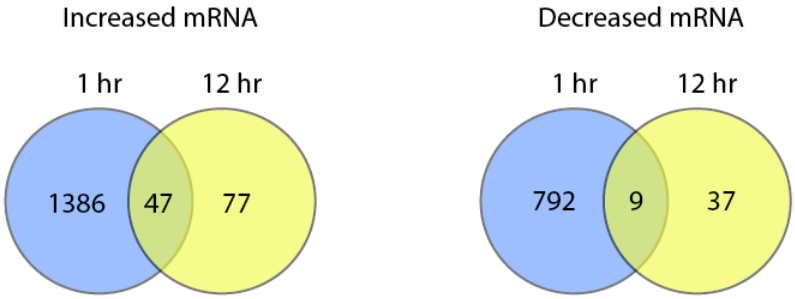

Figure 6: 12 hour IL-6 treatment alters gene expression in rat forebrain culture. (A) An additional set of cultures were treated for 12 hrs with IL-6 / IL-6R. Treatment for 12 hrs upregulated 77 genes ≥ 1.5-fold (366 ≥ 1.2-fold), while 37 genes were downregulated ≤ -1.5-fold (238 genes ≤ -1.2-fold). The heatmap depicts all genes changed ≥ 1.5-fold (red = increase relative to saline; blue = decrease). **(B)** Of the 77 genes upregulated ≥ 1.5-fold by 12 hr IL-6 treatment, 47 (61%) were also upregulated at 1 hr at the 1.5-fold level. Of the 37 genes downregulated ≤ -1.5-fold, 9 (24.3%) were also downregulated at 1 hr.

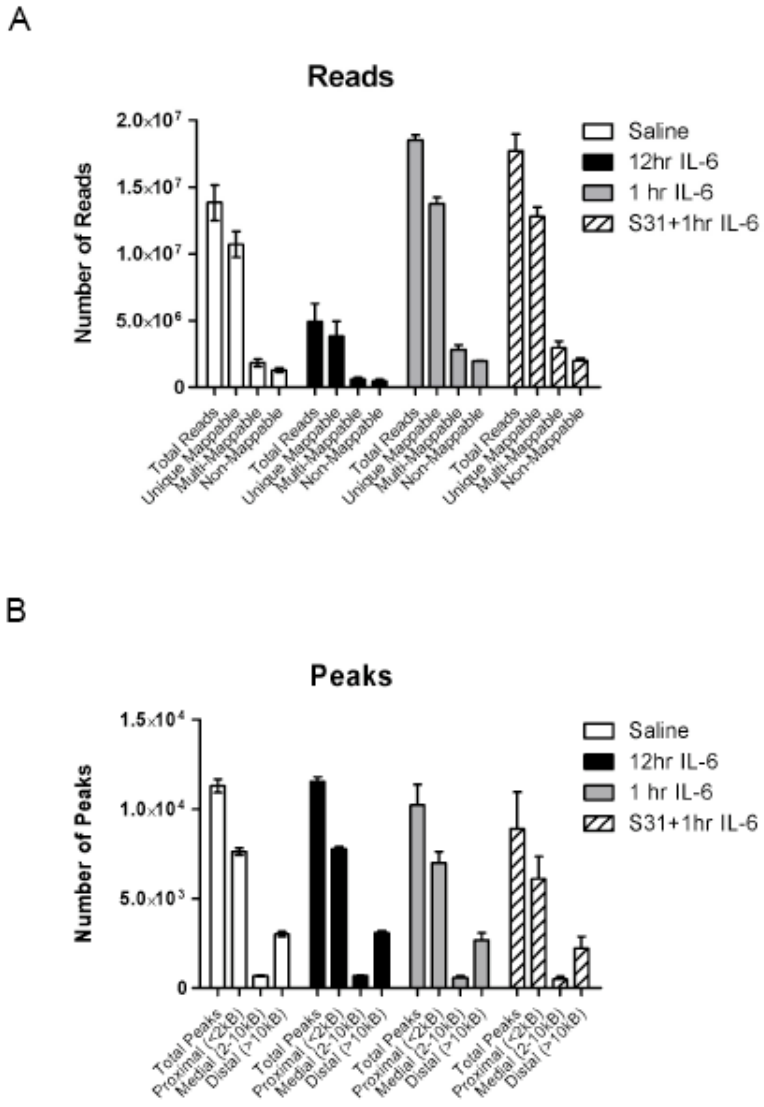

Figure 7: H3K4me3 ChIP-Seq of rat forebrain culture yields a high percentage of uniquely mappable reads and proximal peaks.
(A) A high percentage (72-78%) of reads are uniquely mappable to rat genome for all 4 treatment groups (Saline, 12 hr IL-6, 1 hr IL-6, and 1 hr IL-6 + S31-201). A smaller percentage (13-17%) map to multiple locations in rat genome and 9-11% were not mappable. **(B)** The majority of peaks (68-69%) are proximal (< 2 kb) to annotated transcription start sites (TSS); additionally, 6% of peaks are medial (2-10 kb) and 24-27% are distal (> 10 kb) to TSS.

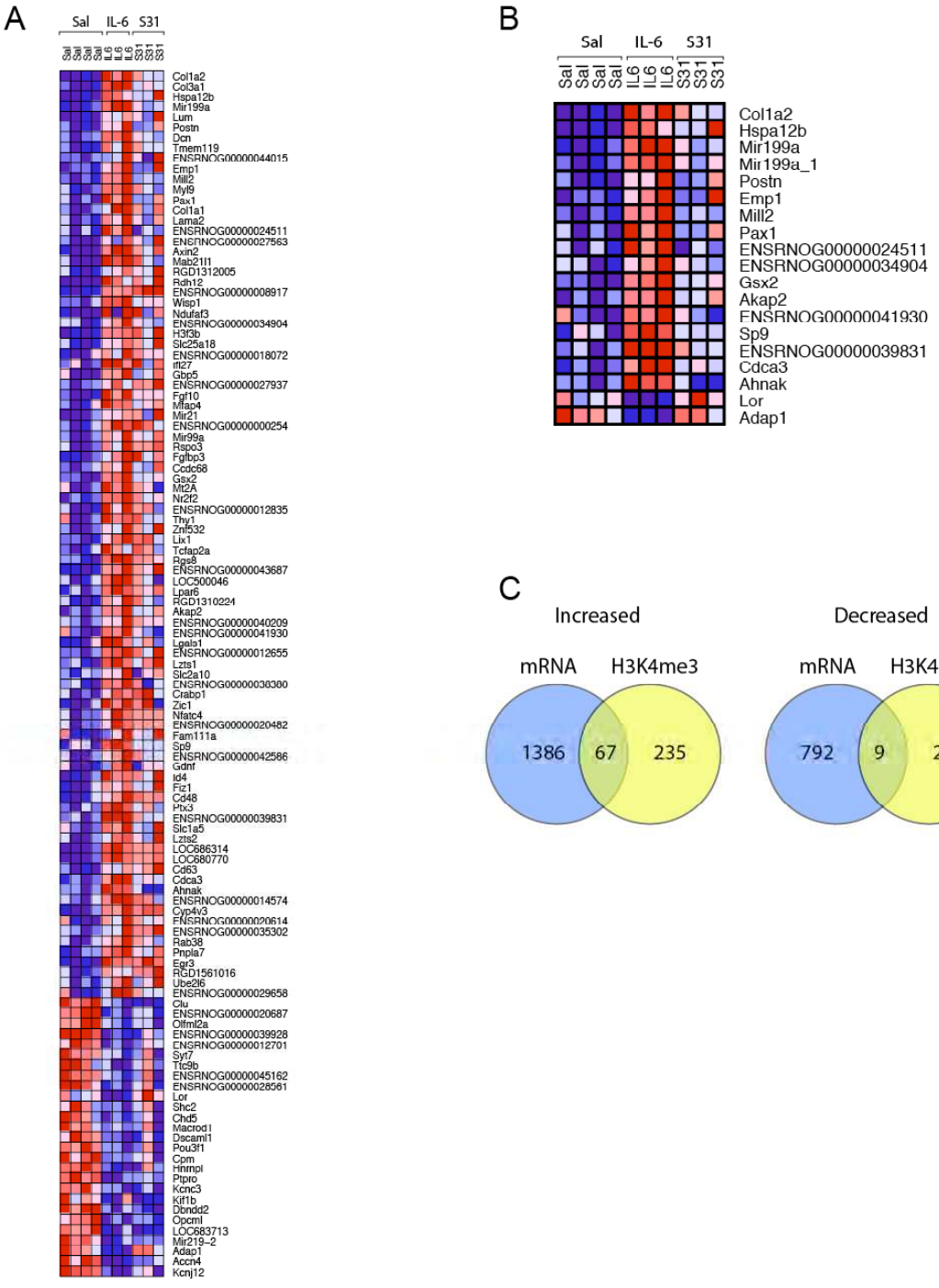
A
Sal
IL-6
S31
Sal Sal Sal Sal IL6 IL6 IL6 S31 S31 S31
Col1a2
Col3a1
Hspa12b
Mir199a
Lum
Postn
Dcn
Tmem119
ENSRNOG00000044015
Emp1
Mill2
Myl9
Pax1
Col1a1
Lama2
ENSRNOG00000024511
ENSRNOG00000027563
Axin2
Mab21l1
RGD1312005
Rdh12
ENSRNOG00000008917
Wisp1
Ndufaf3
ENSRNOG00000034904
H3f3b
Slc25a18
ENSRNOG00000018072
Ifit27
Gbp5
ENSRNOG00000027937
Fgf10
Mfap4
Mir21
ENSRNOG00000000254
Mir99a
Rspo3
Fgfbp3
Ccdc68
Gsx2
Mt2A
Nr2f2
ENSRNOG00000012835
Thy1
Znf532
Lix1
Tcfap2a
Rgs8
ENSRNOG00000043687
LOC500046
Lpar6
RGD1310224
Akap2
ENSRNOG00000040209
ENSRNOG00000041930
Lgals1
ENSRNOG00000012655
Lzts1
Slc2a10
ENSRNOG00000030300
Crabp1
Zic1
Nfatc4
ENSRNOG00000020482
Fam111a
Sp9
ENSRNOG00000042586
Gdnf
Id4
Fiz1
Cd48
Ptx3
ENSRNOG00000039831
Slc1a5
Lzts2
LOC686314
LOC680770
Cd63
Cdca3
Ahnak
ENSRNOG00000014574
Cyp4v3
ENSRNOG00000020614
ENSRNOG00000035302
Rab38
Pnpla7
Egr3
RGD1561016
Ube2l6
ENSRNOG00000029658
Clu
ENSRNOG00000020687
Olfml2a
ENSRNOG00000039928
ENSRNOG00000012701
Syt7
Ttc9b
ENSRNOG00000045162
ENSRNOG00000028561
Lor
Shc2
Chd5
Macrod1
Dscaml1
Pou3f1
Cpm
Hnrnpl
Ptpro
Kcnc3
Kif1b
Dbndd2
Opcml
LOC683713
Mir219-2
Adap1
Accn4
Kcnj12
B
Sal
IL-6
S31
Sal Sal Sal Sal IL6 IL6 IL6 S31 S31 S31
Col1a2
Hspa12b
Mir199a
Mir199a_1
Postn
Emp1
Mill2
Pax1
ENSRNOG00000024511
ENSRNOG00000034904
Gsx2
Akap2
ENSRNOG00000041930
Sp9
ENSRNOG00000039831
Cdca3
Ahnak
Lor
Adap1
C
Increased
mRNA
H3K4me3
1386
67
235
Decreased
mRNA
H3K4me3
792
9
259

Figure 8: 1 hour IL-6 treatment alters H3K4me3 levels at many gene transcription start sites in rat forebrain culture, in part via the pStat3 pathway. (A) Following 1 hr treatment with IL-6, 90 genes demonstrated a ≥ 2-fold increase in H3K4me3 levels within 500 bp of gene TSS (235 ≥ 1.5-fold) and 27 genes decreased ≤ -2-fold (259 ≤ -1.5-fold). The heatmap shows genes with ≥ 2-fold change in H3K4me3 (red = increase relative to saline; blue = decrease). **(B)** Co-treatment with 100 μM of the Stat3 inhibitor, S31-201, attenuated IL-6-induced H3K4me3 changes at 17/91 (18.7%) genes increased ≥ 2-fold and 2/27 (7.4%) of genes ≤ -2-fold. The heatmap depicts the genes whose IL-6-induced expression change was maximally blocked by S31-201. **(C)** A subset of genes with altered H3K4me3 have corresponding changes in mRNA level. Of the 235 genes with a ≥ 1.5-fold increase in H3K4me3, 67 have increased mRNA ≥ 1.5-fold at 1 hr. Of the 259 genes with ≤ -1.5-fold decrease in H3K4me3, 9 have decreased mRNA.

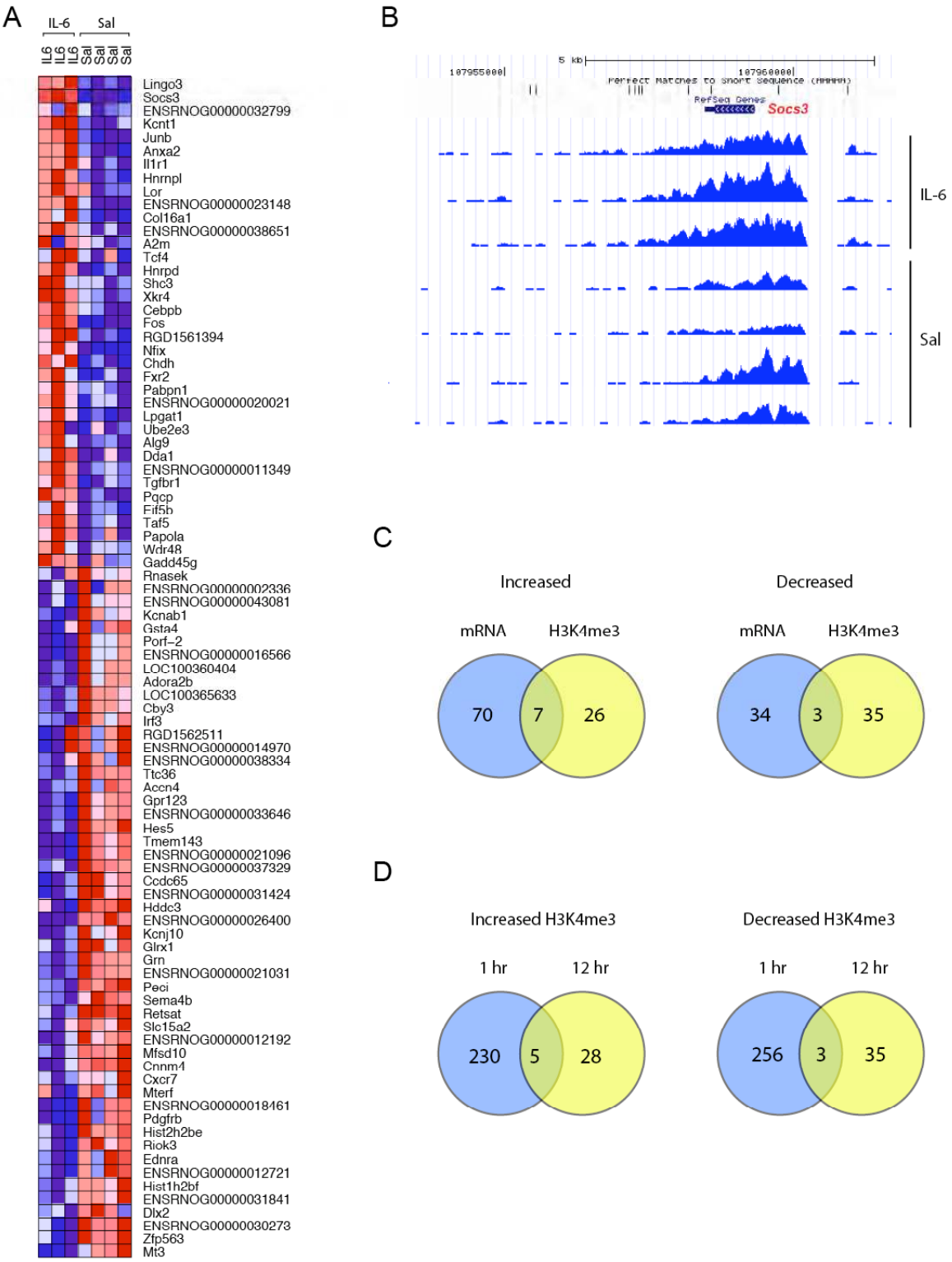
A
IL-6
Sal
IL6
IL6
IL6
Sal
Sal
Sal
Sal
Lingo3
Socs3
ENSRNOG00000032799
Kcnt1
Junb
Anxa2
Il1r1
Hnrnpl
Lor
ENSRNOG00000023148
Col16a1
ENSRNOG00000038651
A2m
Tcf4
Hnrpd
Shc3
Xkr4
Cebpb
Fos
RGD1561394
Nfix
Chdh
Fxr2
Pabpn1
ENSRNOG00000020021
Lpgat1
Ube2e3
Alg9
Dda1
ENSRNOG00000011349
Tgfbr1
Pqcp
Eif5b
Taf5
Papola
Wdr48
Gadd45g
Rnasek
ENSRNOG00000002336
ENSRNOG00000043081
Kcnab1
Gsta4
Porf-2
ENSRNOG00000016566
LOC100360404
Adora2b
LOC100365633
Cby3
Irf3
RGD1562511
ENSRNOG00000014970
ENSRNOG00000038334
Ttc36
Accn4
Gpr123
ENSRNOG00000033646
Hes5
Tmem143
ENSRNOG00000021096
ENSRNOG00000037329
Ccdc65
ENSRNOG00000031424
Hddc3
ENSRNOG00000026400
Kcnj10
Glrx1
Grn
ENSRNOG00000021031
Peci
Sema4b
Retsat
Slc15a2
ENSRNOG00000012192
Mfsd10
Cnnm4
Cxcr7
Mterf
ENSRNOG00000018461
Pdgfrb
Hist2h2be
Riok3
Ednra
ENSRNOG00000012721
Hist1h2bf
ENSRNOG00000031841
Dlx2
ENSRNOG00000030273
Zfp563
Mt3
B
5 kb
107955000
107960000
Perfect matches to short sequence (NNNNN)
RefSeq Genes
Socs3
IL-6
Sal
C
Increased
mRNA
H3K4me3
70
7
26
Decreased
mRNA
H3K4me3
34
3
35
D
Increased H3K4me3
1 hr
12 hr
230
5
28
Decreased H3K4me3
1 hr
12 hr
256
3
35

Figure 9: 12 hour IL-6 treatment alters H3K4me3 levels at many gene transcription start sites in rat forebrain culture.
(A) Following 12 hrs of IL-6 treatment, 33 genes demonstrated increased H3K4me3 levels ≥ 1.5-fold (149 ≥ 1.2-fold); 38 genes showed decreased levels ≤ -1.5-fold (60 ≤ -1.2-fold). The heatmap illustrates all IL-6 induced histone methylation changes ≥ 1.5-fold (red = increase relative to saline; blue = decrease). **(B)** The H3K4me3 profile from the UCSC genome browser for the *Socs3* gene, which demonstrated the most robust and significant increase in methylation following 12 hrs of IL-6 treatment (fold-change = 3.2; $p = 1.94^{-20}$). Note the atypical pattern of H3K4me3, which encompasses the entire *Socs3* gene and surrounding region. **(C)** A subset of genes with altered H3K4me3 have corresponding changes in mRNA levels. Of the 33 genes with H3K4me3 increased ≥ 1.5-fold, 7 also have increased mRNA ≥ 1.5-fold, while 3/38 genes with ≤ -1.5-fold H3K4me3 had decreased mRNA. **(D)** Of the genes with increased H3K4me3 ≥ 1.5-fold at 12 hrs, 5 were also increased at 1 hr; of the genes with decreased H3K4me3 ≤ -1.5-fold, 3 were also decreased at 1 hr.

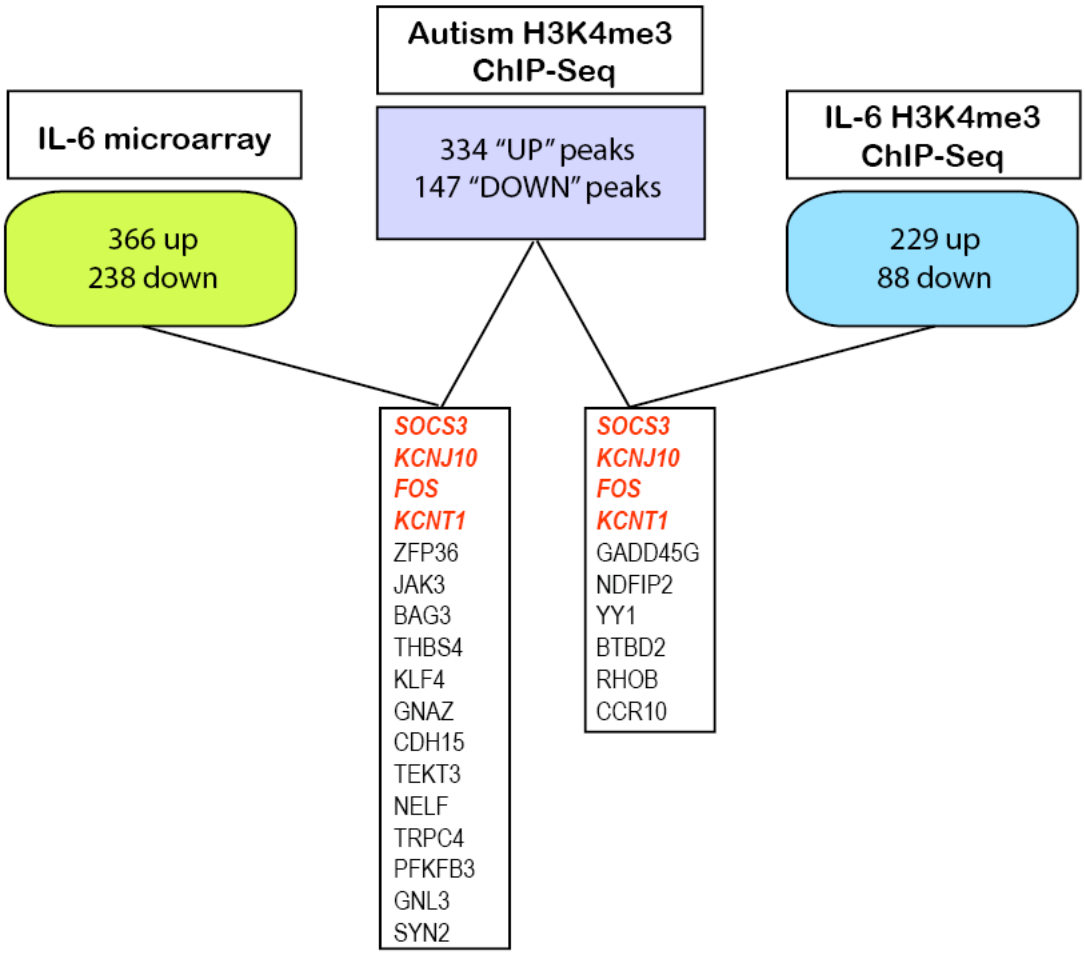

Figure 10: Genes which show altered mRNA and H3K4me3 following IL-6 treatment have altered H3K4me3 in a subset of autism cases.
The genes marked in red demonstrated both altered H3K4me3 and mRNA in cell culture following IL-6 treatment.

Chapter III:

Maternal Immune Activation Induces Subtle Alterations in Histone H3 Lysine 4 Trimethylation in Fetal and Adult Mouse Brain

Introduction

Maternal infection during pregnancy with a variety of infectious agents—including virus (influenza, rubella, herpes simplex virus), bacteria, and parasite (toxoplasma)—has been shown to increase risk of both schizophrenia and autism in offspring [106]. Based on this observation, Fatemi and colleagues developed the maternal immune activation (MIA) mouse model, in which they subjected pregnant rats to influenza infection and examined cellular changes in the brains of offspring [114, 115]. They found altered expression of synaptosome-associated protein 25 (SNAP25) and a reduction of reelin-immunoreactive cells, in addition to decreased cortical and hippocampal thickness, in postnatal animals, suggesting a neuronal migration deficit. Since its initial development, this model has been widely utilized and has been found to recapitulate a variety of molecular, cellular, and behavioral abnormalities observed in both schizophrenia and autism.

In addition to pathogens such as influenza, non-infectious agents of immune-stimulation have been employed to induce immune activation in pregnant rodents. These include the viral mimic and toll-like receptor 3 (TLR3) activator, polyriboinosinic-polyribocytidilic acid, or poly(I:C), as well as lipopolysaccaride (LPS), a bacterial endotoxin that signals via TLR4 [116]. Injection of these substances into mice or rats induces fever and elevated serum cytokines, closely mimicking the effects of actual infection. That inflammation in the absence of a pathogen is capable of producing behavioral

deficits and neuropathology in offspring suggests that it is the maternal immune response, rather than the infectious agent itself, that impacts fetal brain development. This claim has been substantiated by studies demonstrating no detectable virus in fetal brain following maternal infection with influenza [117]. Cytokines from maternal circulation have been shown to cross the placenta and gain access to the fetus, including the brain, and thus represent a means by which immune activation may impact neurodevelopment [118-120].

While it is not possible to induce psychosis in a rodent in the truest sense of the word, various behavioral tests can be used to model aspects of symptoms observed in schizophrenia and autism. Behavioral abnormalities observed in the offspring in the MIA model include impaired sensory motor-gating, including pre-pulse inhibition (PPI) and latent inhibition (LI), working memory deficits, increased anxiety, decreased social interaction, and increased sensitivity to the psychomimetics, amphetamine and MK-801 [83, 119, 121-126]. Additionally, some of these behaviors, including PPI, can be rescued by the administration of antipsychotic drugs [123, 126]. Importantly, the majority of these behaviors do not appear until the adolescent period, mirroring the timing of disease-onset typical in schizophrenia.

In addition to behavioral changes, cellular and molecular alterations have been noted in the brains of rodents prenatally exposed to inflammation. These include pyramidal cell atrophy, decreased Purkinje cells in cerebellum,

increased $GABA_A$ receptor expression in hippocampus, decreased reelin- and parvalbumin-immunoreactive cells in cortex and hippocampus, altered dopamine metabolism, increased microglia, and increased GFAP, all of which reflect the neuropathology of schizophrenia and autism [119, 127-131]. Structural changes, including ventricular enlargement and decreased thickness of the cortex and hippocampus, have also been reported ([114]. The particular alterations induced differ depending upon the specific MIA paradigm, including immune-activating agent employed and the embryonic day on which it is administered.

Despite the large number of studies describing abnormalities in rodent brain following exposure to a prenatal immune stimulus, the precise molecular mechanisms by which pro-inflammatory cytokines mediate their effects on the developing CNS remain unclear. Moreover, it has not been shown that MIA can reproduce chromatin modifications in brain observed in neuropsychiatric disorders such as schizophrenia and autism. In the present study, I sought to determine whether prenatal exposure to an immune stimulus in mice could alter H3K4me3 in brain. I hypothesize that exposure to inflammation *in utero* alters brain development, in part, via chromatin modifications such as H3K4me3 and that some of these changes may be detectable in mature brain.

Materials and Methods

Animals: C57BL/6J mice 10-12 weeks of age were obtained from Jackson Laboratories (Bar Harbor, ME) and housed in a temperature and humidity-controlled environment and maintained on a 12 hour light-dark cycle, with food and water provided ad libitum. Mice were allowed to acclimate for at least one week prior to breeding. Mice were mated overnight and the presence of a vaginal plug constituted embryonic day 0.5 (E0.5).

Poly(I:C) injections: On E12.5 or E17.5, pregnant females received an injection of 5 mg/kg poly(I:C) (potassium salt; Sigma, St. Louis, MO) freshly reconstituted in sterile 0.9% sodium chloride via the tail vein route under mild physical constraint. The injection volume was 5 ml/kg. Control females received an injection of saline solution. Pups were weaned on postnatal day 21 and housed by gender.

Maternal Serum Cytokine ELISA: A subset of females (n = 3 per group) was sacrificed three hours following poly(I:C) or saline injection and blood was collected via cardiac puncture. Blood was allowed to clot at room temperature for 1 hour, centrifuged at 12,000 rpm at 4°C, and the serum aliquoted and stored at -20°C until the cytokine analysis was performed.

Levels of four cytokines (interleukin-6 [IL-6], tumor necrosis factor alpha [TNFα], interleukin 1 beta, [IL-1β], and interferon gamma [IFNγ]) were measured in maternal serum using a SearchLight® Proteome Array (Aushon BioSystems; Billerica, MA), a quantitative multiplexed sandwich enzyme-linked immunosorbent assay (ELISA) containing capture antibodies spotted on the bottom of a 96-well polystyrene microtiter plate. The bound proteins were detected by the subsequent addition of a biotinylated detection antibody, streptavidin-horseradish peroxidase (HRP), and chemiluminescent substrate; chemiluminescent signal was measured with the SearchLight Imaging System's cooled charge-coupled device (CCD) camera.

Fetal Brain Cytokine ELISA: Another group of pregnant females were injected with poly(I:C) at E12.5 or E17.5, sacrificed 3 or 6 hours later, the fetal pups removed, and the brains dissected and frozen at -80°C. Fetal brain tissue was prepared for cytokine ELISA by dounce-homogenizing 3 whole brains per litter in 400 µl 0.1 M phosphate-buffered saline (PBS), pH 7.4, containing 24 µl/ml Complete Protease Inhibitor Cocktail (Roche Diagnostics; Indianapolis, IN) for 1 min on ice. Tissue homogenate was transferred to a 1.5 ml tube, centrifuged for 5 min at 13,000 rpm at 4°C, and the supernatant transferred to a new tube. IL-6 protein was measured as described above.

Behavior: Working memory was assessed in 10-week old offspring employing the T-maze. Mice tend to alternate between the two arms of the maze because they prefer to explore the more "novel" environment, a behavior known as spontaneous alternation, and this behavior is dependent upon an intact working memory [132]. The apparatus was constructed from white plexiglass and consisted of a "home" arm and a perpendicular arm. The mouse was placed in the home arm and allowed to choose between the left and right arms, at which point the opposite arm was blocked off, forcing the mouse to return to the beginning; the blocked arm was then opened and the mouse was then allowed to make another choice. Mice were given 15 choices for a total of 14 possible alternations; the same test was administered on two consecutive days. A total of 78 10-week old E12.5 offspring were tested (saline n = 51, 33♂ and 18♀ [9 litters]; poly(I:C) n = 27, 10♂ and 17♀ [8 litters]) and 62 E17.5 offspring were tested (saline n = 28, 16♂ and 17♀ [10 litters]; poly(I:C) n = 34, 17♂ and 12♀ [12 litters]).

Microarray: Cortex was dissected from 10 fresh frozen E17.5 brains of mice sacrificed at 12 weeks of age (poly(I:C) = 5, 3♂ and 2♀; saline = 5, 3♂ and 2♀) and six E12.5 brains (poly(I:C) = 3, 2♂ and 1♀; saline = 3, 2♂ and 1♀) and the RNA extracted and processed for Affymetrix GeneChIP Mouse Gene 1.0 ST arrays. Total RNA was extracted employing the RNeasy Lipid Tissue

Mini Kit (Qiagen; Valencia, CA). Following dissection, right cortex from each mouse was frozen at -80°C, dounced in 1 mL QIAzol Lysis Reagent and RNA isolated according to the manufacturer's instructions. RNA integrity (RIN) assessed with a 2100 Bioanalyzer (Agilent; Santa Clara, CA). Labeled, fragmented single-stranded cDNA was prepared and submitted to the Genomics Core Facility for hybridization to Affymetrix GeneChIP Mouse Gene 1.0 ST arrays, washing, and scanning as described in the Materials and Methods in Chapter II.

Microarray data analysis: Quality of microarray data was assessed with the Bioconductor package, arrayQualityMetrics, and treatment groups compared with MACE as described in Chapter II.

H3K4me3 ChIP-Seq: Nuclei were extracted from cortex of 6 twelve-week old E17.5 poly(I:C) offspring and 6 saline offspring; mice were derived from 6 independent litters with n = 3 males and 3 females per group. Whole cortex was dissected, frozen at -80°C, dounced in 5 mL Lysis Buffer, and nuclei collected by ultracentrifugation as previously described. Nuclei were resuspended in 200 µl Dounce Buffer for NChIP and processed for H3K4me3 ChIP, library preparation, and deep sequencing as described for rat forebrain culture. In addition, three E12.5 fetal poly(I:C) brain samples and three saline

samples—collected 3 hrs following injection—were processed for H3K4me3 ChIP-Seq.

ChIP-Seq data analysis: As described in Chapter II, raw sequence reads were aligned to mouse genome (version mm9) with Bowtie, the libraries normalized for lowest number of unique reads, and peaks called by MACS. Data were uploaded to the UCSC Genome Browser for visualization and differences in H3K4me3 levels between poly(I:C) and saline measured with DESeq.

Results

Poly(I:C) upregulates IL-6 protein in maternal serum:

In order to determine whether poly(I:C) injections were capable of inducing a measurable immune response in pregnant mice, levels of four cytokines (IL-6, TNFα, IL-1β, and IFNγ) were determined in maternal serum 3 hrs after treatment. As shown in **Fig. 1**, IL-6 protein was upregulated in poly(I:C)-treated mice at both the E12.5 (mean poly(I:C) = 11,426.7$\pm$5425 pg/mL; mean saline = 119.6$\pm$15.9; p = 0.2) and E17.5 time-points (mean poly(I:C) = 3528.9$\pm$426.1 pg/mL; mean saline = 4.2$\pm$1.5; p = 0.002). An outlier in the E12.5 poly(I:C) group with 22,202.4 pg/mL IL-6 precluded detection of statistical significance, even when a non-parametric test was

employed. Additionally, levels of TNFα protein were significantly upregulated in poly(I:C) mice at E12.5 (mean poly(I:C) = 54.2±12.4 pg/mL; mean saline = 2.5±0.44; p = 0.01), but not at E17.5 (mean poly(I:C) = 31.1±9.9 pg/mL; mean saline = 16.9±15.8; p = 0.049). IFNγ and IL-1β were not significantly altered at either time-point by poly(I:C).

It is important to note that, for some cytokines, some mice showed highly variable responses to the poly(I:C) injections. For example, one of the E12.5 poly(I:C) mice showed a dramatic upregulation of IFNγ protein (1597.1 pg/mL) while the other two in this group had levels of 64.2 and 0.8 pg/mL. Additionally, though IL-6 was robustly increased in all poly(I:C)-treated mice, one of the E12.5 mice had much higher levels—22,022 pg/mL versus 7128.5 and 4949.2 pg/mL. In one instance, a saline injection appeared to upregulate a cytokine: for TNFα, two of the three E17.5 saline mice had almost undetectable levels while the third had 48.6 pg/mL (the three poly(I:C) treated mice all had between 20.0 and 50.8 pg/mL). It is not known why saline injection in this particular mouse resulted in upregulation of a pro-inflammatory cytokine, but it could be due to stress induced during tail vein injection, since stress has been shown to result in upregulation of TNFα, IL-1β, and corticosterone in rat [133]. These findings emphasize the variable nature of this mouse model. Ideally, only litters obtained from those poly(I:C) mice showing robust upregulation of cytokines would be included in future studies. However, it is not possible to sample cytokine levels in the pregnant

mice through non-invasive means, and it is critical that stressful procedures be kept to a minimum as this could exert additional effects on fetal brain development. In the future, measurement of maternal temperature with Mini Mitter E-Mitters—implanted intraperitoneally or subcutaneously prior to breeding—could potentially provide a suitable proxy for measurement of cytokine levels.

Poly(I:C) upregulates IL-6 protein in a subset of fetal brains:

In order to determine whether maternal immune activation in pregnant mice results in increased levels of proinflammatory cytokines in fetal brain, we also measured IL-6 protein in fetal brains obtained from pregnant females sacrificed 3 or 6 hrs following injection. Of four E12.5 litters sampled, two had highly upregulated levels of IL-6 (720.0 and 343.5 pg/mL), one had moderately increased levels (43.1 pg/mL), and the fourth (9.8 pg/mL) was not increased relative to saline (mean 5.5±0 pg/mL) (**Fig. 2**). The E12.5 poly(I:C) mean (279.1 pg/mL) was significantly higher when compared to saline (5.5 pg/mL) employing a Mann-Whitney U test ($p = 0.0436$). Of three E17.5 litters sampled, one had increased IL-6 (163.4 pg/mL) relative to saline (mean = 29.6±7.3). No differences in IL-6 levels were observed at the 6 hr time-point in either E12.5 or E17.5 litters.

The variability in IL-6 levels in fetal brains following maternal poly(I:C) injections could be due to several factors. First, differences in maternal

immune system and/or efficacy of the injection itself could result in differences in strength of immune activation between mice, and, subsequently, differing levels of cytokines that reach the fetal brain. Second, the IL-6 levels may not have peaked in fetal brain during the two time-windows selected for cytokine analysis in some mice.

Adult E17.5 poly(I:C) offspring demonstrate impaired working memory:

To assess the effects of prenatal exposure to inflammation on brain function in the adult offspring, working memory was assessed in 10 week old mice from E12.5 and E17.5 litters employing the T-maze. As shown in **Fig. 3**, the E17.5 poly(I:C) offspring demonstrated significantly fewer alternations on both days one and two of testing (Day 1: mean E17.5 poly(I:C) = 6.3±0.4, mean E17.5 saline = 8.2±0.5, $p = 0.002$; Day 2: mean E17.5 poly(I:C) = 7.5±0.4, mean E17.5 saline = 8.9, $p = 0.008$). Though the average percent of alterations in wildtype mice varies, a mean score of 8.9 alternations on day 2 of testing is consistent with what we have previously observed in our laboratory. Additionally, it is important to note that fewer E17.5 poly(I:C) offspring performed above "chance level" (7/14 alternations, or 50%) compared to saline: only 35.3% had a score > 7 on day 1 and 55.9% on day 2, versus 64.3% and 75.0% of saline mice. Moreover, those poly(I:C) mice with a score > 7 on day 2, fewer had a score of 9 or 10 (63.2% and 26.3%) compared to saline (95.2% and 57.1%).

In contrast to the E17.5 offspring, there was no significant difference between E12.5 poly(I:C) and saline mice on either day of testing (Day 1: mean E12.5 poly(I:C) = 6.8±0.05, mean E12.5 saline = 7.5±0.3, p = 0.178; Day 2: mean E12.5 poly(I:C) = 7.9±0.2, mean E12.5 saline = 8.3±0.3, p = 0.393). It should be pointed out that the E12.5 saline mice had somewhat lower numbers of alternations compared to E17.5 saline mice: 7.5 on day 1 (versus 8.2) and 8.3 on day 2 (versus 8.9), and, though this difference is not significant (p = 0.25; p = 0.24), it may have precluded detection of significantly impaired performance in the E12.5 mice. Interestingly, the pregnant mice treated with saline at E12.5 had slightly elevated IL-6 protein in serum (mean = 119.6±15.9) compared to the E17.5 saline group (mean = 4.2±1.5)—it is possible the E12.5 mothers had increased IL-6 due to an increased sensitivity of the immune system to stress earlier in gestation, and that this had a modest effect on the offspring.

Adult E12.5 and E17.5 poly(I:C) offspring display few mRNA changes in cortex:

Next, in order to assess whether prenatal exposure to inflammation resulted in lasting alterations in gene expression in brains of adult offspring, we employed microarrays to measure mRNAs in cortex of E12.5 and E17.5 offspring (**Fig. 4**). Only small changes were observed in poly(I:C) mice

relative to saline, the most significant of which are depicted in the heatmaps in **Fig. 4A** and **Fig. 4B**.

Some genes of interest in the E12.5 poly(I:C) mice include interleukin-1 receptor-associated kinase 3 (*Irak3*), which was increased 1.34-fold ($p = 0.039$); this gene was also found to be increased 1.49-fold following 1 hr IL-6 treatment (see Chapter II). Additionally, interleukin 17 receptor E (*Il17re*) demonstrated a small decrease (-1.31-fold; $p = 0.012$) at this time point. And in the E17.5 poly(I:C) offspring, heat shock protein 1 was modestly increased (*Hspd1*; 1.32-fold; $p = 0.20$). However, given the low signals on microarray (generally < 100) and the marginal significance (p-value range mostly 0.01 to 0.049 prior to correction for multiple comparison), it is unclear whether these represent real changes.

Adult E17.5 poly(I:C) offspring display subtle alterations in H3K4me3 in cortex:

To determine whether prenatal exposure to inflammation was capable of inducing long-lasting changes in H3K4me3 in brain, H3K4me3 ChIP-Seq was performed on cortex of 12 week old E17.5 poly(I:C) and saline mice. We chose to focus on the E17.5 offspring, because these mice displayed significantly impaired working memory as assessed by T-maze.

Alignment of raw reads to mouse genome revealed total library sizes ranging from 2.4×10^6 to 23.0×10^6 total reads (**Fig. 5**). A high percentage of

total reads were uniquely mappable to mouse genome (87% for both saline and poly(I:C) mice), while smaller percentages were multi-mappable or non-mappable (8.5% and 4.0%, respectively) (**Fig. 5A**). Following normalization to the lowest number of uniquely-mappable reads (1.94×10^6), analysis with MACS determined similar numbers of total peaks in poly(I:C) and saline mice (14,907 and 14,847, respectively), a high percentage of which were proximal to annotated TSS (79% in both treatment groups), demonstrating the H3K4me3 immunoprecipitation worked efficiently (**Fig. 5B**).

Comparison of H3K4me3 levels (TSS to +500 bp) in poly(I:C) cortex to saline revealed a small number of subtle fold-changes (**Fig. 6**). In total, 17 genes demonstrated increased H3K4me3 levels between 1.25 and 1.61-fold, while 6 genes were decreased between -1.26 and -2.47-fold. While there were several potentially interesting genes affected—such as *disrupted in schizophrenia 1* (*Disc1*), which was decreased -1.34-fold in the poly(I:C) mice—these results must be interpreted with caution due to the small fold-changes and marginally significant p-values, which were all in the 0.01 to 0.049 range. The variability in mouse-to-mouse tag number for these genes, which can be observed in the heatmap in **Fig. 6**, may have precluded detection of higher significance.

Comparison of poly(I:C) versus saline according to gender revealed more differences in H3K4me3 than the combined analysis. In the male mice, 3 genes demonstrated H3K4me3 increases ≥ 2-fold (109 ≥ 1.5-fold) and 14

genes were decreased ≤ -2-fold (58 ≤ -1.5-fold) (**Fig. 7A**). Several of the genes which showed altered H3K4me3 in the combined gender analysis—including nuclear receptor subfamily 2, group C, member 2 (*Nr2c2*), Sp1 transcription factor (*Sp1*), fragile X mental retardation gene 1, autosomal homolog (*Fxr1*), and *Disc1*—were also found to be altered in male mice. Furthermore, fold-changes of these genes were more pronounced in the males, suggesting that pooled gender analysis may have diluted sex-specific effects of prenatal inflammation on H3K4me3. This is consistent with literature demonstrating gender differences in schizophrenia. For example, one study reported decreased levels of H3K4me3 at the *GAD1* gene in female patients, but not in males [86].

In the female mice, 16 genes were increased ≥ 2-fold (78 ≥ 1.5-fold) in the poly(I:C) offspring and 3 genes were decreased ≤ -2-fold (33 ≤ -1.5-fold). However, these differences are not immediately evident when viewing the heatmap in **Fig. 7B** due to greater variability in signal between female mice compared to male. Alternatively, though the raw reads for each gene were normalized to the geometric mean of all gene signals for each mouse, the normalization protocol may not have been sufficient to reveal group differences when visualized by the heatmap.

Fetal (E12.5) mice display subtle changes in H3K4me3 in brain following maternal poly(I:C) treatment:

Next, in order to determine whether prenatal inflammation is capable of inducing transient alterations in H3K4me3 in mouse brain, which may not be detectable in the adult, H3K4me3 ChIP-Seq was performed on brain tissue from E12.5 poly(I:C) and saline mice collected 3 hrs following injections. In this experiment we chose to focus on the E12.5 time-point, as these litters demonstrated the most robust increase in IL-6 protein in brain following poly(I:C) treatment (**Fig. 2**).

As with the adult mouse H3K4me3 ChIP-Seq libraries, a high percentage of total reads were uniquely mappable (83-84%) to mouse genome in both saline and poly(I:C) mice, while smaller fractions were multi-mappable or non-mappable (13% and 3-4%, respectively). Additionally, a high percentage of total peaks (79%) were proximal to gene TSS; 5% of peaks were medial and 16% were distal (**Fig. 8**).

Similar to the adult mice, alterations in H3K4me3 in fetal mouse brain following maternal poly(I:C) treatment were relatively subtle. Four genes demonstrated H3K4me3 increased ≥ 2-fold (23 ≥ 1.5-fold), while 12 genes were decreased ≤ -2-fold (27 ≤ -1.5-fold) (**Fig. 9**). Though the observed changes were small, there were several interesting candidate genes suggestive of immune activation. For example, interferon regulatory factor 8 (*Irf8*) was upregulated 1.57-fold and BCL2-associated athanogene 3 (*Bag3*) was upregulated 1.39-fold. The latter gene is a member of BAG family of co-chaperones that interacts with heat shock protein 70 (Hsp70) and

increased H3K4me3 was observed at the *BAG3* locus in two autism postmortem brains in our laboratory (unpublished data; ChIP-Seq performed by Iris Cheung and data analyses done by Hennady Shulha and Zhiping Weng).

Global H3K4me3 levels undergo massive changes in brain between fetus and adult:

Comparison of H3K4me3 patterns from the saline fetal brain samples to adult saline mice revealed a large number of highly significant changes, as expected. In total, 163 genes had H3K4me3 levels increased ≥ 2-fold in fetal brain compared to adult (571 ≥ 1.5-fold), and 322 genes were decreased ≤ -2-fold (426 ≤ -1.5-fold).

Discussion

In the present study, I demonstrated measurable immune activation in pregnant mice following poly(I:C) treatment, elevation of IL-6 protein in fetal brain, and significantly impaired working memory in the adult offspring exposed of E17.5 poly(I:C) mice. In contrast, changes in the brain on a molecular level were more subtle. Specifically, small differences were observed in H3K4me3 levels in both fetal and adult mouse brain, and these differences were more pronounced in adult mice when analyzed according gender.

It is a limitation of the field that it is not possible to unequivocally confirm whether a small fold-change in histone methylation levels have functional consequences. Evidence from my experiments in rat forebrain culture suggests that small changes in H3K4me3 levels are associated with similarly small changes on mRNA levels. However, there were no significant changes in gene expression in adult brain of the poly(I:C) offspring; furthermore, the small changes that do occur did not correlate with the H3K4me3 changes. It is possible that such small changes in H3K4me3 do not exert changes in basal mRNA levels but only come into play when exposed to an external stimulus, whether a novel environment or a drug of abuse. In such a situation, a small difference in H3K4me3 levels could influence the way transcriptional machinery is able to modulate gene expression on an acute time scale. Such an example is provided by the study by Branchi and colleagues described in Chapter I that demonstrated adult mice exposed to early environmental enrichment had increased acetylation of histone H3 at the *Bdnf* in hippocampus, but only displayed elevated Bdnf protein following a stressor [26].

Why did poly(I:C) not reproduce the robust alterations in H3K4me3 and gene expression observed in cell culture? One explanation is that the immune stimulus may not have been strong or prolonged enough to induce large changes—multiple injections, a higher dose of poly(I:C), or a different immune activation model entirely, such as infection with the influenza virus,

may be necessary to cause chromatin modification *in vivo*. H3K4me3 may be under even tighter control in the intact brain than *in vitro*, such that the levels of IL-6 achieved in fetal brain were insufficient to alter this histone modification. Alternatively, an underlying genetic abnormality may be required to increase susceptibility of the mice to inflammation, as has been suggested by a recent report showing a combined effect of prenatal inflammation with mutant Disc1 protein on behavior and neuropathology in adult offspring [134]. This idea is also supported by data from human studies showing that prenatal exposure to infection may only increase risk of psychosis in genetically susceptible individuals [37].

Variability in maternal immune response must also be taken into consideration. The cytokine ELISA demonstrates inconsistency in the ability of maternal poly(I:C) injections to result in upregulation of IL-6 protein in fetal brain—only 2/3 E12.5 litters demonstrated a robust increase in IL-6 at 3 hours post-injection and only 1/3 E17.5 litters showed increased IL-6 compared to saline. A recent study reporting variability of maternal immune response and its impact on the offspring highlights the complexity of this rodent model [135]. Specifically, this group demonstrated that a subset of pregnant rats lost weight following poly(I:C) treatment on E14, and that this had a significant impact on locomotor abnormalities induced by MK-801 and amphetamine in the adult offspring.

It is also possible that H3K4me3 changes *in vivo* are more short-lived or confined to a specific window of time following IL-6 stimulus that the current study was unable to capture—the only time points following poly(I:C) administration examined were 3 hours or 12 weeks following exposure to inflammation. Another possibility is that H3K4me3 alterations may be confined to another brain region, such as hippocampus, not sampled in the present study.

The importance of H3K4me3 in brain development has been highlighted in recent literature. For example, Mll1 plays a critical role in neurogenesis in the subventricular zone in mouse [87]. Furthermore, H3K4me3 peaks in neuronal chromatin were recently shown to undergo massive, genome-wide shifts between fetal and adult brain in human, reiterating the critical role that this histone mark plays in brain development [85]. Although lacking the cellular resolution of the former study, my work replicates this finding of developmental changes in H3K4me3 and provides validity for examining the response of this histone modification to environmental stimuli *in utero*.

Due to the inconclusive nature of my findings in mouse brain following prenatal exposure to inflammation, it is difficult to draw parallels to findings from schizophrenia and autism postmortem brain. My data emphasize the limitations of the maternal immune activation model and suggest that paradigms employed by one lab to elicit a particular neuropathology may not

always be reproducible. For example, I did not observe significant gene expression changes in adult brain as has been reported in the literature following poly(I:C) treatment [83]. Furthermore, such paradigms may not be optimized for the investigation of yet-unstudied molecular effects, such as chromatin modifications. Still, such preclinical animal models represent a powerful tool in understanding the role that environmental risk factors play in the pathoetiology of neuropsychiatric disease.

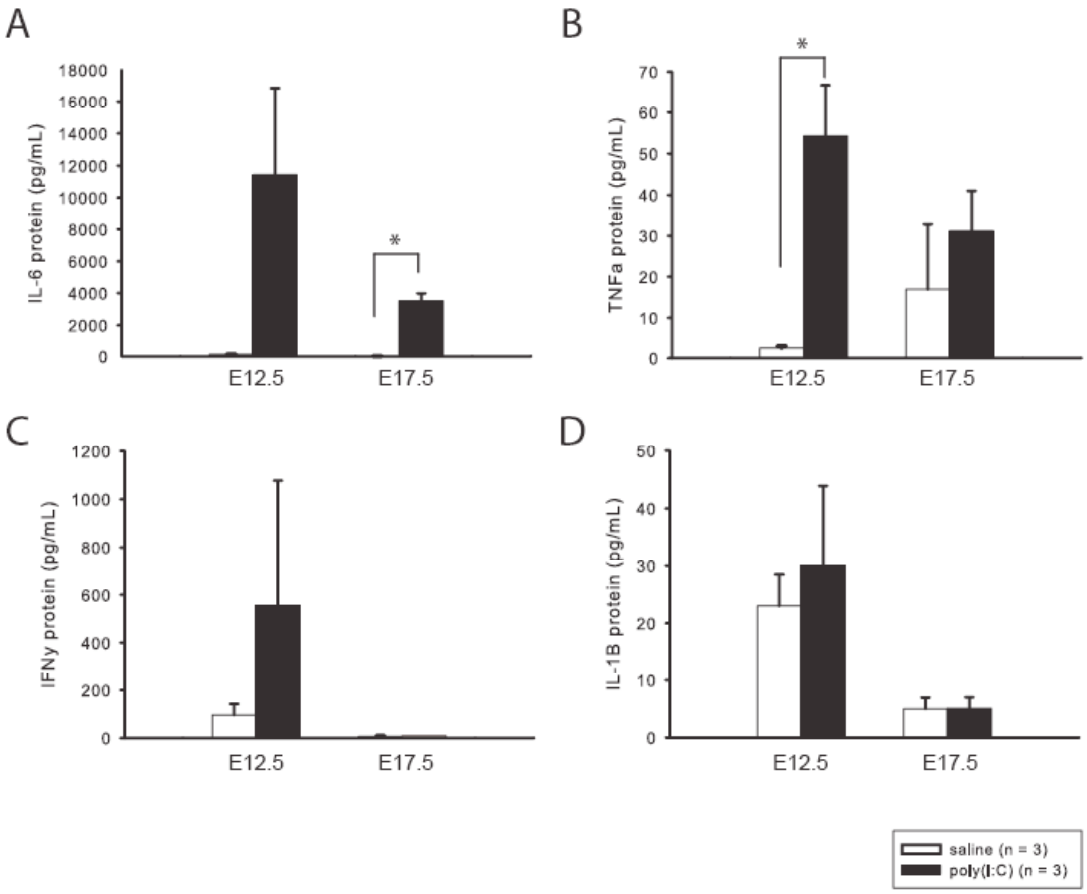

Figure 1: IL-6 is elevated in maternal serum following poly(I:C) injection. **(A)** IL-6 protein is upregulated in maternal serum 3 hours following poly(I:C) injection on embryonic day 12.5 (E12.5) and E17.5 (n = 3 mice per group). Variation in the E12.5 poly(I:C) mice precluded detection of statistical significance. **(B)** TNFα protein is significantly upregulated in maternal serum on E12.5 but not E17.5. **(C)** IFNγ is not altered in maternal serum on E12.5 or E17.5. **(D)** IL-1β is not altered in maternal serum on E12.5 or E17.5.

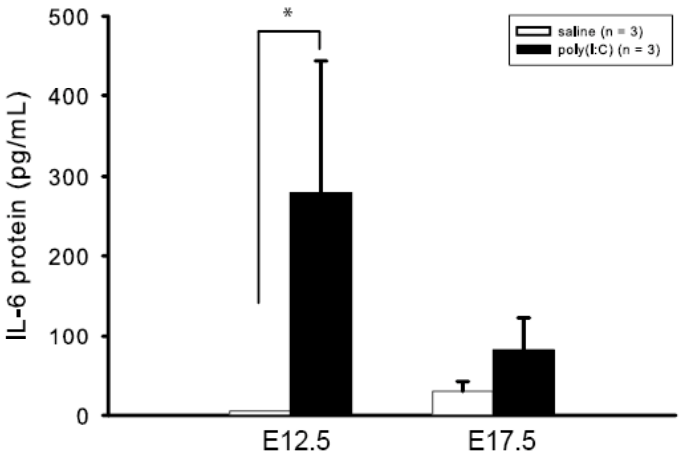

Figure 2: IL-6 is elevated in a subset of fetal brains following poly(I:C) injection. IL-6 protein was elevated in fetal brain in 3/4 E12.5 litters 3 hours following poly(I:C) injection and in 1/3 E17.5 litters. This increase was significant at the E12.5 time point ($p = 0.044$).

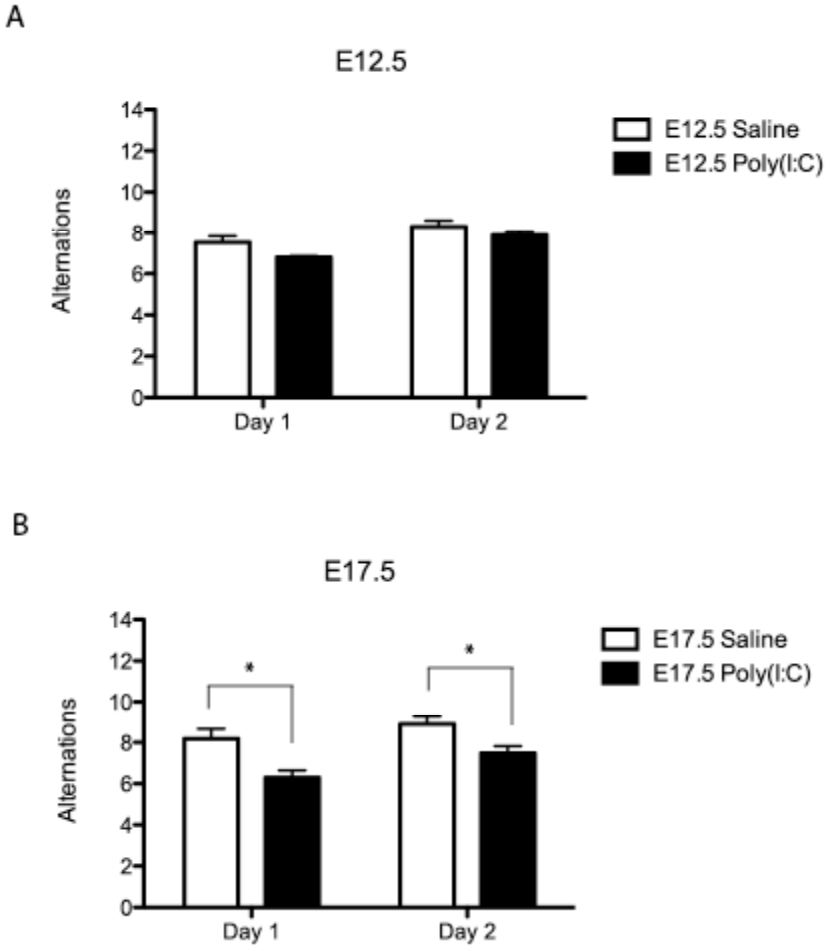

Figure 3: Working memory is impaired in adult E17.5 poly(I:C) mice. **(A)** Adult mice from mothers injected with poly(I:C) on E12.5 do not demonstrate a significantly different number of alternation on day 1 or day 2 of T-maze (saline n = 51 [9 litters]; poly(I:C) n = 27 [8 litters]). **(B)** Adult mice from mothers injected with poly(I:C) on E17.5 demonstrate significantly fewer numbers of alterations compared to saline on both days 1 and 2 of testing (saline n = 28 [10 litters]; poly(I:C) n = 34 [12 litters]).

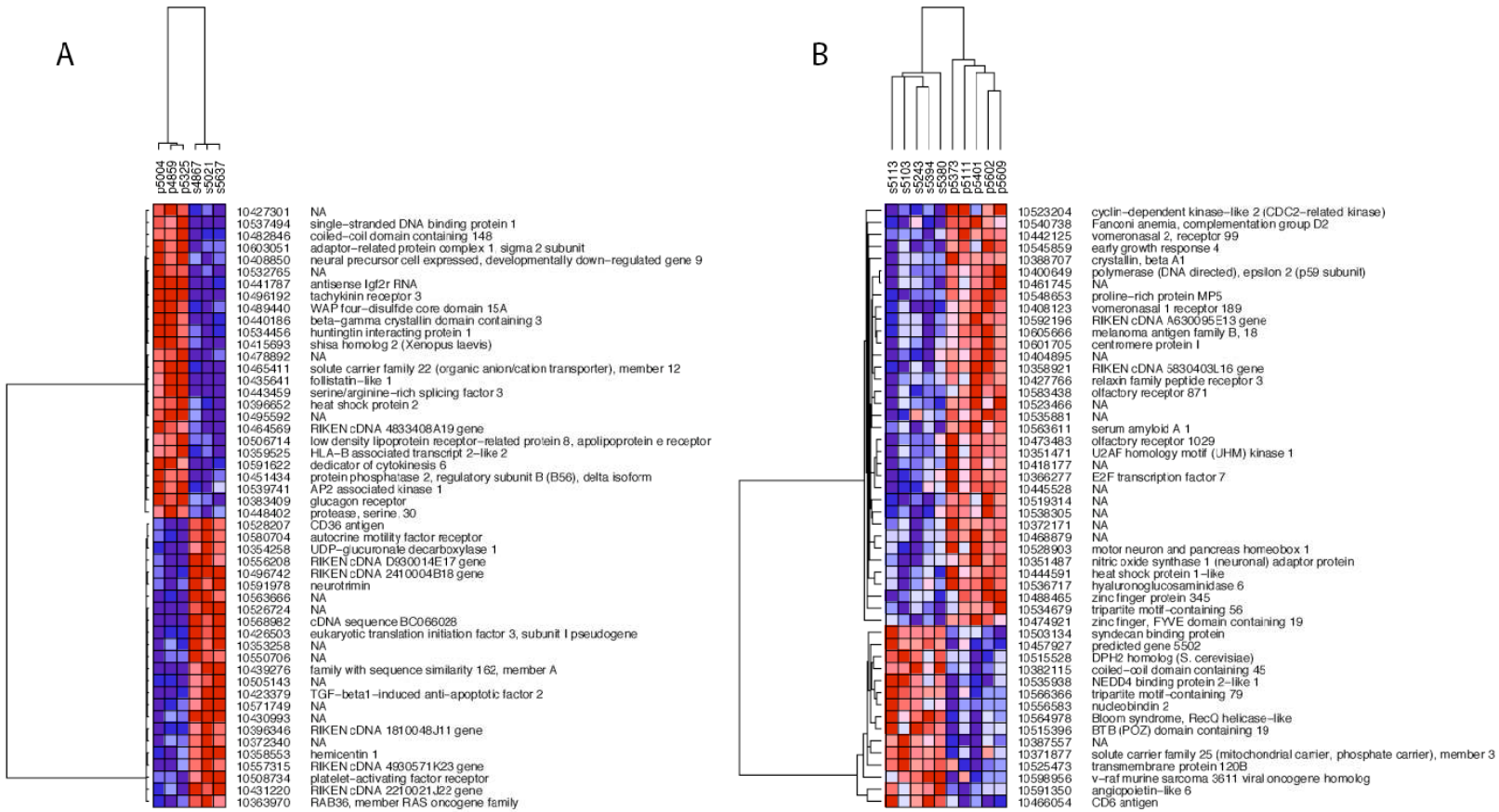
A
p5004
p4859
p5325
s4867
s5021
s5637
10427301 NA
10537494 single-stranded DNA binding protein 1
10482848 coiled-coil domain containing 148
10603051 adaptor-related protein complex 1, sigma 2 subunit
10408850 neural precursor cell expressed, developmentally down-regulated gene 9
10532765 NA
10441787 antisense Igf2r RNA
10496192 tachykinin receptor 3
10489440 WAP four-disulfide core domain 15A
10440186 beta-gamma crystallin domain containing 3
10534456 huntingtin interacting protein 1
10415693 shisa homolog 2 (Xenopus laevis)
10478892 NA
10465411 solute carrier family 22 (organic anion/cation transporter), member 12
10435641 follistatin-like 1
10443459 serine/arginine-rich splicing factor 3
10396652 heat shock protein 2
10495592 NA
10464569 RIKEN cDNA 4833408A19 gene
10506714 low density lipoprotein receptor-related protein 8, apolipoprotein e receptor
10359525 HLA-B associated transcript 2-like 2
10591622 dedicator of cytokinesis 6
10451434 protein phosphatase 2, regulatory subunit B (B56), delta isoform
10539741 AP2 associated kinase 1
10383409 glucagon receptor
10448402 protease, serine, 30
10528207 CD36 antigen
10580704 autocrine motility factor receptor
10354258 UDP-glucuronate decarboxylase 1
10556208 RIKEN cDNA D930014E17 gene
10496742 RIKEN cDNA 2410004B18 gene
10591978 neurotrimin
10563666 NA
10526724 NA
10568962 cDNA sequence BC066028
10426503 eukaryotic translation initiation factor 3, subunit I pseudogene
10353258 NA
10550706 NA
10439276 family with sequence similarity 162, member A
10505143 NA
10423379 TGF-beta1-induced anti-apoptotic factor 2
10571749 NA
10430993 NA
10398348 RIKEN cDNA 1810048J11 gene
10572340 NA
10358553 hemicentin 1
10557315 RIKEN cDNA 4930571K23 gene
10508734 platelet-activating factor receptor
10431220 RIKEN cDNA 2210021J22 gene
10363970 RAB36, member RAS oncogene family
B
s5113
s5103
s5243
s5084
s5379
p5111
p5401
p5602
p5609
10523204 cyclin-dependent kinase-like 2 (CDC2-related kinase)
10540738 Fanconi anemia, complementation group D2
10442125 vomeronasal 2, receptor 99
10545859 early growth response 4
10388707 crystallin, beta A1
10400649 polymerase (DNA directed), epsilon 2 (p59 subunit)
10461745 NA
10548653 proline-rich protein MP5
10408123 vomeronasal 1 receptor 189
10592196 RIKEN cDNA A630095E13 gene
10605666 melanoma antigen family B, 18
10601705 centromere protein I
10404895 NA
10358921 RIKEN cDNA 5830403L16 gene
10427766 relaxin family peptide receptor 3
10583438 olfactory receptor 871
10523466 NA
10535881 NA
10563611 serum amyloid A 1
10473483 olfactory receptor 1029
10351471 U2AF homology motif (UHM) kinase 1
10418177 NA
10366277 E2F transcription factor 7
10445528 NA
10519314 NA
10538305 NA
10372171 NA
10468879 NA
10528903 motor neuron and pancreas homeobox 1
10351487 nitric oxide synthase 1 (neuronal) adaptor protein
10444591 heat shock protein 1-like
10536717 hyaluronoglucosaminidase 6
10488465 zinc finger protein 345
10534679 tripartite motif-containing 56
10474921 zinc finger, FYVE domain containing 19
10503134 syndecan binding protein
10457927 predicted gene 5502
10515528 DPH2 homolog (S. cerevisiae)
10382115 coiled-coil domain containing 45
10535938 NEDD4 binding protein 2-like 1
10566366 tripartite motif-containing 79
10556583 nucleobindin 2
10564978 Bloom syndrome, RecQ helicase-like
10515398 BTB (POZ) domain containing 19
10387557 NA
10371877 solute carrier family 25 (mitochondrial carrier, phosphate carrier), member 3
10525473 transmembrane protein 120B
10598956 v-raf murine sarcoma 3611 viral oncogene homolog
10591350 angiopoietin-like 6
10466054 CD6 antigen

Figure 4: Gene expression is not significantly altered in cortex of E17.5 or E12.5 poly(I:C) mice. (A) The heatmap represents the top 50 differentially expressed genes in E12.5 offspring (red = increase relative to saline; blue = decrease). Note that none of these changes were significant following correction for multiple comparisons. **(B)** The heatmap represents the top 50 differentially expressed genes in E17.5 offspring. As with the E12.5 mice, none of these changes were significant.

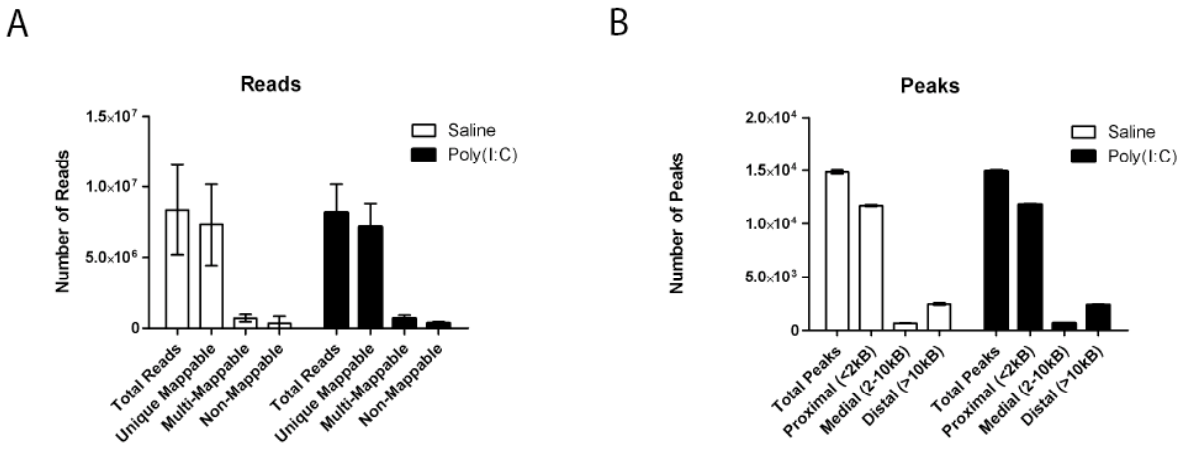

Figure 5: H3K4me3 ChIP-Seq of adult mouse cortex yields a high percentage of uniquely mappable reads and proximal peaks. (A) A high percentage (87%) of reads from H3K4me3 libraries generated from cortex of adult mice are uniquely mappable to mouse genome (version mm9) for both saline and poly(I:C). A smaller percentage (9%) map to multiple locations and 4% are not mappable. **(B)** The majority of peaks called by MACS (79%) are proximal to TSS; additionally, 5% of peaks are medial and 16-17% are distal.

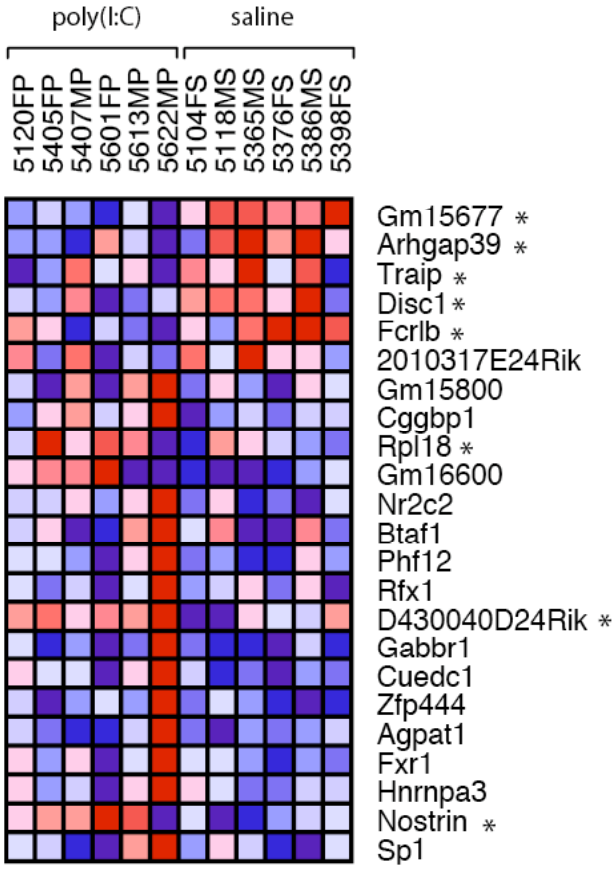

Figure 6: Adult E17.5 poly(I:C) offspring demonstrate subtle H3K4me3 alterations in cortex. Adult poly(I:C) mice show few differences in H3K4me3 levels within 500 bp of gene TSS. The heatmap depicts the 23 genes for which DESeq detected significantly different numbers of tags between groups; however, the fold-changes are all relatively subtle (17 genes were increased 1.25 to 1.61-fold and 6 genes were decreased -1.26 to -2.47-fold). The genes with the most consistent group differences are marked with asterisks.

A

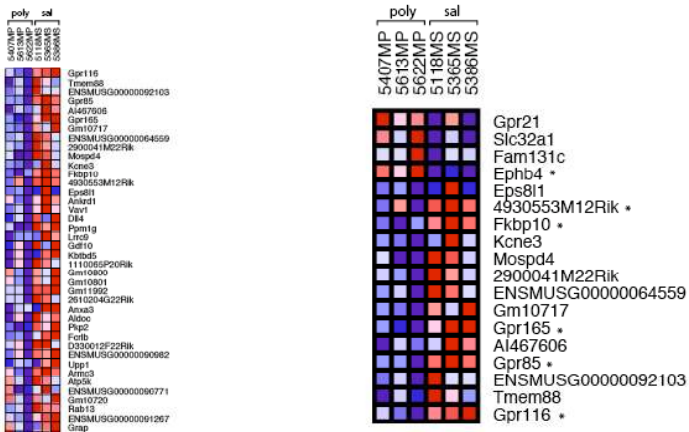
poly
sal
5407MP
5613MP
5622MP
5118MS
5365MS
5386MS
Gpr21
Slc32a1
Fam131c
Ephb4 *
Eps8l1
4930553M12Rik *
Fkbp10 *
Kcne3
Mospd4
2900041M22Rik
ENSMUSG00000064559
Gm10717
Gpr165 *
AI467606
Gpr85 *
ENSMUSG00000092103
Tmem88
Gpr116 *

B

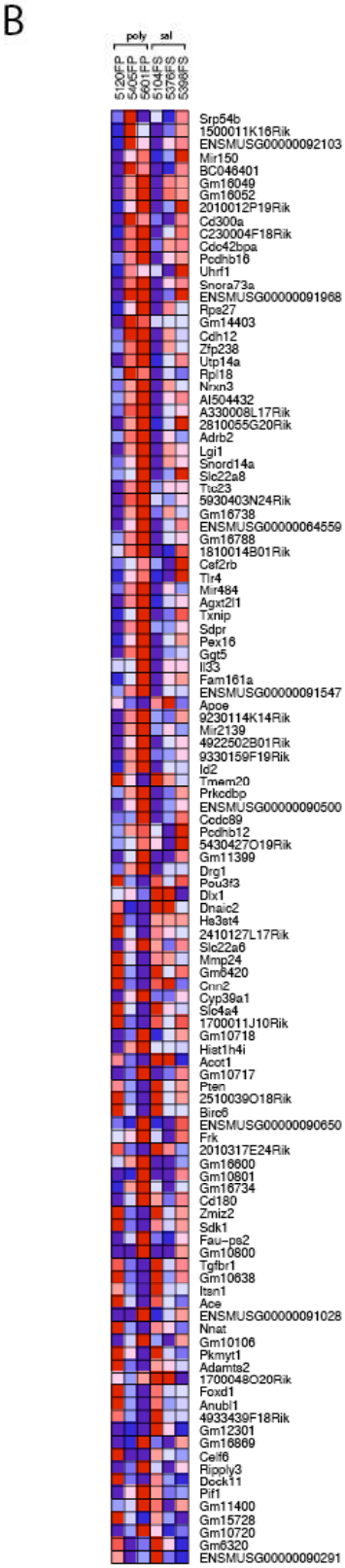
poly
sal
5120FP
5405FP
5601FP
5104FS
5376FS
5398FS
Srp54b
1500011K16Rik
ENSMUSG00000092103
Mir150
BC046401
Gm16049
Gm16052
2010012P19Rik
Cd300a
C230004F18Rik
Cdc42bpa
Pcdhb16
Uhrf1
Snora73a
ENSMUSG00000091968
Rps27
Gm14403
Cdh12
Zfp238
Utp14a
Rpl18
Nrxn3
AI504432
A330008L17Rik
2810055G20Rik
Adrb2
Lgi1
Snord14a
Slc22a8
Tsc23
5930403N24Rik
Gm16738
ENSMUSG00000064559
Gm16788
1810014B01Rik
Cef2rb
Tlr4
Mir484
Agxt2l1
Txnip
Sdpr
Pex16
Ggt5
Il33
Fam161a
ENSMUSG00000091547
Apoe
9230114K14Rik
Mir2139
4922502B01Rik
9330159F19Rik
Igf2
Tmem20
Prkcdbp
ENSMUSG00000090500
Ccdc89
Pcdhb12
5430427O19Rik
Gm11399
Drg1
Pou3f3
Dlx1
Dnaic2
Hs3st4
2410127L17Rik
Slc22a6
Mmp24
Gm8420
Cnn2
Cyp39a1
Slc4a4
1700011J10Rik
Gm10718
Hist1h4i
Acot1
Gm10717
Pten
2510039O18Rik
Birc6
ENSMUSG00000090650
Frk
2010317E24Rik
Gm16600
Gm10801
Gm16734
Cd180
Zmiz2
Sdk1
Fau-ps2
Gm10800
Tgfbr1
Gm10638
Itsn1
Ace
ENSMUSG00000091028
Nnat
Gm10106
Pkmyt1
Adamts2
1700048O20Rik
Foxd1
Anubl1
4933439F18Rik
Gm12301
Gm16869
Celf6
Ripply3
Dock11
Pif1
Gm11400
Gm15728
Gm10720
Gm6320
ENSMUSG00000090291

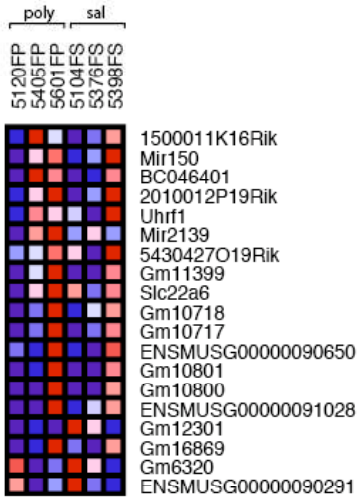
poly
sal
5120FP
5405FP
5601FP
5104FS
5376FS
5398FS
1500011K16Rik
Mir150
BC046401
2010012P19Rik
Uhrf1
Mir2139
5430427O19Rik
Gm11399
Slc22a6
Gm10718
Gm10717
ENSMUSG00000090650
Gm10801
Gm10800
ENSMUSG00000091028
Gm12301
Gm16869
Gm6320
ENSMUSG00000090291

Figure 7: Adult E17.5 poly(I:C) offspring demonstrate differential H3K4me3 alterations by gender. **(A)** Comparison of male poly(I:C) to male saline mice yielded more differences in H3K4me3 levels compared to the pooled gender analysis. In this analysis, 3 genes were increased ≥ 2-fold (109 ≥ 1.5-fold) and 14 genes were decreased ≤ -2-fold (58 ≤ -1.5-fold). The heatmap on the left shows all genes with ≥ 1.5-fold (or ≤ -1.5-fold) change, while the one on the right depicts genes altered ≥ 2-fold. The genes with the most consistent changes (i.e., same direction of change for all 3 mice per group) are marked with asterisks. **(B)** Comparison of female poly(I:C) to female saline mice also yielded more differences in H3K4me3 levels, with 16 genes increased ≥ 2-fold (78 ≥ 1.5-fold) and 3 genes decreased ≤ -2-fold (33 ≤ -1.5-fold). The heatmap on the left shows all genes with ≥ 1.5-fold (or ≤ -1.5-fold) change, while the one on the right depicts genes altered ≥ 2-fold. Note the variability in signal within both poly(I:C) and saline groups.

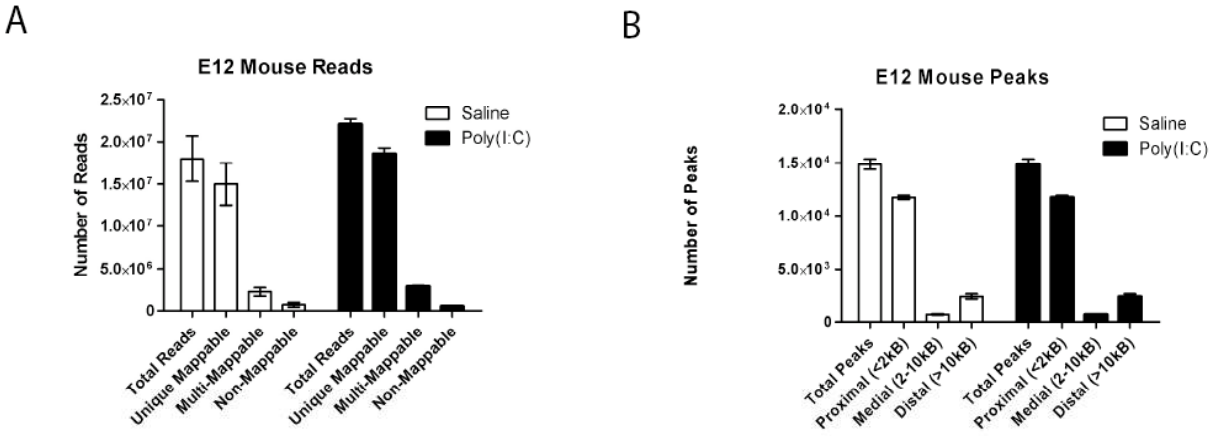

Figure 8: H3K4me3 ChIP-Seq of fetal mouse brain yields a high percentage of uniquely mappable reads and proximal peaks.
(A) H3K4me3 libraries generated from fetal (E12.5) mouse brain yield primarily unique reads (83-84%). A smaller percentage (13%) map to multiple locations and 3-4% are not mappable. **(B)** The majority of peaks in E12.5 mouse brain are proximal (79%) and a smaller percent are medial (5%) or distal (16%).

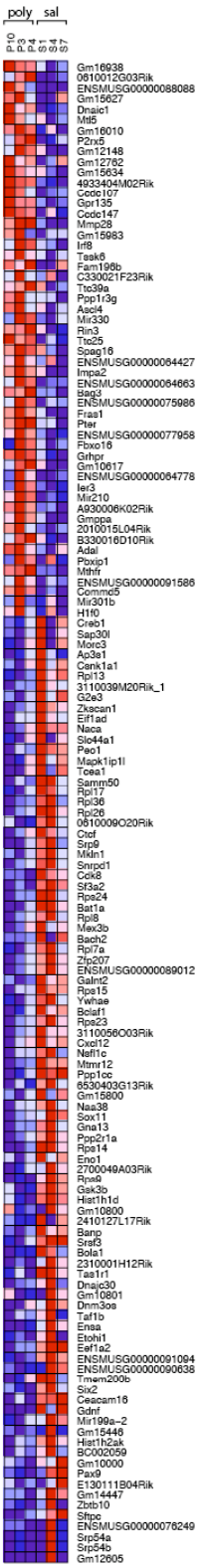
poly
sal
P10
P3
P4
S1
S4
S7
Gm16938
0610012G03Rik
ENSMUSG00000088088
Gm15627
Dnaic1
Mtf6
Gm16010
P2rx5
Gm12148
Gm12762
Gm15634
4933404M02Rik
Ccdc107
Cpr135
Ccdc147
Mmp28
Gm15983
Irf8
Tesk6
Fam198b
C330021F23Rik
Ttc39a
Ppp1r3g
Ascl4
Mir330
Rin3
Ttc25
Spag16
ENSMUSG00000064427
Impa2
ENSMUSG00000064663
Itag3
ENSMUSG00000075986
Fraa1
Pter
ENSMUSG00000077958
Fbxo16
Grhpr
Gm10617
ENSMUSG00000064778
Ier3
Mir210
A930006K02Rik
Gmppa
2010015L04Rik
B330016D10Rik
Adal
Ppxip1
Mthfr
ENSMUSG00000091586
Commd5
Mir301b
H1f0
Creb1
Sap30l
Morc3
Ap3a1
Cenk1a1
Rpl13
3110039M20Rik_1
G2e3
Zkscan1
Eif1ad
Naca
Slc44a1
Peo1
Mapk1ip1l
Tceal
Samm50
Rpl17
Rpl36
Rpl26
0610009O20Rik
Ctcf
Srp9
Mkln1
Snrpd1
Cdk8
Sf3a2
Rps24
Bat1a
Rpl8
Mex3b
Bach2
Rpl7a
Zfp207
ENSMUSG00000089012
Galnt2
Rps15
Ywhae
Bclaf1
Rps23
3110056O03Rik
Cxcl12
Naf1c
Mtmr12
Ppp1cc
6530403G13Rik
Gm15800
Naa38
Sox11
Gna13
Ppp2r1a
Rps14
Eno1
2700049A03Rik
Rps9
Gsk3b
Hist1h1d
Gm10800
2410127L17Rik
Banp
Srsf3
Bola1
2310001H12Rik
Taa1r1
Dnajc30
Gm10801
Dnm3os
Taf1b
Ensa
Etohi1
Eaf1a2
ENSMUSG00000091094
ENSMUSG00000090638
Tmem200b
Six2
Ceacam16
Gdnf
Mir199a–2
Gm15448
Hist1h2ak
BC002059
Gm10000
Pax9
E130111B04Rik
Gm14447
Zbtb10
Sftpc
ENSMUSG00000076249
Srp54a
Srp54b
Gm12605

Figure 9: There are subtle alterations in H3K4me3 levels in fetal (E12.5) mouse brain. As with adult, fetal (E12.5) mice show relatively subtle differences in H3K4me3 levels within 500 bp of gene TSS following poly(I:C) treatment. Four genes were increased ≥ 2-fold (23 ≥ 1.5-fold) and 12 genes were decreased ≤ -2-fold (27 ≤ -1.5-fold). The heatmap shows all genes altered ≥ 1.2-fold between treatment groups.

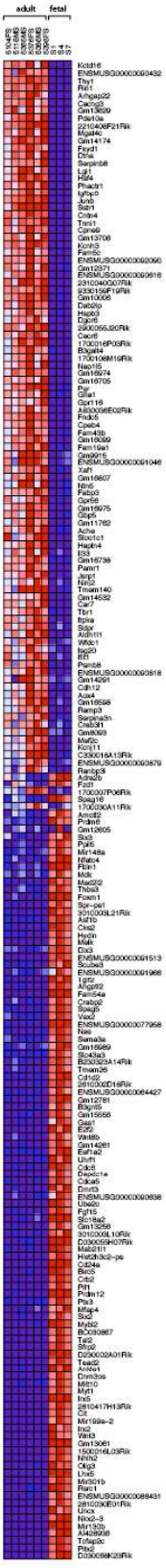
adult
fetal

Figure 10: H3K4me3 levels undergo massive developmental changes in mouse brain. Fetal (E12.5) saline mice demonstrated a large number of robust changes in H3K4me3 levels compared to adult saline mice. Overall, 163 genes were increased ≥ 2-fold in fetal brain compared to adult (571 ≥ 1.5-fold) and 322 genes were decreased ≤ -2-fold (426 ≤ -1.5-fold).

CHAPTER 4: General Discussion

Chromatin modifications, such as DNA methylation and histone modifications, have been suggested to play a role in the pathoetiology of a variety of neuropsychiatric diseases, including schizophrenia and autism. This hypothesis is based upon several lines of evidence, including direct evidence from human postmortem brain tissue and the presence of mutations in genes encoding epigenetic enzymes in the case of autism [13-20]. A role for epigenetics in neuropsychiatric disease has also been emphasized based on knowledge that these disorders are only partially caused by direct genetic mutation and are therefore likely to be caused by environmental factors as well. Recent animal studies demonstrate that exposure to environmental factors during prenatal and early postnatal development can alter chromatin modifications detectable in the brain of adult offspring, sometimes in association with behavioral changes, providing validity to the notion that early environment is capable of changing brain function via epigenetic mechanisms [21, 24, 26-28]. There is also some evidence to suggest that this occurs in human brain as well [29].

In the present thesis I sought to determine whether an environmental factor associated with both schizophrenia and autism—namely, prenatal exposure to inflammation—was capable of inducing changes in the trimethylated form of histone H3 at lysine 4 (H3K4me3) in central nervous system. In Chapter II, I describe experiments demonstrating that IL-6—a pro-

inflammatory cytokine implicated in both schizophrenia and autism—is capable of altering levels of H3K4me3 at a variety of gene loci in rat forebrain culture, providing proof-of-principle for the idea that inflammation can alter a histone modification in a model of the central nervous system. In Chapter III, I describe experiments utilizing the maternal immune activation mouse model of schizophrenia and autism and show that prenatal exposure to inflammation results increased IL-6 in fetal brain tissue, decreased working memory in adult offspring, and subtle changes in H3K4me3 in both fetal and adult brain. These findings suggest that cytokines produced by maternal infection have the potential to alter fetal brain development and adult brain function, in part, by changing gene expression programs through modification of chromatin. Taken together, the results presented in this thesis underscore the importance of environmental stimuli in the regulation of histone modifications in brain.

In the future, association of specific environmental and epigenetic factors with neuropsychiatric disorders will require expansion of medical history information provided by brain banks. There is frequently very little information available for brain donors, including medication history, onset and course of illness, family history of neuropsychiatric disease, and exposure to environmental factors. Some brain banks, such as Mount Sinai School of Medicine Alzheimer's Disease and Schizophrenia Brain Bank, are beginning

to use prospective characterization of brain donors, which includes assessment of neurological, cognitive, and psychiatric status through extensive and structured medical record reviews [136]. Such information will allow more careful correlation between environmental variables and specific cellular and molecular changes—including chromatin modifications—observed in postmortem brain tissue.

Additionally, birth cohort studies, such as the Child Health and Development study (CHDS), provide valuable resources for the investigation of neuropsychiatric disease, including detailed information on prenatal environmental factors and archived maternal serum samples collected throughout pregnancy [137]. This particular birth cohort was utilized by the Prenatal Determinants of Schizophrenia Study (PSD) to show that maternal influenza infection was associated with significantly increased risk of schizophrenia in the offspring [138]. Further investigation of the PSD cohort by the same group demonstrated an association between influenza antibodies in maternal serum during pregnancy and diagnosis of schizophrenia later in life [32]. Such well-characterized birth cohorts provide valuable information on environmental exposures during pregnancy, maternal serum samples, and detailed follow-up of offspring over the course of many years. Thus, collaboration between the investigators leading these studies and brain banks could prove fruitful. Additionally, study participants and their family members may be more amenable to the concept of brain donation,

because they have shown that they are invested in the study of neuropsychiatric disease.

Further complicating the study of chromatin modifications in these diseases, schizophrenia and autism are both characterized by enormous complexity and heterogeneity, in terms of presenting symptoms, genetic susceptibility, and molecular and cellular neuropathology. In addition, they are associated with multiple environmental risk factors. These characteristics suggest that disease in individual patients may have different etiology, though—ultimately—similar signaling pathways, cell types, and neural circuits are affected, producing a recognizable disease phenotype. This heterogeneity makes these disorders particularly challenging to study, because alterations in a cell population, expression of a gene, or epigenetic mark may only be present in a subset of patients, making it difficult for researchers to (1) detect the abnormality in the first place and (2) determine whether the change represents part of the underlying neuropathology or simply a stochastic event. Coupled with the fact that most postmortem studies use relatively small numbers of samples, detection of statistical significance is frequently challenging.

In the future, large-scale studies, including thousands of patient samples, will aid researchers in better understanding this heterogeneity. For example, the genome-wide association studies (GWAS) currently underway are identifying rare single nucleotide polymorphisms (SNPs) and copy

number variations (CNVs) associated with schizophrenia and autism by employing this large-scale study approach [139]. Taking a similar approach with epigenetic modifications may uncover subsets of patient populations affected by a particular alteration. Data from our own laboratory suggests that H3K4me3 marks are altered at specific loci in one or two autism cases compared to all control cases; increasing the subject number in such studies may reveal a larger—and more accurate—percentage of individuals with an autism spectrum disorder affected by these changes.

However, such an undertaking is met with enormous challenges, which should not be underestimated. First, postmortem brain tissue is subject to more limited availability compared to blood samples utilized by GWAS; thus, it will likely take years to amass the number of samples required for such large-scale studies. Secondly, there are a wide variety of chromatin modifications that could potentially be associated with schizophrenia or autism, particularly histone modifications, for which greater than 100 have been identified [140]. Currently, examination of all known histone modifications in postmortem brain samples is not tenable, given the high cost of current technologies such as ChIP-Seq and the amount of tissue this would require. Application of more high-throughput technologies, such as mass spectrometry, could potentially facilitate examination of multiple histone modifications in limited tissue samples by identifying altered marks [141]. Subsequently, these could be selected for further analysis with ChIP-Seq to pinpoint the specific genomic

locations of these changes. Finally, epigenetic research is met with a further complication not faced by genetic studies: each cell population in mammalian organs, including the brain, possesses a unique epigenome. How could an alteration occurring in a specific cell population within a specific brain region possibly be identified? In this case, clues provided by histological studies may point researchers in the right direction. For example, white matter neurons are reportedly increased in multiple subcortical regions in schizophrenia postmortem brain [142]. Additionally, GABAergic interneurons in a variety of brain regions—including cortex, hippocampus, and amygdala—appear to be affected by altered density or changes in mRNA and protein expression, including calcium binding proteins and neurotransmitter receptors [96, 143-145]. And in autism postmortem brain, several studies have reported decreases in numbers of Purkinje neurons in cerebellum [129]. Focusing on specific cell populations known to be affected in schizophrenia or autism may aid in the identification of altered chromatin modifications.

Still, it must be kept in mind that it is also possible for an apparently normal population of cells to possess an aberrant epigenetic signature that influences cell function in the absence of changes in cell density or structure or basal changes in mRNA and protein expression. For example, early exposure to environmental enrichment results in increased acetylation of histone H3 at the brain-derived neurotrophic factor (Bdnf) gene in rat hippocampus, but Bdnf protein levels were only observed to be altered in

these animals following exposure to stress [26]. Additionally, it is possible that altered chromatin modifications influence transient changes in gene expression required for cellular function in brain, such as synaptic plasticity and neural oscillations, both of which are required for cognitive processes; the latter demonstrate abnormalities in schizophrenia and autism patients [146-148]. In this case, this population of cells would not necessarily be identified as possessing altered mRNA or protein levels in postmortem brain tissue, because their abnormal expression is only present within a specified window of time in the living patient. These examples highlight the importance of measuring chromatin modifications in multiple cell populations in schizophrenia and autism brain, not just those currently associated with the disease.

Even if specific chromatin modifications can be associated with specific cell types within subsets of patient populations, there remains the problem of cause-and-effect. For an epigenetic alteration identified in adult postmortem brain, we cannot currently determine: (1) when during the individual's lifespan this aberrant mark was incurred, and (2) whether this alteration plays a role in causing disease or whether it is simply a byproduct of the disease process. At present, answering these questions is not possible, given that this would require sampling of brain tissue from living individuals during fetal and childhood stages, prior to disease onset, which cannot as of yet be predicted based on biomarkers or genetic testing. In addition, it is possible that a

transient epigenetic change during the fetal period could instigate a cascade of events leading to altered brain development and postnatal disease onset; in this instance, this change would not be identified by studying postmortem brain tissue from child or adult cases.

Thus, at least for the time being, researchers are forced to turn to animal models in order to study how a particular alteration in an epigenetic mark occurring at a specific developmental stage influences phenotype. For example, a recent study demonstrated that conditional deletion of mixed-lineage leukemia 1 (*Mll1*)—an H3K4-specific methyltransferase—in neural progenitor cells on embryonic day 13 in mouse brain resulted in decreased neurogenesis, growth retardation and ataxia, and death by postnatal day 30 [87]. It was found that decreased neurogenesis was caused by decreased expression of distal-less homeobox 2 (*Dlx2*)—a transcription factor critical for neuron fate specification—as a consequence of increased levels of H3K27me3 at the promoter region. Another study showed that conditional deletion of DNA methyltransferase 1 (*Dnmt1*) in neuroblasts during the embryonic period resulted in global DNA hypomethylation in forebrain neurons in the postnatal animal, and these cells were eliminated by 3 weeks of age, emphasizing the importance of epigenetics in appropriate neurodevelopment [149]. In contrast, deletion in postmitotic neurons had no effect on DNA methylation levels or cell function. Thus, knockout and transgenic mice provide the means to study how altered chromatin

modifications incurred at specific developmental time-points in specific cell populations impact brain development and function.

In addition to manipulation of chromatin modifications through genetic techniques, researchers have also shown that exposure to specific environmental stimuli during prenatal and early postnatal periods result in altered chromatin modifications in mature brain; moreover, some of these epigenetic changes have functional consequences, at both molecular and behavioral levels [21, 24, 26-28]. These animal models offer a powerful tool to examine how environmental factors associated with neuropsychiatric disease influence chromatin modification in brain and, in turn, influence phenotype in the adult. However, the majority of these studies are limited by the fact that they only examined chromatin in mature brain, long after the environmental stimulus was applied. Thus, these models are susceptible to one of the major limitations of postmortem studies: it is not known whether abnormal chromatin modifications in adult brain are directly caused by the environmental factor during early development or represent a byproduct of other changes. In order to more firmly establish the link between specific stimuli and chromatin modifications, it will be critical to sample brain tissue at multiple time points following the exposure—such experiments will reveal both transient epigenetic changes in fetal brain as well as those that persist throughout the lifespan. Additionally, experiments in which reversal of the chromatin modification induced by environmental exposure also reversed

molecular and behavioral changes, such as those conducted by Weaver and colleagues, provide further evidence that the environmentally-induced epigenetic changes have direct functional consequences [22, 23].

In the future, how could we potentially study chromatin modifications in brain *in vivo* in human populations? Currently, imaging with positron emission tomography (PET) and single-photon emission computed tomography (SPECT) is employed to measure proteins, such as neurotransmitter receptors and transporters, in brains of living patients [150, 151]. Positron-emitting radiotracers have also been developed that bind non-receptor proteins, such as β-amyloid protein [152]. While clearly lacking the fine resolution of methods such as ChIP-Seq, development of molecular imaging technology for measurement of histone modifications in brain of living patients offers a potential means for assessment of how epigenetic marks change over time or whether they are associated with specific phases of illness, such as during a psychotic episode.

In the face of seemingly insurmountable challenges, why should neurobiologists continue to pursue the underlying causes of complex neuropsychiatric disease? Such pessimism can be tempered by bearing in mind the vast scientific achievements that have transpired over the past century. A short 60 years ago, the structure and function of DNA had not yet been identified. And an even shorter time ago, the roots of schizophrenia and autism were ascribed to lack of maternal warmth—anatomical and molecular

changes in the brain had not even been considered. Further elucidation of the mechanisms underlying the onset of neuropsychiatric disease will require extreme dedication, passion, and collaboration by both current and future generations of scientists. The motivation and perseverance necessary for such an undertaking can be derived, in part, from knowledge of—and sympathy for—the extreme suffering caused to patients and their families by these diseases. Also, it will require a more visceral, innate enthusiasm summarized by James Watson: “Understanding the brain is the next great scientific objective…there are real big things out there that seem impossible to explain. But you just want to prove you can do it. You can’t think of anything else. It’s in your blood.”

Appendix I:

A Simple Method for Improving the Specificity of Anti-Methyl Histone Antibodies

Caroline Connor[1], Iris Cheung[1], Andrew Simon[1], Mira Jakovcevski[1], Zhiping Weng[2,3], and Schahram Akbarian[1*]

[1]Brudnick Neuropsychiatric Research Institute, Department of Psychiatry, [2]Program in Bioinformatics and Integrative Biology, and [3]Department of Biochemistry and Molecular Pharmacology,
University of Massachusetts Medical School, Worcester, MA

Epigenetics 5(5):392-5 July 2010

Abstract

Antibodies differentiating between the mono-, di- and trimethylated forms of specific histone lysine residues are a critical tool in epigenome research, but show variable specificity, potentially limiting comparisons across studies and between samples. Using trimethyl histone H3 lysine 4 (H3K4me3)—a mark enriched at transcription start sites (TSS) of active genes—as an example, we describe how simple co-incubation with synthetic peptide of the K4me2 modification leads to increased specificity for K4me3 and a much sharper peak distribution proximal to TSS following chromatin immunoprecipitation and massively parallel sequencing (ChIP-Seq).

Chromatin-immunoprecipitation (ChIP) with site- and modification-specific anti-histone antibodies is a key approach in the field of epigenetics. Enrichment of a given histone modification can subsequently be measured at a defined gene locus with PCR (ChIP-PCR) or, more recently, on a genome-wide scale with massively parallel sequencing (ChIP-Seq) [153]. In particular, methylation of specific histone lysine residues—including H3K4, H3K36, H3K79; H3K9, H3K27, and H4K20—represents one of the most highly regulated types of chromatin modifications [10]. Importantly, these lysine side chains can carry up to three methyl groups, and their mono-, di- and trimethylated forms are differentially localized within the genome and exert distinct effects on transcription. In the case of H3K4, the trimethylated form (H3K4me3) is primarily associated with

transcription start sites, while the monomethylated form, H3K4me1, defines enhancer sequences and other regulatory elements further removed from proximal promoters [12, 154]. Finally, the dimethyl mark, H3K4me2, appears to be more broadly distributed with open chromatin primarily around the 5' portion of genes [12, 154]. Given that the functional effects of each of the three marks is very different, it is critical to perform ChIP with antibodies with selective recognition for either the mono, di, or trimethylated forms.

Many of the commercially available modification-specific antibodies are polyclonal, reflecting a perception of the field that these preparations provide better signal-to-noise as compared to monoclonals. However, we noticed that—while most antibodies are highly selective for a specific histone lysine residue—there can be considerable lot-to-lot variability in me1/2/3 specificity. In particular, cross-reactivity for the H3K4me2 mark was frequently detected with anti-H3K4me3 antibodies (**Figure 1A, B**). This represents a serious problem, as each of the different methylation marks confers specific effects on gene transcription [10, 155]. Here, we describe a simple, but effective, procedure for improving antibody specificity for the H3K4me3 mark.

We describe two slightly different, equally effective protocols for improvement of antibody specificity, both of which include pre-incubation of antibody with peptide of the histone modification for which the antibody demonstrates non-specific immunoreactivity. In the first method, 4 μg rabbit polyclonal antibody against trimethylated histone H3 lysine 4 (H3K4me3;

Millipore, 07-473) was incubated with 9 μg of dimethylated H3K4 peptide (H3K4me2; Abcam, ab7768) spotted onto a 0.5 cm^2 piece of nitrocellulose membrane in 500 μl 1× FSB for 1 hour at room temperature. In the second method, the H3K4me2 peptide was pipetted directly into the antibody solution, incubated for 1 hr at room temperature, and the resulting antibody-peptide solution used for ChIP. To assess the immunoreactivity of anti-H3K4me3 antibody for the mono-, di-, and trimethylated forms of H3K4, we performed dot blots in which peptide for each of the three forms of H3K4 were spotted onto a membrane and allowed to dry; subsequently, membranes were incubated with anti-H3K4me3 antibody. As shown in **Figure 1A, B**, the untreated anti-H3K4me3 antibody demonstrates significant non-specific immunoreactivity for the dimethyl H3K4 peptide. However, pre-incubation of the antibody with H3K4me2 peptide visibly decreases this nonspecific immunoreactivity without altering immunoreactivity for its intended antigen.

To test whether this increased specificity in immunoreactivity translated to improved specificity of DNA sequences pulled down during chromatin immunoprecipitation, we performed ChIP on human and mouse chromatin isolated from brain tissue using untreated or pre-incubated anti-H3K4me3 antibody using a standard protocol for native ChIP [156]. Subsequently, immunoprecipitated DNA was processed for deep sequencing by ligating the Genomic Adaptor Oligo Mix (Illumina) to fragments, PCR-amplified, and fragments around 250 base pairs gel-purified.

As an initial assessment of the DNA immunoprecipitated by treated versus untreated antibody, a fraction of the library was subcloned into the pDrive vector (Qiagen) and transformed into DH5α cells (Invitrogen). Twenty clones were sequenced, aligned with the mouse or human genome, and their proximity to TSS determined. As shown in **Figure 1C**, anti-H3K4me3 antibody pre-incubated with H3K4me2 peptide pulled down significantly more sequences less than 1 kb from annotated TSS as compared to untreated antibody (41% versus 20%; $p = 0.031$). This is consistent with the literature showing that trimethylated H3K4 is highly localized around TSS of actively transcribed genes [12].

Extending the relationship between specificity of immunoreactivity on dot blot to performance of antibody during ChIP, we compared sequences from human brain immunoprecipitated with two commercially available anti-H3K4me3 antibodies: one of which demonstrated significant non-specific immunoreactivity for H3K4me2 peptide on dot blot ("Antibody 1") and the other of which exhibited fairly specific immunoreactivity for H3K4me3 ("Antibody 2"). **Figure 1D, E** show that Antibody 2 pulled down significantly more sequences < 1 kb from TSS (55% versus 27%; $p = 0.0018$) and < 2 kb from TSS (60% versus 31%; $p = 0.001$).

Next, we asked whether pre-incubation of anti-H3K4me3 antibody with H3K4me2 peptide led to increased percentage of sequences in close proximity to annotated TSS genome-wide. Four H3K4me3 ChIP libraries were deep sequenced by an Illumina Genome Analyzer (GA II) and genomic regions containing a significantly large number of reads—called peaks—were detected with the MACS

software [157]. Data from each sample were normalized for sequencing depth and the distribution of H3K4me3 peaks relative to TSS was determined. The percentages of proximal (< 2 kb from TSS), medial (2-5 kb), and distal (> 10 kb) peaks are shown in **Figure 2A**; it is apparent that the two samples prepared with H3K4me3 antibody pre-incubated with 15 μg H3K4me2 peptide in solution contain a higher percentage of proximal peaks (~85%) compared to samples prepared with untreated antibody (~72%). The distribution of peaks relative to TSS is shown in **Figure 2B**. We performed Wilcoxan rank sum tests on the distances of the peaks to the nearest TSS between samples. Peaks in the two samples prepared with peptide (ChIP 3 and 4) were significantly closer to a TSS than peaks in the two samples prepared without peptide (ChIP 1 and 2): p-value < 8.9×10^{-36} for all four pair-wise comparisons. Next, in order to characterize the detailed distribution of sequence tags around TSS, we used the GSA software [158] to produce an aggregation plot, shown in **Figure 2C**. The two samples prepared with pre-incubated antibody have much higher numbers of tags immediately downstream from the TSS, while a faster decline further downstream, compared with the two samples prepared with untreated antibody. As previously reported [12] [158], the periodic behavior of the aggregation plot indicates well-positioned nucleosomes.

In summary, we show that pre-incubation of commercially available anti-H3K4me3 antibody with a peptide of the H3K4me2 epitope results in significant improvement in antibody specificity, and much sharper peaks around TSS genome-wide. These clean-up procedures are particularly important given that the three

forms of methylated H3K4 possess different functions with regards to regulation of transcription.

Acknowledgments: The authors thank Hennady Shulha, Jia Xu, and Jie Wang at the Weng lab for advice on computational analysis. We also thank Dr. Ellen Kittler, Dr. Maria Zapp, and the staff of the UMMS Deep Sequencing Core for expert advice and support. Supported by grants from the NIH.

Figure 1: Preincubation of anti-H3K4me3 antibody with H3K4me2 peptide reduces nonspecific immunoreactivity and improves performance during ChIP. (A, B) Preincubation of anti-H3K4me3 antibody with increasing amounts of H3K4me2 peptide on membrane (A) or in solution (B) decreases immunoreactivity of the antibody for this modification on dot blot. **(C, D)** ChIP performed with anti-H3K3me3 antibody pre-incubated with 15 μg H3K4me2 peptide in solution results in significantly more sequences < 1 kb from TSS compared to untreated antibody (C). There was no significant difference at < 2 kb from TSS (D). **(E, F)** An anti-H3K4me3 antibody which demonstrates low immunoreactivity for H3K4me2 peptide on dot blot ("Antibody 2") results in significantly more sequences < 1 kb (E) and < 2 kb (F) from TSS post-ChIP compared to an anti-H3K4me3 antibody with high immunoreactivity for H3K4me2 peptide on dot blot ("Antibody 1").

Figure 2: ChIP-Seq performed with pre-incubated anti-H3K4me3 antibody results in a greater percentage of proximal peaks.

(A) ChIP performed with pre-incubated anti-H3K4me3 antibody results in a greater percentage of proximal peaks (~85% of total peaks) compared to untreated antibody (~72% of total peaks). **(B)** The two ChIP samples prepared with pre-incubated anti-H3K4me3 antibody show a higher proportion of peaks in close proximity to TSS and a proportional decrease in those distal to TSS. **(C)** The two ChIP samples prepared with pre-incubated anti-H3K4me3 antibody demonstrate a higher proportion of sequence tags directly downstream from TSS compared to

samples prepared with untreated antibody. In addition, the number of tags in the pre-incubated samples decline more quickly with increasing distance from TSS.

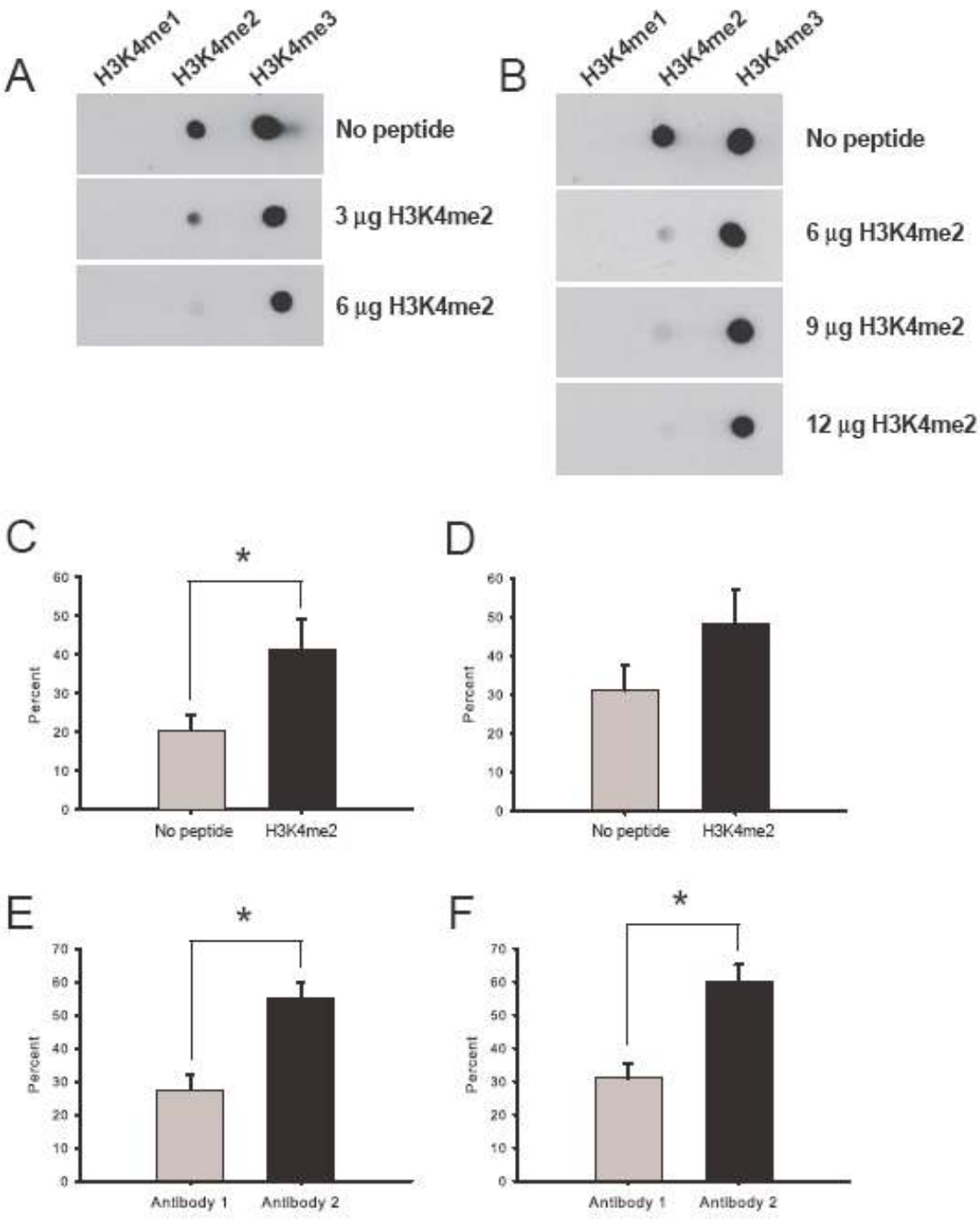
A
H3K4me1
H3K4me2
H3K4me3
No peptide
3 µg H3K4me2
6 µg H3K4me2
B
H3K4me1
H3K4me2
H3K4me3
No peptide
6 µg H3K4me2
9 µg H3K4me2
12 µg H3K4me2
C
*
Percent
No peptide
H3K4me2
D
Percent
No peptide
H3K4me2
E
*
Percent
Antibody 1
Antibody 2
F
*
Percent
Antibody 1
Antibody 2

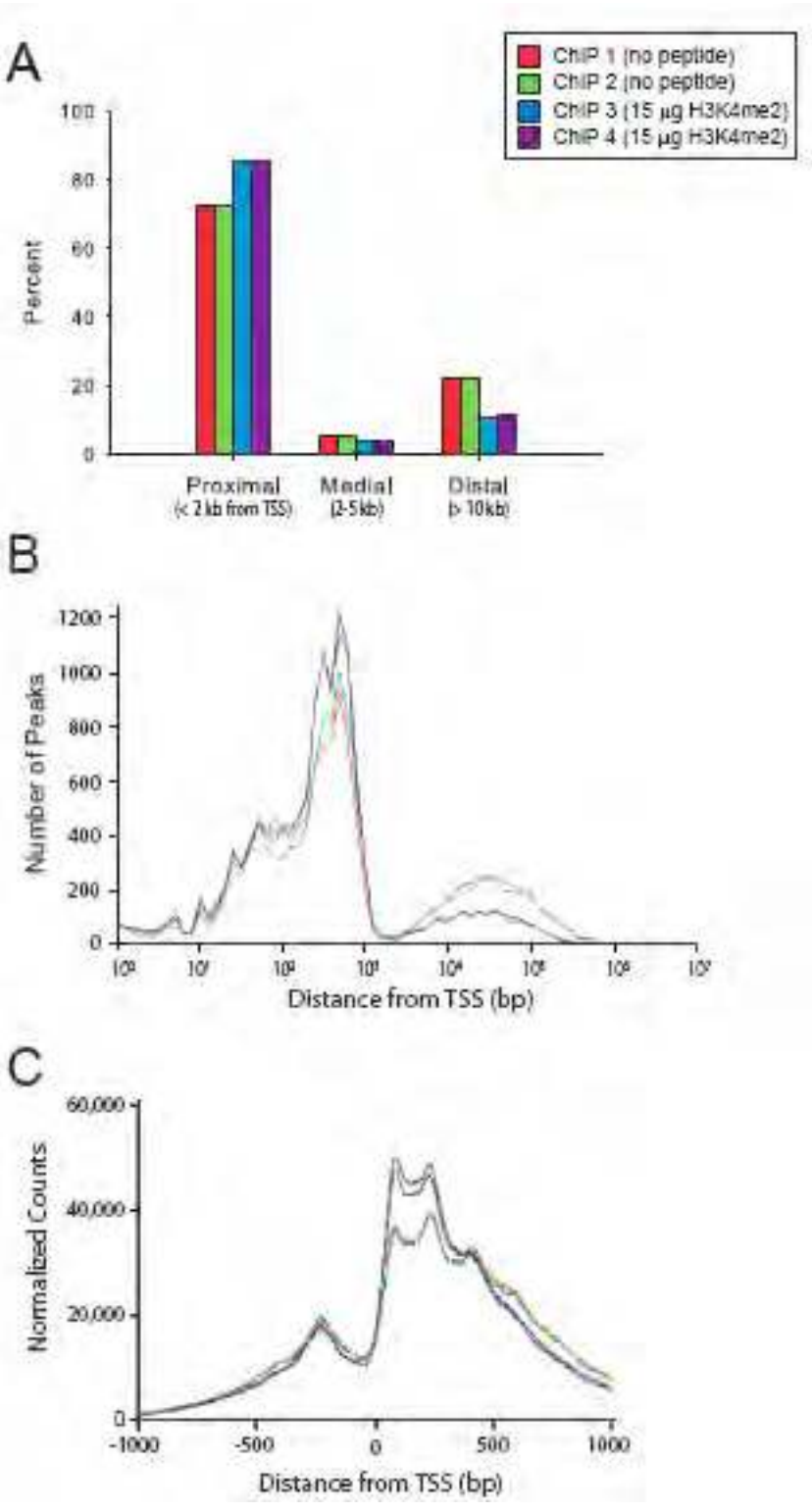
A
ChIP 1 (no peptide)
ChIP 2 (no peptide)
ChIP 3 (15 µg H3K4me2)
ChIP 4 (15 µg H3K4me2)
Percent
100
80
60
40
20
0
Proximal
(< 2 kb from TSS)
Medial
(2-5 kb)
Distal
(> 10 kb)
B
Number of Peaks
1200
1000
800
600
400
200
0
Distance from TSS (bp)
C
Normalized Counts
60,000
40,000
20,000
0
-1000
-500
0
500
1000
Distance from TSS (bp)

Appendix II:

Cingulate White Matter Neurons in Schizophrenia and Bipolar Disorder

Caroline M. Connor[1, 2#], MA, Yin Guo[2#], MD, and Schahram Akbarian[2*], MD, PhD

[1] Program in Neuroscience, Graduate School of Biomedical Sciences, [2] Department of Psychiatry, University of Massachusetts Medical School, Worcester MA 01604

# The two first authors made an equal contribution to this study.

Biological Psychiatry 66(5):486-93 September, 2009

ABSTRACT

Objective: Increased neuronal density in prefrontal, parietal and temporal white matter of schizophrenia subjects is thought to reflect disordered neurodevelopment; however, it is not known if this cellular alteration affects the cingulate cortex and whether similar changes exist in bipolar disorder.

Method: 82 postmortem specimens (bipolar 15, schizophrenia 22, control 45) were included in this clinical study. Densities for two neuronal markers, neuron-specific nuclear protein (NeuN) and neuregulin 1 alpha (NRG), were determined in white matter up to 2.5 mm beneath the anterior cingulate cortex; NeuN+ density was also determined for a subset of cases in prefrontal cortex. Changes during normal development were monitored in a separate cohort of 14 brains.

Results: Both the schizophrenia and bipolar cohorts demonstrated a two-fold increase in NeuN+ density in cingulate white matter; this effect could be attributed to ~25% of cases that exceeded the second standard deviation from controls. Similar changes were observed in prefrontal cortex. In contrast, NRG+ neuronal density was unaltered. Cases with increased NeuN+ densities in 2-dimensional (2D) counts also showed a pronounced, > 5-fold elevation in NeuN+ nuclei/mm^3. Additionally, the developmental cohort demonstrated a 75% decline in NeuN+ neuronal density during the first postnatal year, but was stable thereafter.

Conclusions: Increased neuronal density in white matter of cingulate cortex in schizophrenia provides further evidence that this alteration occurs in multiple cortical areas. Similar changes in some cases with bipolar illness suggests that the two disorders may share a common underlying defect in late prenatal or early postnatal neurodevelopment.

INTRODUCTION

Alterations of subcortical white matter in schizophrenia are thought to reflect the neurodevelopmental origins of this disorder. For example, recent neuroimaging studies describe changes in morphology and integrity of white matter tracts that are present from the earliest stages of these disorders [159, 160]. There is also progressive reduction of frontal lobe white matter [161] and—in striking contrast to overlying cortex—a relative glucose hypermetabolism in unmedicated schizophrenia subjects [162]. Of note, the 22q11.2 deletion syndrome (22qDS)—one of the strongest genetic risk factors for bipolar disorder and schizophrenia [163]—was associated with heterotopias and numerous ectopic neurons scattered throughout the white matter of the frontal lobe [164]. While heterotopias and other markers of more severe migration defects are not known to be characteristic of schizophrenia, these changes observed in some cases may be indicative of a more subtle developmental defect that is present in a larger proportion of the patient population.

In support of this idea, increased densities, or altered distribution, of white matter neurons have been reported in 11 out of 13 studies on

schizophrenia postmortem brain [165-178]. Some of these cells are thought to be derived from the embryonic subplate, a transient structure during pre- and early postnatal development that plays a pivotal role in orderly development of cortical connectivity [179, 180]. The majority of studies reported either a generalized increase of neurons [165, 167, 168, 171-174, 178], or redistribution towards deeper white matter space [165, 177]. However, there is little consensus as to which regions of subcortical white matter are definitively affected. This lack of agreement is not unexpected due to methodological differences between studies—even those studies which focused on the same brain region vary in terms of sulcogyral position sampled, neuronal markers employed, tissue processing, and characteristics of the clinical cohort. Furthermore, there is evidence that a robust increase in white matter neuron density is not a uniform feature in psychosis, but limited to approximately one third of cases diagnosed with schizophrenia [166]. Therefore, while it is difficult to reach a firm conclusion regarding white matter neuron changes in schizophrenia, the studies—when taken together—strongly suggest that this cell population is affected and may reflect defective brain development during the second half of gestation, when neurons are migrating through the interstitial zone, or, alternatively, during early postnatal life, when the majority of these cells undergo apoptosis [181].

The goal of the present study was: (1) to determine whether or not white matter neuron abnormalities extend beyond the diagnosis of

schizophrenia and also occur in bipolar disorder; (2) to estimate the proportion of schizophrenia or bipolar cases affected by this alteration; (3) to find out whether these alterations affect widespread portions of the frontal lobe, including the white matter space beneath the cingulate cortex, a region strongly implicated in the pathophysiology of both bipolar disorder and schizophrenia [182, 183]; (4) to monitor white matter neuron densities during the course of normal development and aging. We chose NeuN (neuron-specific nuclear antigen) [184], because neurons immunoreactive for this protein were previously reported to be elevated in frontal lobe white matter in schizophrenia [171, 172], and the alpha splice form of neuregulin 1, a schizophrenia risk gene implicated in neuronal migration [185-187]. (5) Finally, because microglial activation appears to be associated with increased NeuN-immunoreactive neurons in white matter in multiple sclerosis, we also assessed immunoreactivity for Iba1 (ionized calcium-binding adaptor molecule 1), a ubiquitous marker for microglia that is upregulated upon activation [188, 189].

METHODS

***Brain Tissue*:** 82 postmortem brain specimens (22 schizophrenia, 15 bipolar, and 45 controls) (**Table 1**) were obtained from the Harvard Brain Tissue Resource Center (HBTRC, Belmont, MA). A prospective design was chosen to ensure that each specimen that newly arrived at the brain bank would be

processed in a similar manner. Tissue blocks (~1.5 – 2 cm^3) were resected from each case from cingulum at an anterior-posterior level immediately rostral to the central sulcus, corresponding to the caudal sector of Brodmann area (BA) 24 (**Fig. 1A**). Care was taken to include portions of the adjacent corpus callosum and cingulate gyrus in each resected block. Immediately after resection, blocks were immersion-fixed in 10% phosphate-buffered formalin for a period of 4 days, then cryoprotected for 1 week in phosphate-buffered 30% sucrose; subsequently, tissue was frozen and 25 μm coronal sections cut on a cryostat. In addition, for a select group of clinical cases with elevated white matter neuron densities in cingulate (and controls matched for age, gender and autolysis time), additional sections were obtained from paraffin-embedded superior frontal gyrus (BA 9) (**Table 1**). Furthermore, fresh frozen cingulate tissue was also obtained for such cases for counting nuclei (see below) (**Table 1**).

For the developmental study, unfixed frozen tissue blocks from the pole of the frontal lobe were obtained for 14 additional subjects ranging in age from 40 weeks of gestation to 51 years of age. None of these subjects had been diagnosed with neurological or psychiatric disease. We chose the pole of the frontal lobe, instead of the anterior cingulate, as this region can be identified unambiguously in both young and old brain. These samples were obtained from the Brain and Tissue Bank for Developmental Disorders, University of Maryland (National Institute of Child Health and Human

Development Contract NO1-HD-8-3284) and the University of California, Davis (Center for Neuroscience) (**Table 1**). Tissue blocks were fixed in 4% formaldehyde for 20 hours, after which 25 μm coronal sections were cut and directly mounted on glass slides; subsequently, tissue was fixed again for 5 minutes in 100% acetone and re-hydrated prior to immunostaining. This additional acetone-based fixation was necessary due to the fragility of some of the younger samples.

See **Supplementary Methods** for details on immunohistochemistry, microscopy (including both 2D and 3D-like counting procedures), and statistics.

RESULTS

In all cases and controls, the massive callosal fiber tracts were readily discernable from bordering cingulum bundle and subcortical white matter (**Fig. 1A,B**). The ventral portion of the cingulate cortex in cases and controls showed the expected bipartition with the six-layered cortex of BA24, bordering upon the less laminated BA33, which is defined by "merging" of prominent pyramidal cell laminae of lower layer III and layer V [190] (**Fig. 1B, C**).

NeuN+ neuronal density is increased in cingulate white matter in schizophrenia and bipolar disorder

In sections immunostained for NeuN, the gray/white matter border was readily discernable, particularly at low magnification (**Fig. 1B, C**). The NeuN+ neurons were

defined by robust immunoreactivity in the nucleus and more lightly stained cytoplasm and processes, which were overall more readily discernable in gray matter than in white matter (**Fig. 1D**). In the gray matter, a large majority of neurons were NeuN+, resulting in a Nissl-type staining patterns (**Fig. 1B,C**).

In controls, NeuN+ neuronal density was highest in the most superficial white matter (4.25 cells/mm^2), and subsequently declined in the deeper white matter to densities of 0.794 cells/mm^2 (**Fig. 3A**). Both schizophrenia and bipolar groups were observed to have greater overall mean NeuN+ neuronal densities compared to controls (2.87 ± 0.50 and 2.29 ± 0.44 cells/mm^2 versus 1.28 ± 0.13 cells/mm^2; mean $\pm$ standard error). Diagnosis had a significant effect on overall mean NeuN+ density ($K = 14.0$; $p = 0.001$). The increased NeuN+ densities observed in schizophrenia and bipolar groups were both significantly different from control density ($Q = 13.6$, $p < 0.01$ and $Q = 7.24$, $p < 0.01$), but the two patient groups were not significantly different from one another ($Q = -2.51$, $p > 0.05$). When each compartment was analyzed individually, diagnosis was found to have a significant effect on NeuN+ density in all five compartments ($K = 6.32$, $p = 0.042$; $K = 10.5$, $p = 0.005$; $K = 6.83$, $p = 0.033$; $K = 11.8$, $p = 0.003$; $K = 12.4$, $p = 0.002$), with fold increases ranging from 1.17 to 3.75 (**Fig. 3A, B**). The increased NeuN+ densities observed in schizophrenia were significantly different from controls in all compartments ($Q = 8.83$, $p < 0.01$; Q 7.93, $p < 0.01$; $Q = 8.43$, $p < 0.01$; $Q = 10.8$, $p < 0.01$; and $Q = 9.90$, $p < 0.01$). NeuN+ densities in the bipolar cohort

were significantly different from controls in compartments II-V ($Q = 8.90$, $p < 0.01$; $Q = 4.42$, $p < 0.01$; $Q = 6.87$, $p < 0.01$; and $Q = 9.66$, $p < 0.01$).

Notably, 7 out of 22 schizophrenia subjects and 3 of 15 bipolar subjects demonstrated overall NeuN+ densities more than two standard deviations above the control mean (**Fig. 3C**); this increased proportion of cases exceeding the 95th percentile of control mean was significant for both schizophrenia ($\chi^2 = 12.3$, $p < 0.0001$) and bipolar groups ($\chi^2 = 5.7$, $p = 0.017$). We conclude that approximately 25% of cases diagnosed with bipolar disorder or schizophrenia show a more robust increase in cingulate white matter neuron densities. Importantly, when these 10 clinical cases were removed from the analyses, differences between the remaining schizophrenia, bipolar and the control subjects for each of the five compartments were not significant when corrected for multiple comparisons. No demographic or other factor was identifiable that could distinguish between the 10 cases with white matter neuron density above the 95th percentile of controls and the remaining patients. For example, 3/7 (4/7) affected schizophrenia subjects were male (female), while all 3 affected bipolar subjects were female. Approximately one half of these cases were from the left and from the right hemisphere, and ages were not significantly different from the cohort means.

Also of note, NeuN+ neurons were present in the deeper white matter in only 24/45 of control subjects, but were found in 12/15 of bipolar subjects

and in 20/22 schizophrenia subjects. These differences in distribution were significant for both schizophrenia (χ^2 = 10.3, p = 0.001) and bipolar groups (χ^2 = 8.4, p = 0.004). These findings also resonate with several previous reports suggesting elevated neuronal numbers in deeper white matter [166, 177, 178]. Among the 4 cases that were not on antipsychotic medication prior to death, 3 cases (75%) were found to harbor NeuN+ neurons in white compartments III-V. Therefore, the much higher proportion of subjects with NeuN+ neurons in deeper white matter in the two disease cohorts is unlikely to be due to antipsychotic medication. No association was observed between NeuN+ densities and age (r = 0.050) or PMI (r = -0.029); additionally, there was no significant difference in NeuN+ density between left and right hemispheres (U = 154.5; p = 0.480). Furthermore, there were no significant differences between genders within the 3 diagnostic categories (*control*: U = 65.5, p = 0.552; *schizophrenia*: U = 36.0, p = 0.335; *bipolar*: U = 18.0, p = 0.087). Finally, among 5 factors tested by ANCOVA (diagnosis, hemisphere, PMI, age, gender) only diagnosis had a significant effect on overall NeuN density (F = 8, p = 0.0007). Therefore, the observed increases in white matter NeuN+ neuronal density in the clinical samples of our cohort are most likely related to the disease itself and not due to other factors.

NRG+ neuronal density is unaltered *in cingulate white matter in schizophrenia and bipolar disorder*

Next, we wanted to study additional white matter neuron populations. To this end, we noticed that while immunostaining with the anti-Neuregulin α (NRG) antibody (see Methods) resulted in robust labeling of a subpopulation of bi- or multipolar neurons residing in cortex and white matter (**Fig. 2C**), none of the NeuN+ neurons in white matter (**Fig. 2A, B**) expressed NRG. Therefore, the white matter neuronal population expressing NeuN does not overlap with NRG+ cells, which is consistent with previous reports that NeuN is expressed in some—but not all—subpopulations of neurons [191, 192].

We determined the density of NRG+ neurons in both gray and white matter in a subset of 10 bipolar, 16 schizophrenia, and 26 control subjects. (We had previously observed increased NeuN+ white matter neurons in these clinical cases, similar to the ones reported above for the larger cohorts (data not shown).) For each of the 3 diagnostic groups, NRG+ density was lower in the cortical gray matter of cingulate as compared to the white matter (**Fig.3C**), which is consistent with a previous report demonstrating that NRG+ neurons are less common in gray matter compared to white in adult human brain [185]. In white matter, both schizophrenia and bipolar groups demonstrated similar mean NRG+ densities compared to controls (1.34 ± 0.099 and 1.31 ± 0.18 cells/mm^2 versus 1.26 ± 0.13 cells/mm^2), and there was no significant effect of diagnosis on overall, or compartment-specific, NRG+ density (K =

1.8, p = 0.406) (**Fig. 3E, F**). These findings further confirm that the observed increase in NeuN+ density in cingulate white matter bipolar disorder and schizophrenia is specific for that neuronal population.

NeuN+ neuronal density in cingulate gray matter is unaltered in schizophrenia and bipolar disorder

NeuN+ densities in gray matter were typically 50-150 fold higher than in white matter, but there was no significant correlation between the two (*bipolar* r = 0.0005; *schizophrenia* r = 0.004; *control* r = 0.0319; *all subjects* r = 0.0013) (**Supplemental Figure 1**). We conclude that the variation in neuronal densities in cingulate white matter is dissociated from any density changes of the overlying cortex.

Size of NeuN+ neurons in cingulate white matter is unaltered in schizophrenia and bipolar disorder

To rule out that the observed increase in NeuN+ density in bipolar disorder and schizophrenia could be an artifact due to a larger size of the NeuN-immunoreactive cells, we determined the average area of these cells in bipolar, schizophrenia, and control subjects, and no significant differences between diagnostic groups were found (0.092 ± 0.006; 0.099 ± 0.003; and 0.101 ± 0.003 mm^2) ($F = 1.09$; $p = 0.367$).

NeuN+ neuronal density is also increased in dorsolateral prefrontal cortex (BA9) white matter in schizophrenia

In the control subjects of the current study, the average density of NeuN+ neurons in cingulate white matter near the sulcal bottom ranged from 0.79 to 4.31 cells/mm^2. This contrasts with a previous study conducted on the middle banks of dorsolateral prefrontal cortex that reported NeuN+ densities of up to 40 cells/mm^2 in sections of similar thickness [172]. These differences are not unexpected, because the number of interstitial white matter neurons tend to decline towards sulcal fundi and, moreover, the thickness of the neuronal layer in the embryonic interstitial zone (future white matter), is thinner underneath the cingulate in comparison to the lateral cortex [181].

Therefore, we wanted to determine whether neuronal densities show regional differences in frontal lobe white matter and whether increased NeuN+ densities in the cingulate could be extrapolated to other areas. Indeed, NeuN+ densities in white matter beneath the sulcal bottom of the superior frontal gyrus (BA9) of 5 μm thick sections (see Methods) ranged from 0.21–2.48 cells/mm^2 in control subjects. If adjusted for differences in section thickness, NeuN+ neuron density in BA9 is 5-fold higher when compared to the cingulate. NeuN+ densities in the 6 schizophrenia cases showed a significant increase in BA9, compared to controls matched for age, gender and autolysis time (**Fig. 3D**); these same 6 subjects also demonstrated

increased NeuN+ densities in cingulate cortex as compared to the 6 controls (mean = 4.01 cells/mm^2 versus 1.28 cells/mm^2). Therefore, altered NeuN+ densities in psychosis potentially affect widespread portions of the frontal lobes.

NeuN+ nuclei are increased in cingulate white matter in schizophrenia

Next, we wanted to confirm that the elevated two-dimensional (2D) NeuN+ cell density can be replicated with a three-dimensional counting method. However, optical dissectors are not ideal for white matter neuron quantifications because neuronal numbers are low overall and unevenly distributed [144]. To bypass these limitations, we calculated the total number of NeuN+ and NeuN- nuclei extracted from a standardized column of white matter tissue from frozen, unfixed anterior cingulate (see Methods) (**Fig. 4A-C**). These additional studies were conducted on 6 schizophrenia cases that—in comparison to 5 matched controls—showed a 6.6-fold increase in overall NeuN+ densities as determined by the 2D approach (*schizophrenia*: 3.59 ± 0.70 cells/mm^2; *controls*: 0.55 ± 0.41 cells/mm^2, Mann-Whitney U = 31, $p < 0.05$). As shown in **Fig. 4D**, these 6 schizophrenia cases also showed a significant, 7.4-fold increase in NeuN+ nuclei per mm^3 white matter tissue (*schizophrenia*: 376 ± 253 nuclei/mm^3; *controls*: 51 ± 38 cells/mm^3; Mann-Whitney U = 0, $p = 0.006$). Across the 11 subjects, there was a good linear correlation between the 2D and 3D counts ($R = + 0.72$). In contrast to the

observed increase in NeuN+ nuclei, the schizophrenia group did not show increased numbers of overall nuclei (neuronal and non-neuronal) (**Fig. 4B, E**). This increase in NeuN+ nuclei—in the absence of an increase in DAPI+ nuclei—makes sense given that less than 4% of the white matter nuclei population is neuronal (**Fig. 4D-F**), and, thus, an increase in neuronal nuclei will not necessarily be reflected by an increase in all nuclei. From these findings, we draw two conclusions: First, increased numbers and densities of NeuN+ white matter neurons in our clinical cases are apparent when employing two different methodologies. Second, this alteration is highly specific, because overall numbers of cells in the white matter remained unaltered.

Iba1 immunoreactivity is unaltered in cingulate white matter in schizophrenia and bipolar disorder

Next, we wanted to explore whether the observed alterations in NeuN+ density in white matter were related to a change in the microglia population, because a recent study in multiple sclerosis suggests a potential link between microglial activation—a hallmark of the inflammatory response in brain—and increased white matter neuron densities [188]. To this end, we graded immunoreactivity for the microglial marker, Iba1 (see Methods), on a scale of 0-4 in all schizophrenia and bipolar subjects, together with a subset of controls (**Supplemental Figure 2A**). We found no significant difference in

Iba1 immunoreactivity between groups, nor was it associated with NeuN+ density in white matter (**Supplementary Figure 2B,C**). We conclude that increased presence of NeuN+ neurons in white matter of a subset of schizophrenia and bipolar subjects is not associated with microglial activation.

NeuN+ neuronal density in white matter decreases during development

Interstitial white matter neurons of adult brain are thought to be vestiges of the subplate, a transient structure of the developing brain that shows a progressive involution starting in the 3rd trimester [193]. Previous studies utilized Nissl, Golgi and acetylcholinesterase staining to determine developmental changes in subplate neuronal densities subjacent to visual, somatosensory, motor, and prefrontal cortices [181, 194]. While there is general consensus that neuronal density in subcortical white matter declines during the first year of postnatal life, the specific timing of this event varied depending upon the cell markers used. Presently, it is not known whether NeuN-immunoreactive white matter neurons undergo changes in numbers or densities during development. Therefore, we monitored the temporal course of NeuN+ neuronal density in postmortem specimens of a new postmortem cohort ranging in age from 40 weeks of gestation to 51 years of age (**Table 1**). To avoid variability of frontal lobe anatomy as potential confound, we focused on white matter space underneath the lobe's rostral pole, which is unambiguously identifiable in both young and old brain. There was a steep decline in NeuN+ densities during the first year of life, after which the density plateaued and remained relatively

constant throughout childhood, adolescence, and adulthood (**Fig. 5**). The mean NeuN+ density for the 10 subjects > 1 year (14.6 ± 6.42 cells/mm^2) demonstrated a 76.7% decrease as compared to the mean density of 4 subjects < 1 year (62.7 ± 29.6 cells/mm^2); this difference was significant ($U = 0$, $p = 0.005$; 1 degree of freedom).

DISCUSSION

We report that approximately 25% of subjects diagnosed with bipolar disorder or schizophrenia show an elevated density of NeuN-immunoreactive cells in cingulate white matter. These changes were observed both by 2- and 3-dimensional counting techniques. The alteration was specific, because (i) no association between NeuN+ densities in gray and white matter was observed and (ii) the density of a different population of white matter neurons, immunoreactive for NRG, in the disease cohorts was not significantly different from controls. Increased NeuN+ density in cingulate white matter was paralleled by a similar increase in dorsolateral prefrontal white matter, suggesting that these cellular alterations affect widespread portions of the frontal lobe. Additionally, the density of NeuN+ neurons in white matter during normal development was found to decline during the first year of postnatal life, but remained stable thereafter, suggesting that the observed alterations in the schizophrenia and bipolar cohorts may reflect a disturbance during the late prenatal or early postnatal period. In multiple sclerosis, chronic

lesions within subcortical white matter harbor increased numbers of neurons [188] in conjunction with increased microglia, but, in the present study, there was no association between these two white matter cell populations.

The fact that NeuN+ neuronal density was increased in cingulate white matter not only in schizophrenia, but also in bipolar disorder, was unexpected because two earlier studies on the dorsolateral prefrontal cortex had reported negative findings [169, 175]. However, the overall smaller sample sizes in those studies may have precluded the recognition of a subgroup of approximately 20-30% of affected subjects that, according to the present study, show a robust elevation in white matter neuron numbers. In either case, the findings presented here add to the emerging evidence that neurodevelopmental mechanisms play a role in some cases with bipolar illness [195] and, moreover, that such mechanisms may represent a common underlying pathophysiology of psychotic spectrum disorders.

The mechanism by which this increase in white matter neurons in psychosis occurs is unclear, but failure of neuronal migration or decreased cell death could be involved [165-178]; the latter hypothesis adds to the notion of faulty apoptosis in some cases with psychosis [196]. It is unlikely that the increase in NeuN+ cells in white matter of clinical cases is due to newly generated neurons later in life, because—thus far—evidence for neurogenesis in postnatal human cerebral cortex is lacking [197].

Strikingly, a number of the emerging susceptibility genes and pathways for schizophrenia and bipolar disorder—including *Disrupted-in-schizophrenia*

1 (*DISC1*) and the *Neuregulin 1 (NRG1)*-erbB4 tyrosine kinase—are important regulators of migration, positioning, and formation of functional circuits of immature neurons during the development of cerebral cortex and other forebrain structures [198, 199]. As mentioned above, the 22q11.2 deletion syndrome (22qDS), a genetic cause for bipolar disorder and schizophrenia [163]—is associated with heterotopias and numerous ectopic neurons scattered throughout the white matter of the frontal lobe [164]. Therefore, further study of these risk genes and genetic syndromes may provide important insights into the mechanisms underlying white matter abnormalities in psychotic disorders.

The pathophysiological consequences of increased white matter neuron density in cingulate and prefrontal cortices remain unknown. Notably, white matter neurons surviving preprogrammed cell death during development are known to become functionally integrated with the circuitry of the mature cortex [200] and, furthermore, remain interconnected with the thalamus [201], suggesting that any excess of white matter neurons in schizophrenia and bipolar disorder could indeed impair cortical and subcortical circuitries. It is intriguing to speculate that elevated neuronal numbers in adult white matter reflect a defect present from the prenatal period onwards, because a subset of the neurons residing beneath the developing cortical plate in the fetal brain are essential for orderly development of the GABAergic circuitry in the overlying cortex [202]. Therefore, the dysfunction of

inhibitory interneurons—a core component in the pathophysiology of some types of psychosis [203, 204]—ultimately may have its roots in a neurodevelopmental defect of the future white matter.

Acknowledgements

The authors would like to thank Dr. F.M. Benes, Mr. George Tejada, and Mr. Louis Fernandez from the Harvard Brain Tissue Resource Center at McLean Hospital, Belmont MA; Dr. E.G. Jones, Dr. W.E. Bunney Jr, and Mr. Phong Nguyen from the Center for Neuroscience at the University of California at Davis; Dr. R. Zielke and Mr. R. Johnson of the Brain and Tissue Bank for Developmental Disorders, University of Maryland, for providing brain tissues, and Dr. A. Chang and Dr. B.D. Trapp for generously providing us with Iba1 antibody. Supported by grants from the National Institute of Mental Health.

Table 1. Postmortem Cohorts

Diagnosis	*N*	Age Years	PMI Hours	Gender M/F	Hemisphere L/R	APD %	MS %	ADD %
Cingulate Cortex (BA 33)								
Bipolar	15	74.3 ± 2.29	22.5 ± 2.40	4/11	9/6	80% (4/5)	60% (3/5)	40% (2/5)
Schizophrenia	22	67.8 ± 2.94	20.6 ± 1.71	9/13	8/14	64% (7/11)	36% (4/11)	36% (4/11)
Control	45	69.8 ± 1.87	23.2 ± .85	24/21	21/24	0	0	0
Cingulate Cortex for Nuclei Counts								
Schizophrenia	6	69.5 ± 6.53	24.0 ± 2.44	2/4	3/3	80% (4/5)	40% (2/5)	20% (1/5)
Control	5	71.8 ± 6.68	21.5 ± 4.10	2/3	2/3	0	0	0
Dorsolateral Prefrontal Cortex (BA 9)								
Schizophrenia	6	69.2 ± 6.60	21.5 ± 2.52	3/3	4/2	100% (4/4)	50% (2/4)	25% (1/4)
Control	6	66.7 ± 6.10	25.4 ± 2.67	3/3	3/3	0	0	0
Prefrontal Cortex (BA 10)								
Perinatal/infant	4	40 ewg–9 months[a]	15 ± 6.58	2/2	4/0			
Child and adult	10	2–51 years[a]	15.7 ± 6.06	6/4	9/1			

Age and PMI expressed as mean ± standard error.

ADD, antidepressant drugs (Zoloft, Paxil, Wellbutrin, Effexor, trazodone, remeron); APD, antipsychotic drugs (typical and atypical); BA, Brodmann area; ewg, estimated weeks gestation; F, female; L, left; M, male; MS, mood stabilizers (lithium, depakote); PMI, postmortem interval; R, right.

[a]Age range.

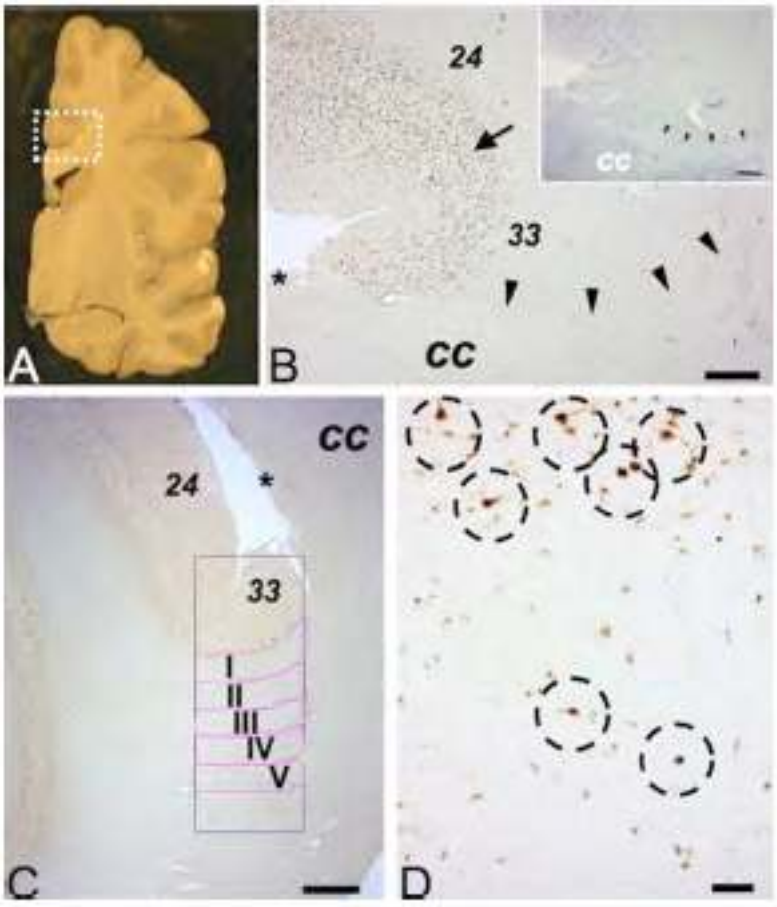

Figure 1: Gray and white matter structures surrounding cingulate cortex. (**A**) Representative coronal slab of a hemisphere (postmortem), rectangle outlines approximate position and size of tissue block destined for present study. (*Image courtesy of Mr. L. Fernandez, Harvard Brain and Tissue Resource Center.*) (**B**) Parallel sections stained for NeuN immunoreactivity or Nissl (insert) showing cingulate cortex with dorsal BA24 and ventral BA33, transition marked by arrow. See text for details. The border between the cingulate white matter (including cingulum bundle) and the fiber tracts of bordering corpus callosum (cc) is demarcated by arrowheads. (**C**) Digitized image from region-of-interest, including the position of counting frame and white matter compartments I-V each 500 micron deep and 2000 microns wide (see Methods). * in **B,C** marks dorsal line of corpus callosum with induseum griseum. (**D**) Higher resolution image from superficial white matter bordering cingulate cortex, showing several NeuN+ neurons (marked by dotted circles), including two cells completely surrounded by WM tissue (bottom). Size bars (in μm), (B) 500, (C) 1000 and (D) 100.

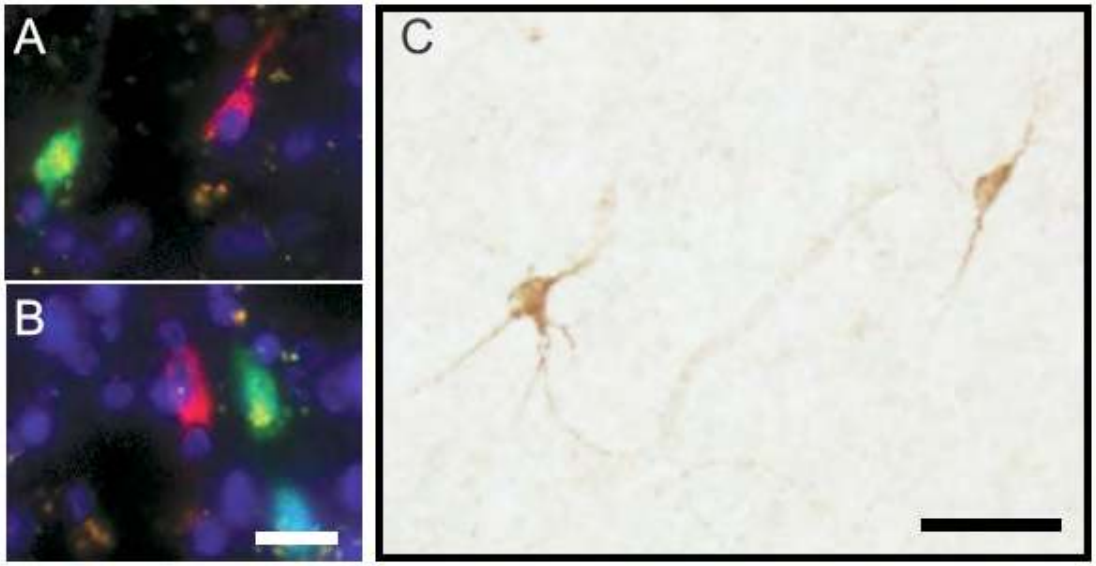

Figure 2: NeuN and NRG1α (NRG) immunoreactivity define two non-overlapping neuronal subpopulations. (**A, B**) Digitized images from cingulate white matter sections triple-stained with the nucleophilic dye, DAPI (blue), and anti-NeuN (green) and anti-NRG (red) antibodies, showing both NeuN+ and NRG + neurons, but no double-labeled cells. (**C**) Representative image from white matter of section processed for NRG immunoreactivity with DAB/peroxidase labeling (brown), showing neurons with robust staining of cytoplasm and dendrites. Size bars: (A,B) 20 μm, and (C) 50 μm.

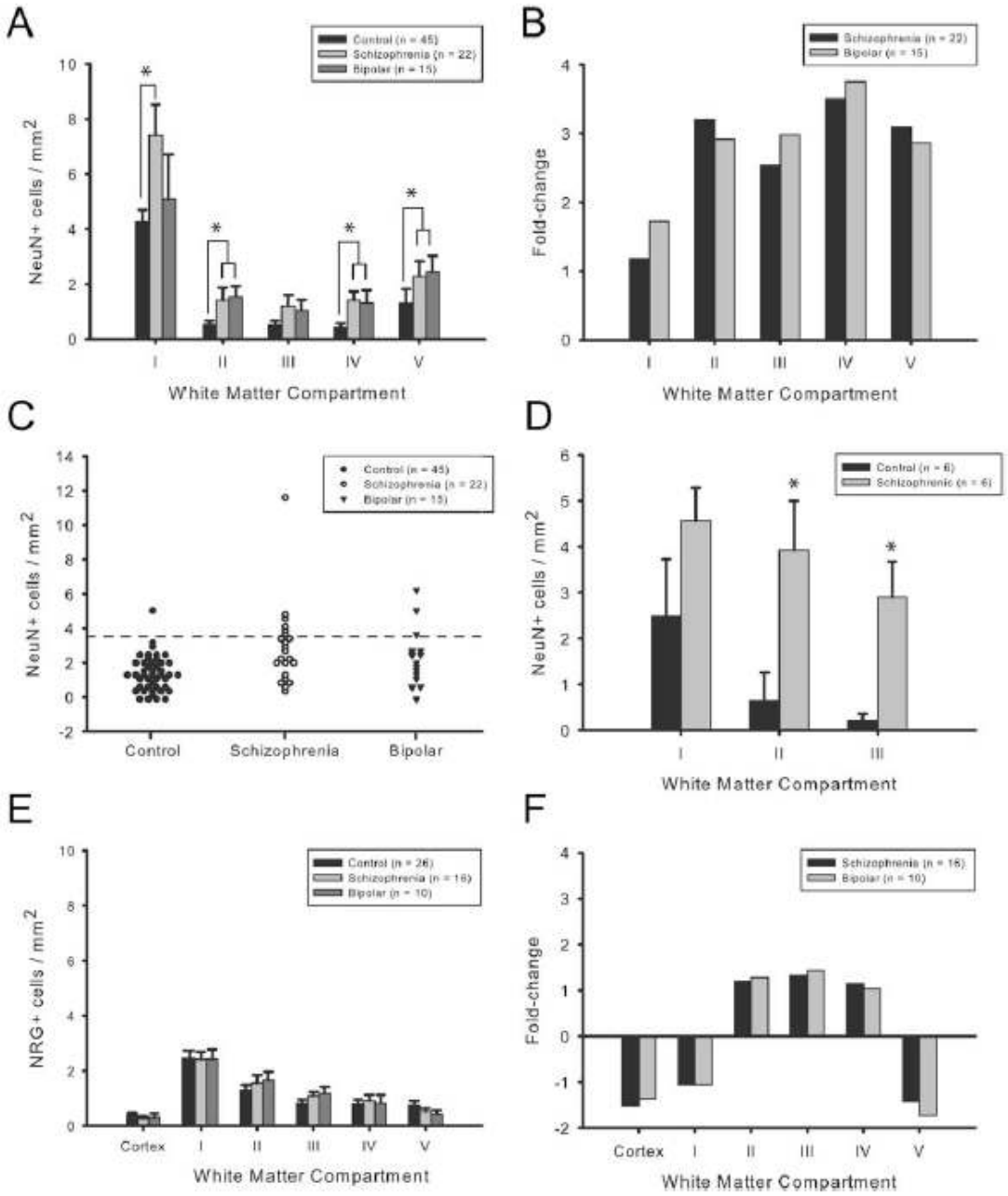

Figure 3: Increased NeuN+ neuronal density in white matter in schizophrenia and bipolar disorder. (**A**) NeuN+ neuronal density (presented as cells/mm^2, y-axis) in white matter compartments I-V (x-axis) beneath cingulate cortex of controls (N = 45, black), schizophrenia (N = 22, light gray), and bipolar disorder (N = 15, dark gray). Notice decline in NeuN+

neuronal density in white matter > 500 micron apart from overlying cortex (compartments II-V). Also notice higher overall densities in the two disease groups, as compared to controls. (**B**) Fold-change in NeuN+ neuronal densities in white matter compartments of schizophrenia (black) and bipolar subjects (gray), relative to control cohort. A -2-fold change is equivalent to a 50% decrease. (**C**) Frequency distribution of NeuN+ cell densities in cingulate white matter of the 3 cohorts, as indicated. Dotted line demarcates second standard deviations above the mean from controls. (**D**) NeuN+ neuronal density in the superior frontal gyrus white matter of 6 schizophrenia and 6 control subjects; the 6 clinical cases also showed increased NeuN+ density in the cingulate (see Results). (**E**) NRG+ cell densities, including (**F**) fold-change from controls, in cingulate cortex and white matter beneath BA33 of schizophrenia and bipolar subjects, as indicated (control N = 26; schizophrenia N = 16; bipolar N = 10). Notice that fold-changes in NRG+ neuronal densities in the clinical cohorts are < 2 from controls.

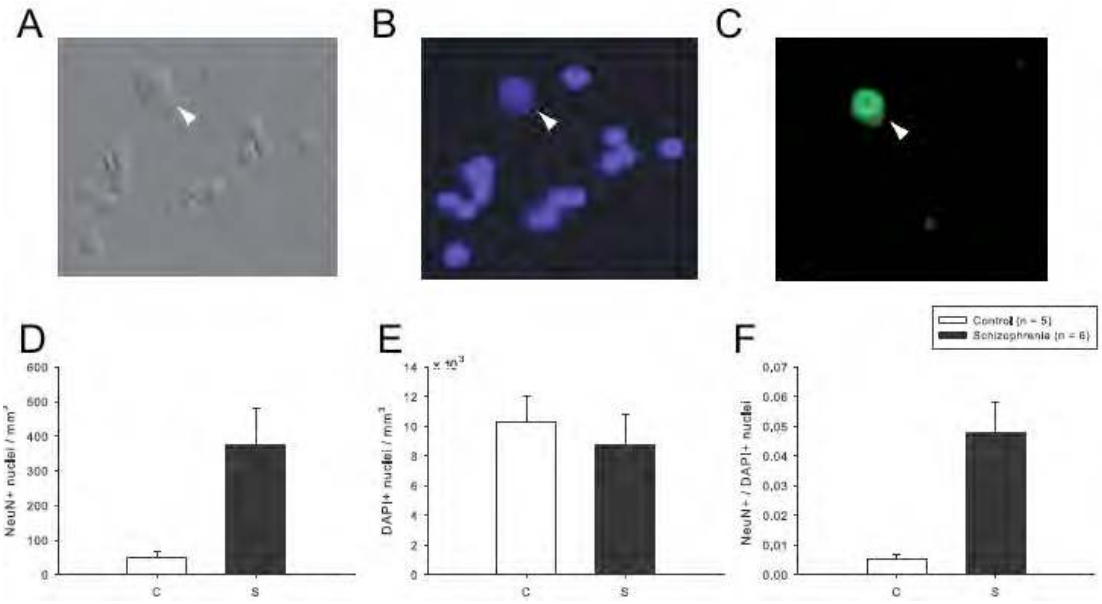

Figure 4: Isolation and quantification of nuclei from cells residing in white matter. (**A-C**) Representative digitized photomicographs from purified nuclei extracted from cingulate white matter (see Methods). (**A**) Differential Interference Contrast (DIC), (**B**) DAPI nucleophilic dye counterstain, and (**C**) NeuN immunoreactivity. Arrow demarcates nucleus of NeuN+ white matter neuron, notice comparatively larger size and the prominent nucleolus. Bar in (**C**) = 20 μm. (**D-F**) Bar graphs showing numbers of (**D**) NeuN+ and (**E**) DAPI stained nuclei per mm^3 white matter, and (**F**) proportion of NeuN+ nuclei in 6 schizophrenia and 5 control subjects (see Results). Data expressed as mean ± S.E.M.

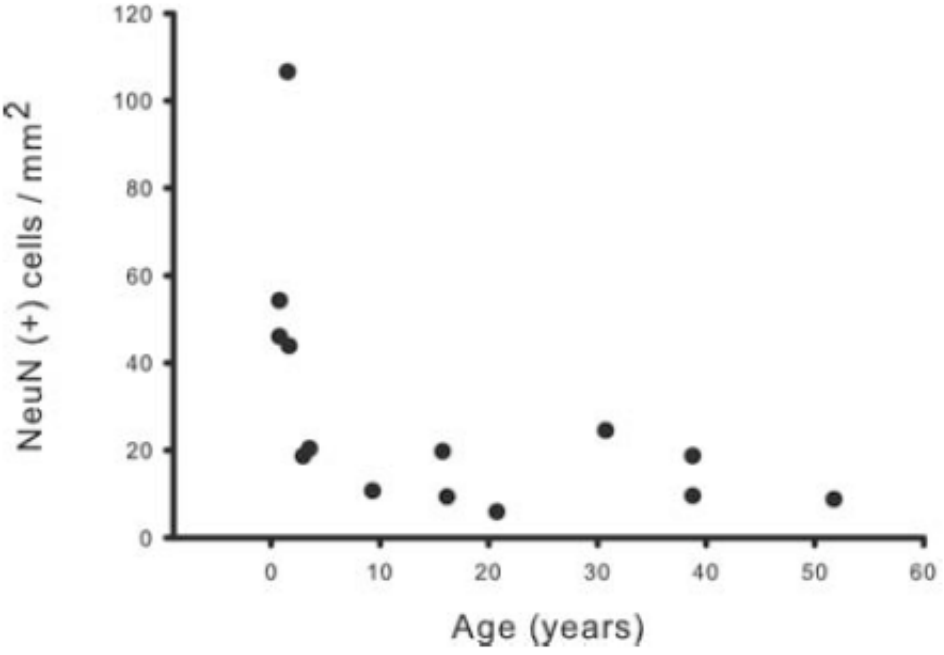

Figure 5: White matter NeuN+ neuronal density demonstrates an age-associated decline during development. Age (in years) was plotted against overall NeuN+ density (cells/mm^2) for each of the 14 subjects in the developmental cohort. Notice the steep decline in density during the first postnatal year.

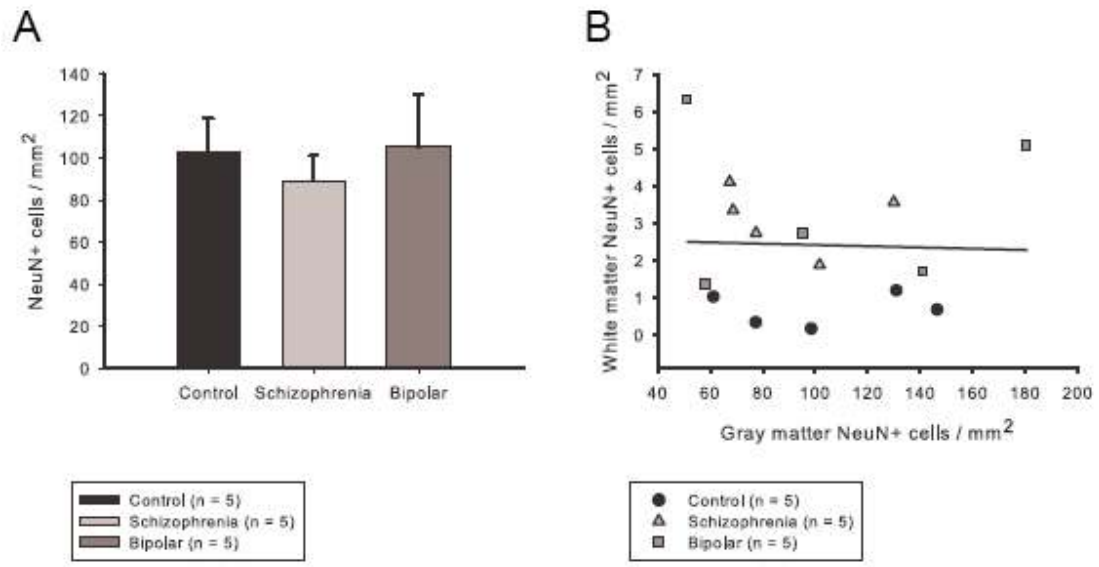

Supplemental Figure 1: NeuN+ neuronal density is unaltered in gray matter in schizophrenia and bipolar disorder. (**A**) NeuN+ neuronal density (presented as cells/mm2, y-axis) in BA33 gray matter of controls (N = 5, black), schizophrenia (N = 5, light gray), and bipolar disorder (N = 5, dark gray) subjects. There was no significant difference in NeuN+ neuronal density between diagnostic groups. (**B**) Correlation between NeuN+ neuronal densities in gray matter (x-axis) versus white matter (y-axis) for control, schizophrenia, and bipolar subjects. Notice that there was no appreciable correlation between gray and white matter NeuN+ neuronal densities (r = 0.0013).

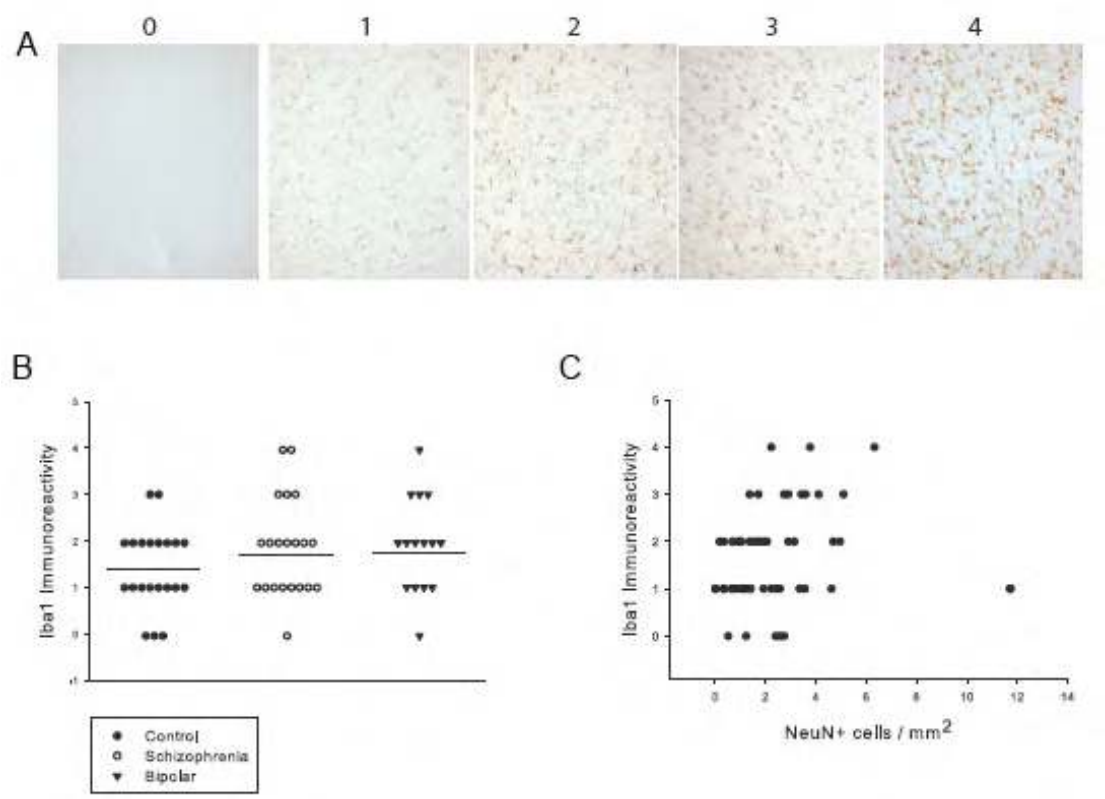

Supplemental Figure 2: Iba1 immunoreactivity is unaltered in cingulate white matter in schizophrenia and bipolar disorder. (**A**) Digitized images from cingulate white matter processed for Iba1 immunoreactivity with DAB/peroxidase labeling, depicting the grading scale used for assessment of microglia. 0 = indistinguishable from background; 1 = occasional fiber staining; 2 = numerous fibers and occasional cell bodies; 3 = numerous fibers and cell bodies; 4 = intensely stained fibers and cell bodies. (**B**) Frequency distribution of Iba1 immunoreactivity levels for control (N = 21), schizophrenia (N = 22), and bipolar disorder (N = 15) subjects. Note that the mean Iba1 immunoreactivity levels were not significantly different between the 3 diagnostic groups. (**C**) Correlation between Iba1 immunoreactivity levels and NeuN+ neuronal densities in white matter. There was no appreciable correlation between these two cell populations.

Study	Cohort	Brain region	Marker & counting	White matter (WM) space examined	Disease-specific alterations
Akbarian et al (1993a)	Control 5 Schizophr. 5	Frontal lobe, superior frontal gyrus (BA 9)	NADPH-d 2-dimens.	WM space 0 - 4.8 mm beneath cortex divided into six 0.8 mm wide bins.	**3 out of 5 cases showed significant increase** in one or more deeper WM compartments
Akbarian et al (1993b)	Controls 7 Schizophr. 7	I) Hippocampus and entorhinal ctx. II) Temporal neocortex (BA 21)	NADPH-d 2-dimens.	I) **Lateral temporal neocortex**: Three 1.0 mm compartments II) **Pre-/Parasubiculum**: Two 1.0 mm compartments. III) **Entorhinal cortex**: Two 1.0 mm compartments.	I) **45-90% increase** in NADPH-d neuron density in lateral temporal WM, 1-3 mm beneath cortex. II) No alterations in WM space of hippocampus and entorhinal cortex.
Akbarian et al. (1996)	Controls 20 Schizophr. 20	Frontal lobe, middle frontal gyrus (BA 46)	a) MAP2-ir, b) NF-H, ir c) NADPH 2-dimens.	WM space beneath cortex divided into six 1.0 mm wide bins.	**Altered distribution in schizophrenia** cohort due to deficits in superficial bins and **increased density in deep WM**. (Effect primarily due to 7 out of 20 schizophrenia cases.)
Anderson et al. (1996)	Controls 5 Schizophr. 5	Frontal lobe, middle frontal gyrus (BA9/46)	MAP2-ir, 2-dimens.	WM space 0-4.8 mm beneath cortex divided into six 0.8 mm wide bins.	**44% increase** in MAP2+ neuron density in schizophrenia; significant changes confined to WM < 3.2mm beneath gray matter.
Kirkpatrick et al. (1999)	Controls 9 Schizophr. 9 *Deficit S. 3* *Non-deficit S. 6*	Parietal lobe (BA 39)	MAP2-ir, 3-dimens.	WM space < 2.25 mm beneath gray matter at depth of sulcus.	**115% increase** in MAP2+ neuron density in deficit syndrome schizophrenia.
Beasley et al. (2002)	Controls 15 Schizophr. 15 Bipolar Dis. 15 Major Dep. 15	Frontal lobe (BA9/46) Middle frontal sulucs	MAP2-ir, 2-dimens.	WM space beneath cortex divided into five 0.5 mm wide bins.	No significant differences between control and psychiatric groups.
Rioux et al (2003)	Controls 15 Schizophr. 41	Anterior parahippo-campal gyrus	MAP2-ir, 2-dimens.	Measured distance of all neurons to closest gray/white boundary; cells were then grouped into 0.03 mm bins.	Altered neuronal distribution, with more MAP2+ neurons **located in deeper WM** in schizophrenia.
Eastwood & Harrison (2003)	Controls 14 Schizophr. 12	Temporal lobe, Sup.temporal gyrus. (BA 22)	NeuN-ir, 2-dimens.	WM space < 1.5 mm beneath gray matter.	**16% increase** in NeuN+ neuronal density in superficial WM in schizophrenia. (Effect mainly due to 4 subjects with negative syndrome schizophrenia.)
Kirkpatrick et al., (2003)	Controls 5 Schizophr. 7 *Deficit S. 3* *Non-deficit S.4*	Frontal lobe (BA 46)	MAP-2 ir., 3-dimens.	WM space < 2.5 mm beneath gray matter.	**60% increase** in MAP-2 neurons in schizophrenia subjects with deficit syndrome.
Molnar et al (2003)	Controls 18 Bipolar Dis. 8 Major Dep. 10	Frontal lobe (BA 9)	NADPH-d Enzyme 2-dimens.	WM space beneath cortex divided into six 1.0 mm wide bins.	No significant differences between cases and controls.

Ikeda et al., (2004)	Controls 6 Schizophr. 13 *Disorgan. 7* *Paranoid 6*	Frontal lobe (BA 9)	NPY-ir, 2-dimens.	WM space divided into 0-0.8 and 0.8 – 1.6 mm beneath gray matter.	**23% increase** in proportion of NPY+ neurons in the deeper WM of disorganized schizophrenia subjects.
Eastwood & Harrison (2005)	Controls, 12 Schizophr. 11	I) Frontal lobe (BA 9/46) II) Parahippoc.gyrus	NeuN-ir, 2-dimens.	Superficial WM space < 2 mm beneath gray matter.	**20% increase** in NeuN+ neuronal density in superficial WM of frontal lobe of schizophrenia; Effect mainly in 4 schizophrenia subjects
Bertram et al. (2007)	Controls, 22 Schizophr. 22 Bipolar Dis. 5 Major Dep. 7	I) DLPFC II) Orbitofrontal gyrus III) Cingulate cortex	NRG-1α-ir, 2-dimens.	Not specified.	I) **−50% reduction** in NRG-1α-ir neuronal density in superficial & deep WM in schizophrenia. II) **−60% reduction** in gray matter in schizophrenia and **−50%** in major depression.

Supplemental Table 1: Overview on previous studies of white matter neurons in schizophrenia and affective disorder subjects. Red shading demarcates studies demonstrating significant increases in the clinical cohorts.

Supplemental Methods

Immunohistochemistry: Given the large number of specimens included in this study (N = 96), it was not possible to process the entire cohort simultaneously; however, to reduce inter-assay variability, multiple sets of randomly mixed cases and controls were processed in parallel, using the same antibodies and reagents. Incubation times were kept constant across the entire study. Adjacent sections were stained for (i) Nissl, or immunoreactivity for (ii) Neuron-specific nuclear protein (NeuN), (iii) Neuregulin 1 alpha (NRG), (iv) Ionized calcium-binding adaptor molecule 1 (Iba1). Sections were incubated in mouse anti-NeuN antibody (Upstate; Billerica, MA) diluted 1:500, rabbit anti-NRG antibody (Lab Vision; Fremont, CA) diluted 1:200, or mouse anti-Iba1 antibody 1:500 (a generous gift from Dr. A. Chang and Dr. B.D. Trapp) overnight and processed using a standard protocol for immunoperoxidase-based labeling (Vector Laboratories; Burlingame, CA). For two subjects, double-immunofluorescence was performed for NeuN and NRG in conjunction with AlexaFluor 488 and 594-conjugated secondary antibodies (Invitrogen; Carlsbad, CA). For a subset of 6 cases and 6 controls, NeuN immunohistochemistry was conducted for the superior frontal gyrus (BA9), using 5 μm thick sections from paraffin-embedded blocks.

Microscopy: Two-dimensional (2D) cell counts for NeuN or NRG immunostained sections were conducted under 1.25x and 20x objectives,

using an Olympus BX51 upright microscope in conjunction with a motorized stage and BIOQUANT Life Science software version 8.00.20. Under the 1.25x objective, the gray/white matter border along BA33 was demarcated, and the white matter space (subcortical white matter and cingulum bundle but excluding the corpus callosum) was divided into compartments each 500 microns deep and 2000 microns wide (**Fig. 1C**). After compartments were drawn, the NeuN+ neurons were counted using the 20x objective. A cell was defined as NeuN+ if immunoreactivity was detectable in the nucleus with weaker stained neuron-like cytoplasm or processes visible (**Fig. 1D**). A cell was defined as NRG+ if cut through the level of nucleus with robust staining confined to cytoplasm and processes (**Fig. 2D**). For each specimen, NeuN+ and NRG+ cells were counted in each of the 5 white matter compartments in two tissue sections per marker by a counter blind to diagnosis. In BA9, sampling was limited to the upper 3 white matter compartments, because we could not rule out what white matter greater than 1500 micron from overlying cortex was potentially in closer proximity to surrounding cortex not present in the plane of the section. To assess potential differences in cell size between diagnostic groups, average somal area of NeuN+ neurons in cingulate white matter was estimated by tracing 5 cells per subject using Bioquant software and 20x magnification (n = 5 per group). All NeuN counts were performed by Y.G. NRG-counts and microglial ratings (see below) were done by C.C. and S.A., and no significant differences between raters were observed. For the

NeuN counts, intra-rater reliability (counting the same subject, but not necessarily the same section, twice) approached 90**%.**

In addition, NRG+ cells were counted in the gray matter of BA33; NeuN+ cells were counted in BA33 gray matter for a subset of subjects (n = 5 for each of the 3 cohorts). For the NeuN counts, the clinical cases were chosen randomly, and then matched to controls with similar age and postmortem interval, and same sex. As in the white matter, a two-dimensional counting method was used. For each section, a rectangular box 2000 microns wide was placed across the full vertical thickness of BA33 and the numbers and density of NeuN+ or NRG+ neurons were calculated per mm^2.

Finally, all cases (bipolar = 15; schizophrenia = 22) and a subset of controls (n = 21) were immunostained with the anti-microglial antibody, Iba1, and blindly graded as 0 (staining indistinguishable from background), 1 (occasional fiber staining), 2 (numerous fibers and occasional cell bodies), 3 (numerous fibers and cell bodies), and 4 (intensely stained fibers and cell bodies) (**Supplemental Figure 2**).

Isolation and quantification of nuclei in cingulate white matter: For a subset of subjects (**Table 1**), a column of white matter adjacent to the gray/white border of the ventral portion of BA24 from frozen cingulate was isolated with a metal borer with a diameter of 3.15 mm and the length measured with calipers. The borer was placed perpendicular to the

gray/white matter border after visual inspection ensured that the border had not shifted on the opposite of the block. Subsequently, tissue was dounced in lysis buffer [205], layered onto a sucrose cushion, and ultracentrifuged at 28,000 rpm at 4°C for 2.5 hrs. The nuclei pellet was dissolved in 500 µl PBS, incubated with 200 µl antibody solution (anti-NeuN, 1:500; anti-mouse AlexaFluor 488) for 45 min at 4°C, and fixed with 70 µl 10% formalin. A 5 µl aliquot was removed, diluted with 495 µl PBS, and ten 5 µl aliquots from this solution applied to 10 separate slides and coverslipped with Vectashield Mounting Medium with the nucleophilic dye, DAPI.

The total number of NeuN+ and DAPI+ nuclei was counted for each the 10 slides and then averaged. The following formula was used to estimate the total number of NeuN+ and DAPI+ nuclei per tissue column:

$$[(\#\ \text{NeuN+ or DAPI+ nuclei counted} / 5\ \mu l)\ (500\ \mu l) / 5\ \mu l] \times 770\ \mu l$$

To determine the number of nuclei per mm tissue cubed (mm^3), the estimated total number of nuclei was divided by the volume of tissue for that particular sample.

Statistics: For each subject, NeuN+ and NRG+ cell densities were calculated for each white matter compartment as cells per square millimeter and the densities from the two slides per subject averaged. A Kruskal-Wallis one-way ANOVA was used to compare NeuN+ or NRG+ cell densities

between bipolar, schizophrenia, and control groups. The Dunn's test was utilized to conduct post-hoc comparisons between diagnostic categories. Additionally, presence or absence of NeuN+ cells in deeper white matter (compartments III-V) were determined for each subject and each patient group was compared to the control group with Pearson chi-square. Effects of potential confounds on overall white matter NeuN density— including postmortem interval (PMI), subject age, gender, hemisphere, and medication status—were examined by Pearson correlation, Mann-Whitney U-test, and also with ANCOVA for a mixed model by REML (restricted estimation by maximal likelihood).

Appendix III:

DNA Methylation Changes in Schizophrenia and Bipolar Disorder

Caroline M. Connor[1,2], MA and Schahram Akbarian[2*], MD, PhD

[1] Program in Neuroscience, Graduate School of Biomedical Sciences, [2] Department of Psychiatry, University of Massachusetts Medical School, Worcester MA 01604

Epigenetics 3(2):55-8 March-April, 2008

Abstract

The etiology of the major psychotic disorders, including schizophrenia and bipolar disorder, remains poorly understood. Postmortem brain studies have revealed altered expression of multiple mRNAs, affecting neurotransmission, metabolism, myelination and other functions. Epigenetic mechanisms could be involved, because for a limited number of genes, the alterations on the mRNA level were linked to inverse DNA methylation changes at sites of the corresponding promoters. However, results from independent studies have been inconsistent, and when expressed in quantitative terms, disease-related methylation changes appeared to be comparatively subtle. A recent study identified approximately 100 loci with altered CpG methylation in schizophrenia or bipolar disorder, the majority of which were gender-specific. Additional work will be necessary to clarify the origin and timing of these methylation changes in psychosis, and to determine the specific cell types affected in CNS.

Aberrations in DNA methylation have been implicated in a wide variety of brain disorders. Examples include (1) mental retardation syndromes resulting from certain imprinting disorders (example: Angelman and Prader-Willi syndromes), [206, 207] triplet repeat expansions (Fragile X syndrome), [208, 209] mutations in DNA methyltransferase encoding genes (ICF syndrome) [210] and (2) a subset of gliomas [211-214] and neuroectodermal [211, 215, 216] tumors which show promoter hypermethylation of tumor suppressor genes. More

recently, however, DNA methylation has been studied in the context of a very different category of brain malady: the major psychotic disorders, including schizophrenia and bipolar disorder, which are defined by delusions, hallucinations, and mood alterations. While a variety of radiological, histological, and molecular alterations have been observed in schizophrenic [217] and bipolar brain [218], a definitive diagnostic neuropathology or molecular phenotype is lacking. The etiologies of these disorders are complex, demonstrating concordance rates of less than 70% in monozygotic twins, non-Mendelian inheritance patterns, and sexual dimorphism [219]; these features, obviously, provide fertile ground for "epigenetic" disease models. Of note, the molecular pathology of the major psychotic disorders is thought to involve alterations in gene expression, including a down-regulation of transcripts involved in cellular metabolism [220-222], inhibitory neurotransmission [96], and myelination and other oligodendrocyte functions [223, 224]. Therefore, it is tempting to speculate that at least some of these transcriptional defects could be due to aberrant increases in CpG methylation and repressive chromatin remodeling at 5' regulatory sequences. However, to date, DNA methylation has only been assayed for a small number of genes (namely, *REELIN* [15, 225-227], *COMT* [228-230], *DRD2* [231], and *SOX10* [232]) in postmortem brain of subjects diagnosed with schizophrenia or other major psychoses.

Recently, Mill and colleagues published the first comprehensive methylation study of major psychosis [233] in which they assayed methylation at

approximately 7800 loci — primarily within CpG islands of gene promoter regions — in frontal cortex of a comparatively large set of postmortem brain samples (35 schizophrenia, 35 bipolar, and 35 control subjects). Based on figure 2 of Mill *et al.*, approximately 100 loci demonstrated significant disease-related methylation changes. Interestingly, a subset of the loci that were hypermethylated showed altered gene expression in previous studies employing some of the same brain samples studied by Mill *et al.*, with approximately an equal portion of up- and down-regulated transcripts. That schizophrenia and bipolar disorder showed methylation changes of similar magnitude and direction for a number of loci resonates with some of the clinical, genetic, and neurochemical features common to both disorders [234]. Strikingly, the list of genes showing altered methylation in Mill *et. al.* includes at least one locus, *DYSBINDIN*, which confers genetic risk for psychosis [235-237]. This is interesting, because information regarding interactions between sequence polymorphisms and epigenetic modifications in human brain is available only for very few psychosis genes, including *BDNF* [233], *GAD1* [86], and *5-HT2A* [238].

Perhaps one of the most intriguing discoveries by Mill *et al.* [233] was the finding that the vast majority of disease-related DNA methylation changes differentially affected male and female patients. At present, straightforward explanations for this puzzling phenomenon are lacking because the genes involved are located on autosomes and, until now, not known to show sex-specific regulation. It remains to be determined whether or not these loci are differentially

methylated or show monoallelic expression in normal brain, and which, if any, of the corresponding gene transcripts are differentially expressed in female and male brain. Sex steroids may play a role; estrogen, for example, is an important modulator of frontal lobe function in females [239, 240], and there is ample evidence that the hormone is involved in the regulation of chromatin structures, including DNA and histone methylation, at a number of gene promoters [219, 241, 242]. Furthermore, gender-specific chromatin alterations in schizophrenia may extend beyond the level of DNA methylation —both androgens and estrogens are known to interact with chromatin remodeling complexes [219, 243-245] and recent evidence suggests that promoter-associated histone methylation changes at select GABAergic gene loci may be more prominent in female schizophrenia subjects, compared to their male counterparts [13]. Given the sexual dimorphism of schizophrenia and bipolar disorder — including differences in rate of occurrence, symptoms, and time course — the differential methylation changes observed in male and female patients should not come as a surprise.

It is noteworthy that absolute methylation differences between psychosis and control samples were relatively small in the Mill *et al.* study [233], even for some of the more significant loci (for example, 17% vs. 25% for *WDR18*). Therefore, DNA methylation changes in psychosis appear to be more subtle compared to those observed in brain neoplasia or some of the above-mentioned mental retardation syndromes. These features emphasize that DNA methylation analysis in psychosis samples is best approached by quantitative methodology,

for which bisulfite sequencing remains the gold standard [246]. Given this lack of dramatic methylation changes in schizophrenia or bipolar brain, it comes as no surprise that earlier studies reporting positive findings (*REELIN* [15, 225], *COMT* [228]) were not consistently replicated in subsequent work [226, 227, 229, 230, 233]. Some of these inconsistencies may be due differences in methodology, specific CpG dinucleotides assayed, brain regions examined, and clinical populations from which the postmortem specimens were obtained. Furthermore, it must be noted that for these genes, the *degree* of DNA methylation may not necessarily correlate with functional consequences (i.e., decrease in mRNA transcript levels); rather, the specific location of the methylated CpG dinucleotide — for example, within a transcription factor binding site — may be more critical for mediating transcriptional repression.

In addition to the overall subtle nature of these psychosis-related alterations, the interpretation of DNA methylation studies on postmortem brain is complicated by additional factors:

(1) To date, most methylation studies in brain have utilized DNA extracted from whole tissue homogenates. This represents a major confound, as different cell types are known to possess unique methylation patterns and brain tissue is comprised of multiple types of neurons, glia, and other cells. Moreover, specific sub-populations of cells within specific brain regions are thought to be affected in the psychotic disorders, such as parvalbumin-immunoreactive neurons [140, 247-250], oligodendrocytes [251-254], and astrocytes [182, 255, 256]. Thus, if

alterations in DNA methylation within specific cell populations do indeed play a role in the pathoetiology of psychosis, some methylation changes may be “diluted” — or even undetectable — due to the averaging of methylation signals from a heterogeneous pool of cells. Furthermore, neuron-to-glia ratios show considerable variation during the course of normal maturation and aging [257]. This is not a trivial point, because there is evidence that, for select gene loci, the DNA methylation signal from postmitotic neurons differs considerably from tissue homogenate. Specifically, when DNA methylation was selectively assayed for neuronal nuclei obtained from postmortem human brain, 4/10 loci showed age-related methylation changes similar to DNA from tissue homogenate, but 6/10 loci did not [258].

(2) Furthermore*, in vitro* studies in cell culture suggest that DNA methylation is dynamically regulated—on the scale of minutes to hours—in response to DNA methyltransferase inhibitors [259, 260] and depolarization [146]. Thus, it will be important to more fully elucidate how diverse environmental stimuli impact the regulation of DNA methylation in human brain, as these factors could potentially result in methylation changes unrelated to disease etiology. Indeed, recent studies have demonstrated that the DNA methyltransferases and methylation patterns in a variety of tissues, including CNS, are influenced by a variety of factors, including social environment [21, 261], ischemia [262], environmental toxins [263-265], nicotine [266], alcohol [267], psychostimulants [268, 269], and antipsychotic drugs [233, 270, 271].

However, the above-mentioned factors could also play a role in the pathogenesis of schizophrenia and bipolar disorder. Thus, it will be important to explore both the origin and timing of DNA methylation changes in schizophrenia and bipolar disorder: whether they arise from stochastic events during embryogenesis, are secondary effects of psychosis in the patient (or even in an affected parent), or reflect exposure to different environmental stimuli during subsequent development, maturation, and aging remains to be determined. The latter hypothesis gains credence from work by Fraga et. al. (2005) [272] which shows that methylation patterns of monozygotic twins become increasingly different with age; furthermore, twins who were raised apart demonstrated greater differences in DNA methylation patterns than those raised together. In addition to environmental influences, accumulating evidence suggests that epigenetic marks can be inherited across multiple generations [273-275], providing an alternative explanation for the aggregation of schizophrenia and bipolar disorder in families. However, to date, evidence for DNA methylation changes in germ cells of individuals diagnosed with major psychosis is lacking [233].

Therefore, while important issues remain to be resolved, including the origin of methylation changes in schizophrenia and bipolar disorder, ante- and postmortem confounds, and cellular heterogeneity of brain tissue, one can expect that epigenetic studies on human brain, such as the one undertaken by Mill *et al.* [233] will significantly advance our understanding of the molecular pathology underlying complex psychiatric disorders.

Acknowledgements

Supported by NIMH grant R01MH071476

Appendix IV:

DNA methylation in the human cerebral cortex is dynamically regulated throughout the life span and involves differentiated neurons

Kimberly D. Siegmund[1]*, Caroline M. Connor[2,3]*, Mihaela Campan[4], Tiffany I. Long[4], Daniel J. Weisenberger[4], Detlev Biniszkiewicz[5], Rudolf Jaenisch[5] , Peter W. Laird[4] and Schahram Akbarian[3#]

[1]Departments of Preventive Medicine and [4]Biochemistry and Molecular Biology, Keck School of Medicine, University of Southern California, Los Angeles, CA 90089-9176; [2] Program in Neurobiology, Graduate School of Biomedical Sciences and [3] Department of Psychiatry, University of Massachusetts Medical School, Worcester, MA 01604; [5]The Whitehead Institute for Biomedical Research, Nine Cambridge Center, Cambridge, MA 02142.

* These authors contributed equally to this manuscript.

PLoS ONE 2(9):e895 September, 2007

ABSTRACT

The role of DNA cytosine methylation, an epigenetic regulator of chromatin structure and function, during normal and pathological brain development and aging remains unclear. Here, we examined by MethyLight PCR the DNA methylation status at 50 loci, encompassing primarily 5' CpG islands of genes related to CNS growth and development, in temporal neocortex of 125 subjects ranging in age from 17 weeks of gestation to 104 years old. Two psychiatric disease cohorts—defined by chronic neurodegeneration (Alzheimer's) or lack thereof (schizophrenia)—were included. A robust and progressive rise in DNA methylation levels across the lifespan was observed for 8/50 loci (*GABRA2, GAD1, HOXA1, NEUROD1, NEUROD2, PGR, STK11, SYK*) typically in conjunction with declining levels of the corresponding mRNAs. Another 16 loci were defined by a sharp rise in DNA methylation levels within the first few months or years after birth. Disease-associated changes were limited to 2/50 loci in the Alzheimer's cohort, which appeared to reflect an acceleration of the age-related change in normal brain. Additionally, methylation studies on sorted nuclei provided evidence for bidirectional methylation events in cortical neurons during the transition from childhood to advanced age, as reflected by significant increases at 3, and a decrease at 1 of 10 loci. Furthermore, the DNMT3a *de novo* DNA methyl-transferase was expressed across all ages, including a subset of neurons residing in layers III and V of the mature cortex. Therefore, DNA methylation

is dynamically regulated in the human cerebral cortex throughout the lifespan, involves differentiated neurons, and affects a substantial portion of genes predominantly by an age-related increase.

INTRODUCTION

Epigenetic modification of chromatin, including DNA methylation at the sites of CpG dinucleotides, is a key regulator of gene expression, growth and differentiation in virtually all tissues, including brain [276-279]. Dysregulated DNA methylation, or methyl-CpG-dependent chromatin remodeling, is thought to underlie *ICF* syndrome (*I*mmunodeficiency, *C*entromere instability and *F*acial anomalies), Rett's disorder and other mental retardation syndromes [280, 281]. Furthermore, changes in methylation status at selected genomic loci may affect social cognition [282], learning and memory [283] and stress-related behaviors [21] and is believed to contribute to dysregulated gene expression in a range of adult-onset neuropsychiatric disorders, including autism, schizophrenia, depression and Alzheimer's disease [15, 225, 238, 284, 285]. Finally, there is strong evidence that aberrant methylation of tumor suppressor genes contributes to the molecular pathology of a subset of astrogliomas and other types of brain cancers [212, 286].

However, despite its clinical importance, the regulation of DNA cytosine methylation, particularly in the human brain, remains poorly understood. To date, there are no comprehensive studies which have monitored methylation at multiple loci during the course of brain development and aging, or in chronic psychiatric disease. Furthermore, all previous studies of DNA methylation in human or animal brain utilized tissue homogenates comprised of a highly heterogeneous mixture of neurons and glia [21, 225,

283, 287], or examined DNA methylation in subfractions of chromatin defined by site-specific histone modifications [13] and therefore it remains to be determined whether or not DNA methylation is dynamically regulated in terminally differentiated neurons.

Given this background, the present study was undertaken to provide a first insight into the dynamics of DNA methylation in the human cerebral cortex. Altogether, we examined 50 loci, mostly CpG islands within the 5' end of genes, during the course of development, maturation and aging. Additionally, we assessed the methylation status for these same loci in Alzheimer's disease and schizophrenia; the former condition is characterized by chronic neurodegeneration and the latter by widespread transcriptional and metabolic perturbations [288-290] in the absence of large scale loss of neurons. While disease-associated alterations were limited to 2/50 sequences in the Alzheimer's cohort of the present study, the majority of genomic loci, including genes implicated in neural development and CNS tumors, showed a striking age-associated increase in methylated CpGs. Furthermore, we show that DNA methylation is dynamically regulated in differentiated neurons during the transition from childhood to advanced age. Collectively, our results suggest that DNA methylation in the human cerebral cortex, including its neuronal constituents, is dynamically regulated across the full lifespan and potentially affects a substantial portion of the genome.

RESULTS

Four types of age-related DNA methylation profiles in the human cerebral cortex

Using a real-time PCR-based technique called MethyLight [291, 292], we analyzed DNA methylation at 50 loci, most of them representing promoter CpG islands of genes expressed in the cerebral cortex; a portion of these genes is also implicated in cancer biology (Supplemental Tables 1, 2). Most of the cancer-related genes included in this study show aberrant methylation in various types of neoplasia, including CNS tumors (Supplemental Table 1), and hence we were interested to monitor potential methylation changes within these genes during the course of normal brain development and aging. Other genes included in this study play a role in the molecular pathology of some cases diagnosed with schizophrenia and other psychiatric illness (e.g., *BDNF, DRD2, GABRA2, GAD1, HOXA1, NTF3*) or are linked to chronic neurodegeneration (*LDLR, PSEN1, S100A2*). We screened altogether 125 pre- and postnatal, child and adult samples of rostro-lateral temporal cortex, yielding 7,500 quantitative measurements (**Fig. 1**). Two of the CpG islands (*AR* and *FAM127A*) are from X-linked genes, which become methylated only on the inactive X-chromosome in females, and were included as internal controls to validate the DNA methylation measurements (**Fig.1**). For 124 (out of 125) samples, *AR* and *FAM127A* methylation levels were in agreement with the gender information provided by the brain bank, and for the remaining

one case, the discrepancy was resolved upon re-review of the chart on file with the bank. Therefore, all of the female postmortem samples, but none of the males, showed substantial DNA methylation of both of these X-linked genes, as expected.

Unsupervised hierarchical clustering of the remaining 48 gene loci, excluding the X-linked genes, revealed a strong age association (**Fig. 1**). All prenatal samples were contained in a single cluster, shown at the top of **Fig. 1** (blue cluster). The subjects over 40 years of age were divided into two other major clusters with either moderate amounts (red cluster at bottom) or high density of CpG island methylation (black cluster in middle). The majority of loci showed a statistically significant increase of DNA methylation associated with age, adjusted for diagnosis, but the chronology of these age-associated changes varied remarkably among different loci. Altogether, four different types of age-related methylation changes were discernible: (1) Eight of the 50 gene loci showed a linear increase of DNA methylation with age, as exemplified by *HOXA1* (**Fig. 2** and Supplemental Figure). (2) Half of the genomic loci showed a statistically significant biphasic age distribution (Supplemental Figure). Among these, 18 genes revealed a sharp shift in slope at some time-point within the first decade of life, mostly in the newborn period, as indicated by *PAX8* (**Fig. 2** and Supplemental Figure). (3) One locus (*MGMT*) showed a highly unusual, non-linear stochastic accumulation of hypermethylation starting at about age 50 (**Fig. 2** and Supplemental Figure).

The stochastic nature of this hypermethylation event is of particular interest, since variation in *MGMT* CpG island hypermethylation in gliomas is associated with clinical response to alkylating agents [293]. Interestingly, the incidence of malignant gliomas peaks around age 40-50 [294, 295], which is the same age period when *MGMT* hypermethylation emerged in the samples of the present study. (4) Finally, in striking contrast to the age-related progressive increase in DNA methylation at single copy genes (described above under type 1,2,3), *ALU* and other repetitive elements either showed a significant *decrease* in DNA methylation during the first decade of life, followed by relatively little change during subsequent maturation and aging (1/5 repetitive sequences) (**Fig. 2**), or showed relatively little change across the lifespan (4/5 repetitive sequences) (Supplemental Figure). For the majority of loci showing an age-related increase in DNA methylation, the effect was extremely robust ($p < 0.0001$) (**Fig. 2** and Supplemental Figure).

While it was beyond the scope of this study to assess the relationship between the observed age-related methylation pattern and corresponding changes in gene expression for all loci, we hypothesized that genes showing a linear and robustly progressive increase in methylation throughout the lifespan ("type 1" genes, see above and **Fig. 2**) would show a decline in mRNA levels at advanced age. To examine this, we profiled temporal cortex mRNA levels by qRT-PCR for 4 of the "type 1" genes listed in **Fig.2** (*SYK, NEUROD2, GABRA2, GAD1*) in a cohort of six child brains (range: 1.3-11.5

years) and 11 adults (range: 32-87 years), carefully matched for RNA quality (see Methods) and normalized to *18S* rRNA levels (data not shown). Indeed, all four genes showed an inverse correlation between mRNA levels and age, to a moderate degree (R^2 = 0.29-0.42 for *SYK*, *NEUROD2*, *GAD1* and *GABRA2*). In contrast, mRNA levels of *B2M* and *GUSB*, two housekeeping genes commonly used to assess RNA quality in human postmortem specimens [296], and of *MGMT*–a gene with a highly unusual age-related methylation profile (**Fig.2**)–did not show a correlation with age (R^2 = 0.02 for *MGMT*, and < 0.002 for *B2M* and *GUSB*). Therefore, the age-related decline in mRNA levels observed for a subset of the "type 1" genes is not explained by generalized RNA deficit or decay in the older specimens. We conclude that the progressive, age-related increases in DNA methylation at the 5' sequences of these genes could contribute to the observed age-related decline in corresponding mRNA levels.

Disease-associated alterations

Taking a false discovery rate into account, Alzheimer's cases showed a statistically significant difference in DNA methylation for *SORBS3* and *S100A2*. In both cases, the Alzheimer patients tend to show an acceleration of the age-associated changes in DNA methylation (**Fig. 3**). *SORBS3* (also known as *vinexin, SCAM-1* or *SH3D4*), which encodes a cell adhesion molecule expressed in neurons and glia [297], becomes progressively more

likely to be methylated with age, and is methylated to a greater degree in Alzheimer patients (median PMR = 38.5, N = 18) than in all other cases (schizophrenia, controls) older than 60 years (median PMR = 16.9, N = 39, *P*=0.00081). *S100A2*, a member of the S100 family of calcium binding proteins, displays a complex chronology, with a rapid prenatal increase, followed by an infrequent stochastic decrease in DNA methylation later in life, particularly among Alzheimer patients (median PMR = 12.9, N = 18) versus all other subjects older than 60 years (median PMR = 20.5, N = 39, *P*=0.00197). The age- and disease-associated loss of *S100A2* DNA methylation in Alzheimer's disease is consistent with the observation of S100A2 protein in corpora amylacea, or polyglucosan bodies, which accumulate in aging human brains [298]. Therefore, the significant DNA methylation changes in Alzheimer's disease, including the decrease of *S100A2* and increase in *SORBS3* CpG methylation, appear to represent accelerations of the normal, age-associated DNA methylation changes in these genes. Notably, previous in vitro studies provided evidence that DNA methylation is involved in transcriptional regulation of *PSEN1* [284] an Alzheimer's disease-associated gene and regulator of amyloid precursor protein and Notch signaling pathways [299]. However, *PSEN1* showed only very low levels of methylation in our samples, and we did not find age- or disease-associated changes (Supplemental Table 3a). This lack of consistent change in PSEN1 methylation in diseased or aging tissue, however, may not

be surprising given that this gene exhibits significant variability in interindividual methylation, according to a study in male germ cells [300].

The methylation of *PAX8*, a gene encoding a paired box-containing transcription factor important for CNS and thyroid development [301], was higher in schizophrenics than in controls (P=0.0025) (Supplemental Table 3b), but this was not considered statistically significant after adjusting for multiple comparisons by controlling the false discovery rate (set at 0.05)[302]. We conclude that schizophrenia is not accompanied by consistent DNA methylation changes at the 50 gene loci included in this study.

The *de novo* DNA methyltransferase, DNMT3a, is expressed in developing and aging cerebral cortex

The DNA methylation data described above strongly suggest that DNA methylation events in the cerebral cortex are ongoing across a wide age range, extending beyond the developmental period and continuing into old age. If this hypothesis is correct, then one would expect expression of the *de novo* DNA methyltransferase enzymes, DNMT3a and/or DNMT3b [303, 304], at all ages. In mouse cerebral cortex, Dnmt3a expression remains detectable in adults, albeit at lower levels than observed during earlier periods of postnatal development; in contrast, Dnmt3b is found in murine CNS only during a narrow period of prenatal development [305]. To find out when DNMT3a protein is expressed in the human cerebral cortex, we employed

immunoblotting on cortical homogenates from fetal, child and adult samples. We observed, across all ages, an immunoreactive band of approximately 120 kDa, corresponding to full-length form of DNMT3a [306, 307] (**Fig. 4A**). Immunolabeling of intact nuclei from child and adult cortex revealed that the bulk of the DNMT3a-like immunoreactivity is derived from neuronal nuclei (**Fig. 4B-E**). Expression of DNMT3a in neurons was confirmed by in situ hybridization studies with full length DNMT3a cRNA (**Fig. 4F-H**); a subset of neurons, including some with pyramidal neuron-like morphology (**Fig. 4G**) residing in layers III and V of the adult cortex expressed DNMT3a mRNA. We conclude that DNMT3a in human cerebral cortex is expressed primarily in neurons, which is in agreement with similar findings in mice [305] and, furthermore, is expressed across the lifespan from the 2nd trimester of pregnancy through old age.

Age-related DNA methylation changes in nuclei of differentiated neurons

Notably, studies in rat and mouse identified a number of stimuli or environmental conditions that alter expression of selected mRNAs in immature, or mature brain, in conjunction with–often bidirectional–changes in CpG methylation of the corresponding promoters [21, 146, 260, 283]. The conclusion drawn by these studies, either explicitly or implicitly, is that neuronal gene expression is subject to epigenetic regulation. However, most

CNS tissues, including cerebral cortex, are comprised of a highly heterogeneous mixture of various dividing and postmitotic cell populations, which are likely to show important differences in the methyl-CpG patterning of their genomes. This uncertainty regarding the cellular specificity of any DNA methylation signal obtained from brain homogenates places limitations on the interpretation of the age-related changes in methylation as described above. Nonetheless, the presence of DNMT3a in cortical neurons across a wide age range (**Fig 4**), in conjunction with the robust, age-related methylation changes at >50% of the gene loci (**Fig. 1, 2**), strongly suggests an ongoing modification of the neuronal DNA long after the exit from the cell cycle, which in primate cerebral cortex occurs during fetal mid-development [308]. To find out whether DNA methylation is dynamically regulated in postmitotic neurons and to rule out the potential confound of changes in glia numbers during the course of development [309, 310], we isolated nuclei of differentiated neurons from child and adolescent (1-16 years) and aged (>60 years) cortex using NeuN immunolabeling in conjunction with fluorescence-activated cell sorting (FACS) (**Fig. 5A,B**). Then, the methylation levels for 10 gene loci were analyzed in the neuronal DNA by MethyLight PCR. When compared to child and adolescent specimens, DNA from aged neuronal nuclei showed a significant increase in methylation at 3/10 loci (*HOXA1, PGR, SYK*), and a significant decrease in 1/10 loci (*S100A2*) (**Fig. 5C**). Therefore, during the

transition from childhood to old age, differentiated cortical neurons undergo bidirectional changes in DNA methylation.

SUMMARY AND DISCUSSION

The present study examined DNA methylation changes for 50 genomic loci during the course of development, maturation and aging of the human cerebral cortex. The majority of loci showed significant age effects: eight loci showed a progressive increase in methylation that continued across the entire lifespan and another 18 loci were defined by a sharp rise within the first months or years after birth. We present direct evidence that, for a subset of loci, genomic DNA from differentiated cortical neurons undergoes methylation changes during the course of maturation and aging. In addition, one locus, *MGMT*, showed a stochastic accumulation in methylation starting around age 50, with potential implications for the tumor biology of astrogliomas, as discussed above. While DNA methylation changes related to development or aging were extremely robust in the present study, disease-associated changes, on the other hand, were surprisingly limited. Schizophrenia, a chronic psychiatric disease condition associated with psychosis and widespread cortical dysfunction in the absence of large-scale loss of neurons [311-313], was not associated with significant methylation changes in the present study. On the other hand, cases diagnosed with Alzheimer's disease, which is defined by a neurodegenerative process in cerebral cortex and other

brain regions, showed significant methylation changes in 2/50 loci. One locus (*S100A2*), which is methylated in neurons (**Fig. 5C**) was significantly less methylated in the DNA from Alzheimer cases compared to age-matched controls (**Fig.3**), possibly due to large-scale loss of neurons associated with that disease. In addition, methylation of another locus (*SORBS3*) was higher in the Alzheimer samples than in controls. Thus, the DNA methylation alterations in both genes appear to reflect an enhancement, or acceleration, of the age-associated changes that we observed in normal brain (**Fig. 3**).

It is noteworthy that the overwhelming majority of loci analyzed in the present study demonstrated age-related *increases* in DNA methylation in cerebral cortex (26/50 loci), and only one gene–*S100A2*--showed a change in the opposite direction; this decrease was even more pronounced in the Alzheimer's cohort. Likewise, in DNA samples derived selectively from differentiated neurons of controls, only *S100A2* showed an age-related loss of methylation, while significant increases were found for 3/10 genes (**Fig. 5C**). Collectively, these findings support the notion that DNA methylation levels progressively increase in the cerebral cortex at many genomic loci during the course of maturation and aging. On the other hand, according to the findings presented here, DNA de-methylation events appear to play a less prominent role. Therefore, it remains to be clarified whether or not there is active de-methylation in brain, and if DNA repair-related mechanisms are involved similar to those recently reported for dividing cells and *Xenopus* oocytes

[314]. Additionally, further studies will be required in order to determine whether or not DNA methylation/demethylation in human brain is subject to more acute alterations—on the scale of hours or days—as has been previously demonstrated in cell cultures and animal models [146, 259, 260].

It is important to realize that our study had several limitations, including the focus on one area of the cerebral cortex, i.e. the neocortex of the anterior and lateral temporal lobe. Therefore, additional studies will be necessary to confirm that the developmental DNA methylation changes as observed in this study are a generalized feature operating throughout all areas of the human cerebral cortex. Furthermore, we monitored DNA methylation changes at a limited number of genomic sequences, hence it will be necessary to confirm the findings reported here on a more comprehensive, genome-wide scale. Such studies will be necessary in order to find out (i) whether or not the developmental DNA methylation changes reported here represent a more generalized, age-dependent drift towards increased methylaton levels and (ii) whether or not schizophrenia or Alzheimer's disease are associated with DNA methylation changes affecting wide-spread portions of the genome. Finally, while our study presents some of the first and direct evidence for methylation changes in the DNA of terminally differentiated neurons, our analyses was limited to samples obtained from children and adults, because isolation of neuronal nuclei from fetal specimens via FACS was not feasible for technical reasons. Hence, it remains to be determined whether or not neurons, or

various types of glia and other non-neuronal cells, contribute to the observed sharp rise in DNA methylation during the perinatal and early childhood period that was observed at 18/50 loci in this study. These highly dynamic methylation increases postnatally could either be related to the relatively high levels of neuronal DNMT3a methyl-transferase in the immature brain [305] or , alternatively, result from developmental shifts in cell composition of the postnatal cortex, including a rise in the number of oligodendrocytes and other glia-related changes [257]. In light of these findings, it is tempting to speculate that certain nurturing, feeding and other “environmental” conditions could potentially result in sustained DNA methylation and gene expression changes affecting many parts of the genome. Indeed, emerging evidence from animal models is in support of this hypothesis [21, 315]. Based on the results of the present study, we predict that approximately one half of genes encoded in the genome will show age-related DNA methylation changes in the human brain, many of which will directly, or indirectly, affect neuronal gene expression and thus cognition and behavior.

MATERIAL AND METHODS

Human brain tissue

Fresh frozen, postmortem brain tissue from fetuses, newborns and children were obtained through the Brain and Tissue Banks for Developmental Disorders, University of Maryland and University of Miami (NICHD contract #

NO1-HD-8-3284). Adult tissue samples were obtained from three brain banks (i) the Center for Neuroscience, University of California at Davis, CA, (ii) the Harvard Brain Tissue Resource Center at McLean Hospital, Belmont, MA, and (iii) the Massachusetts General Hospital, Boston, MA. All brain banks provided tissue to us without personal identifiers, and all collection and written consent procedures (donors or family members) were approved by the institutional review boards of the brain banks' institution. Small blocks of frozen, unfixed tissue were dissected from the developing cortical plate (fetus) or cerebral cortex (children, adults) of the anterior lateral temporal lobe. Altogether, 17 fetal, 15 child and 93 adult specimens were included in the present study. Among the adult samples, there were 18 cases meeting CERAD criteria of definite Alzheimer's disease and 30 cases meeting DSM-IV based criteria for schizophrenia (Supplemental Table 4).

Methylation and mRNA analyses

From all specimens, DNA was extracted from the cortical plate (fetus) or gray matter (children, adults) using a standard procedure, with modifications [316] and analyzed by MethyLight PCR after bisulfite conversion [291, 292, 317] (for primer sequences, see Supplemental Table 2). In addition, RNA was extracted from cortical gray matter of child and adult samples with the RNeasy Lipid Tissue Mini Kit (Qiagen, Valencia, CA) and treated with DNAse I. RNA quality for all samples was assessed using high-resolution capillary

electrophoresis on the Agilent Bioanalyzer 2100 (Agilent Technologies, Palo Alto, CA). Samples with a RIN < 4.0 were discarded [296]. RNA was reverse-transcribed and amplified with TaqMan One-Step RT-PCR Master Mix Reagent in 7500 Real Time PCR System machine (Applied Biosystems, Foster City, CA, U.S.A.), in conjunction with unlabeled primers and SYBR Green (*GAD1*) or FAM-labeled primer sets purchased from Applied Biosystems (all other genes). Quantifications were performed by positioning the cycle threshold within the linear range of amplification curve. Each value of mRNA was calculated with the equation $V = (1+E)^{Ct}$ (E: amplification efficiency) and normalized to 18S ribosomal RNA.

DNMT3a expression studies

For western blotting, 100 mg aliquots of cortical tissue were homogenized in 1x Laemmli buffer for SDS-PAGE, then processed for anti-DNMT3a immunoreactivity (rabbit polyclonal, Abcam Inc., Cambridge, MA) at a final dilution of 1:250; or, for loading control, mouse anti-β-actin (Sigma, St. Louis, MO), final dilution 1:10,000.

To extract nuclei for DNMT3a-like immunolabeling, cortical tissue was homogenized in 2mL 1× RSB buffer (100mM NaCl, 30mM $MgCl_2$, 100mM Tris-HCl, pH 7.5) with 1% NP-40, mixed with 8mL 1× RSB, and centrifuged in a swing-bucket rotor at 1000 *x g* for 10 min at 4°C. Subsequently, the pellet was dissolved in 4mL 4% phosphate-buffered paraformaldehyde (PFA) and

incubated for 10 min at room temperature. This homogenate was layered onto a 30% sucrose cushion, centrifuged, and the resulting pellet dissolved in 0.1% Triton X-100/ 0.32M sucrose/5mM $CaCl_2$/ 0.1mM EDTA/ 10mM Tris-HCl, pH 8.0, mixed with 1mL 1.8 M sucrose, and centrifuged at 1500 *x g* at 4°C for 10 min on a 1mL 1.2 M sucrose cushion. Nuclei pellets were dissolved in 1x PBS, and then dried on glass slides and blocked with 1xPBS/10% normal goat serum/0.2% Triton X-100 for 1 hour. For double immunolabeling, primary antibodies (anti-DNMT3a and anti-NeuN as a neuron-specific marker [191, 192]) were labeled with the Zenon Alexa Fluor 594 Rabbit IgG Labeling Kit or the Enhanced Zenon® (Alexa 488) Mouse IgG Labeling Kit (Invitrogen, Carlsbad, CA) and applied at 1:500 final dilution to the slides for 4 hrs. Following incubation, slides were rinsed repeatedly, incubated in tyramide solution according to the manufacturer's instructions, washed, counterstained with DAPI and coverslipped.

To prepare for in situ hybridization histochemistry, tissue blocks were allowed to thaw, then immersion-fixed with 4% phosphate-buffered PFA for up to 4 days, and then cryoprotected in 30% phosphate-buffered sucrose; 20 μm sections were cut on a cryostat, mounted on glass slides, and stored at -80° C until use. Sense and antisense digoxigenin (DIG)-labeled DNMT3a cRNA probes were generated from full-length human DNMT3a cDNA (Genbank BC043617) in the presence of DIG-11-UTP (Roche Applied Science, Indianapolis, IN), according to the manufacturer's instructions.

Templates were digested with DNase I and the cRNA purified by LiCl precipitation. Sections were treated with 0.2 M HCl and then acetylated with 0.25% acetic anhydrate in 0.1 M triethanolamine, and prehybridized with hybridization buffer (50% formamide, 2X SSC, 10% dextran sulfate, 0.5 mg/ml sperm DNA, 0.25 mg/ml yeast tRNA, 0.2 mg/ml BSA, 50 ug/ml Heparin, 2.5 mM EDTA and 0.1% Tween-20) at 60^{o}C for 1 hr. Sections were then hybridized with DIG-labeled probes diluted 1:50 in hybridization buffer (50 µl/section) at 60^{o} C overnight. Sections were washed with 2X SSC at R.T., 1XSSC at 37^{o}C and then treated with RNase A at the same temperature. After RNase A digestion, sections were washed sequentially with 1X SSC at 37^{o}C, 1X SSC: 50% formamide at 52^{o}C, 0.1X SSC at 52^{o}C and then developed with the DIG Nucleic Acid Detection kit (Roche Applied Science, Indianapolis, IN), in conjunction with sheep anti-digoxigenin-alkaline phosphate conjugated antibody (1:1000) (Roche) and NBT/BCIP chromogen (1:50) (Roche) according to the manufacturer's instructions. Sections were mounted with mounting medium (VetctaMount^{TM} AQ, Vector Laboratories, Burlingame, CA) and coverslipped with glass.

Flow cytometry

Intact nuclei were prepared from up to 3 gram of frozen-thawed tissue as described above, with the exception of the fixation step, and further purified by ultracentrifugation through a sucrose cushion at 25,000 *x g* for 2.5 hrs at

4°C. The pelleted nuclei were dissolved in 1 mL 1× PBS, centrifuged for 5 min at 14,000 *x g* , and the nuclei pellets stored at -80°C until further processed. Nuclei were immunolabeled with anti-NeuN antibody (see above) and sorted using a FACSVantage DiVa system (BD Biosciences), the DNA extracted and processed by Methylight PCR as described above.

ACKNOWLEDGEMENTS

We would like to thank Dr. David Siegmund (Department of Statistics, Stanford University) for introducing us to the methods used for evaluating the biphasic age associations, Ms. Jing Chang for help in conducting statistical analyses, Dr. Yin Guo for technical assistance, and Dr. F. M. Benes and Dr. Stephan Heckers (Harvard Brain Tissue Resource Center, McLean hospital, Belmont), Dr. W. E. Bunney Jr. and Dr. E. G. Jones (Center for Neuroscience, University of California at Davis), Dr. B. Hyman (Massachusetts General Hospital, Boston, MA) for providing adult brain tissues and Dr. Ron Zielke and staff from the Brain and Tissue Bank for Developmental Disorders at University of Maryland for providing fetal and child specimens.

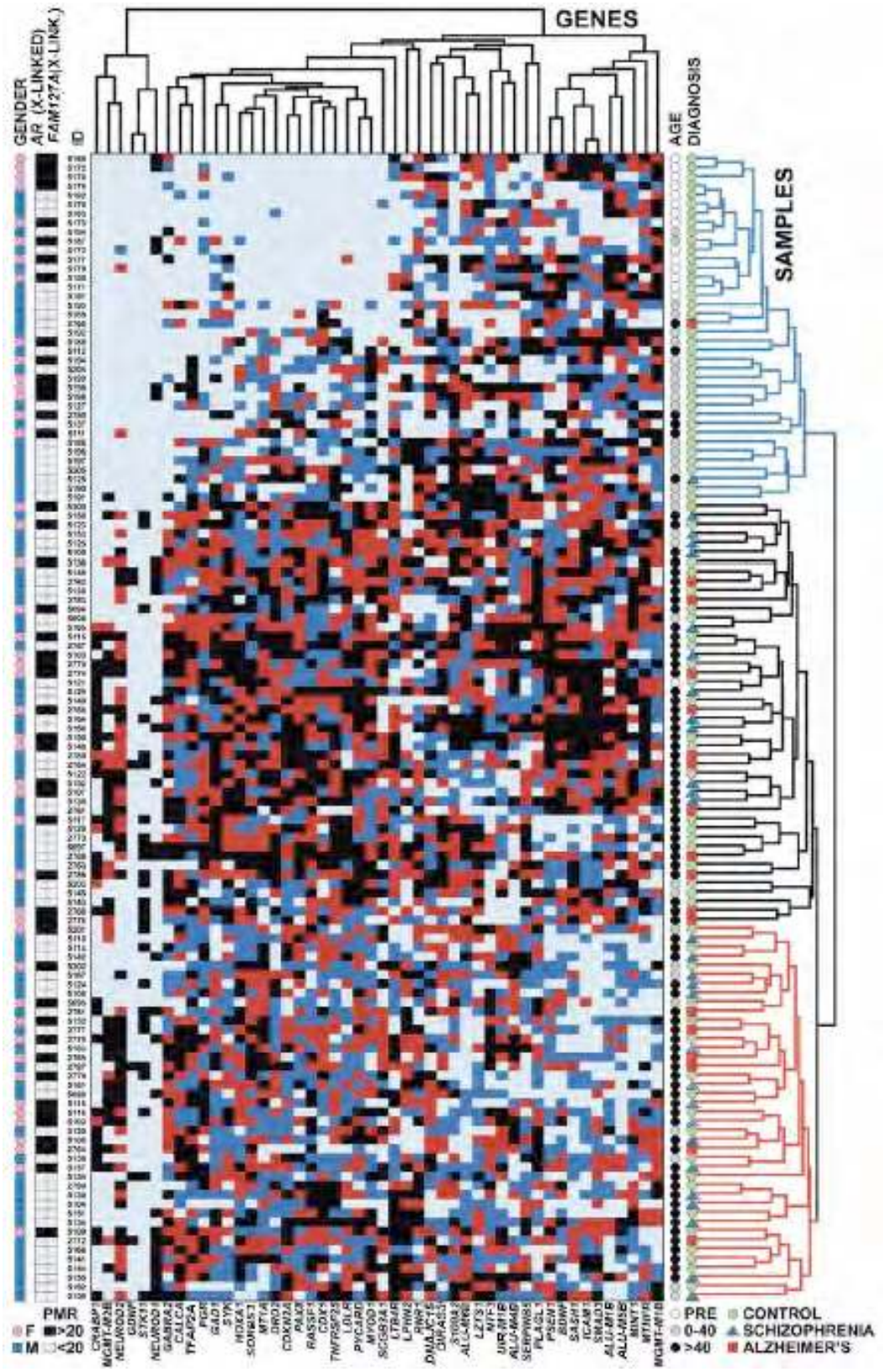
GENES
SAMPLES
GENDER
AR (X-LINKED)
FAM127A(X LINK.)
ID
AGE
DIAGNOSIS
PMR
F
M
>20
≤20
PRE
0-40
>40
CONTROL
SCHIZOPHRENIA
ALZHEIMER'S

Figure 1: DNA methylation changes at 50 loci in temporal neocortex across the lifespan. Two dimensional hierarchical cluster analysis using Manhattan distance and average linkage (N=48 regions, 125 subjects). DNA (rostro-lateral temporal neocortex) was extracted and analyzed by MethyLight for the genes indicted as described (see Methods). Each gene is grouped into quartiles (Dark Light Blue =1 low, Dark Blue =2 medium-low, Red=3 medium high, Black=4 high extent of methylation). The larger the number of samples with no detectable methylation, the fewer the number of observations coded dark blue and red. Gender (Blue squares = Male, Pink circles = Female), Age (White circles = Prenatal (PRE); Gray circles = 0-40 years old; Black circles = older than 40 years), and Diagnosis (Green circles = controls; Blue triangles = Schizophrenia cases; Red squares = Alzheimer's cases) are indicated with symbols explained below each variable. *AR* and *FAM127A* are two additional X-linked genes with DNA methylation occurring on the inactive X-chromosome in females, and are dichotomized at a PMR value of 20, as indicated. PMR = Percent of Methylated Reference [292, 318]. Three major sample clusters are indicated on the right hand side in blue (consisting mostly of prenatal and young adult samples), black, consisting mostly of subjects over 40 years old with high density CpG island methylation, and red, mostly subjects over 40 years old with lower density CpG island methylation.

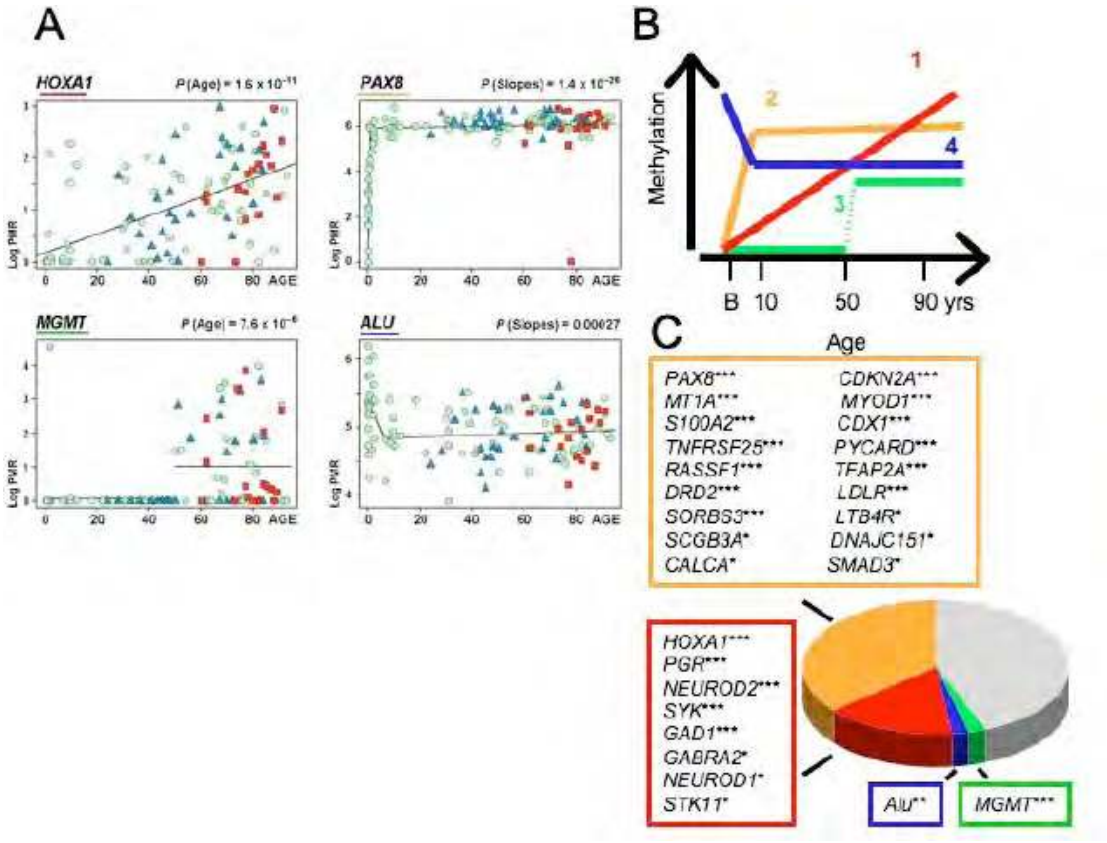

Figure 2. Four developmental profiles for cortical DNA methylation. (A) Associations of log-transformed PMR values (ln(PMR+1); y-axis) with age (x-axis) for several representative genes. Trends are studied using linear regression. *HOXA1* shows a linear association. *MGMT*-M2B shows a non-linear shift, with the *P*-value referring to a *T*-test of the difference in mean methylation value for subjects under or over 50 years of age. For the biphasic linear trends of *PAX8* and the *ALU* sequence *ALU-M1B* (Supplemental Table 2) the *P*-values refer to a test of change of slope. Green dots = controls, blue triangles = schizophrenia and red squares = Alzheimer's subjects. **(B)** Schematic summary of the four different types (1-4, see text for details) of developmental methylation profiles in human temporal cortex across the lifespan (x-axis, B = birth), as illustrated by the representative examples in (A). (**C**) Listings and proportion of gene loci (total = 48; excluding *AR* and *FAM127A* which showed gender-specific methylation) that show significant age-dependent methylation changes: colors refer to the scheme in (B). Gray sector refers to the subset of loci without a significant age effect. N= 125 subjects. All p-values are adjusted for diagnosis; *** $p < 0.0001$, ** $p < 0.001$, * $p < 0.05$.

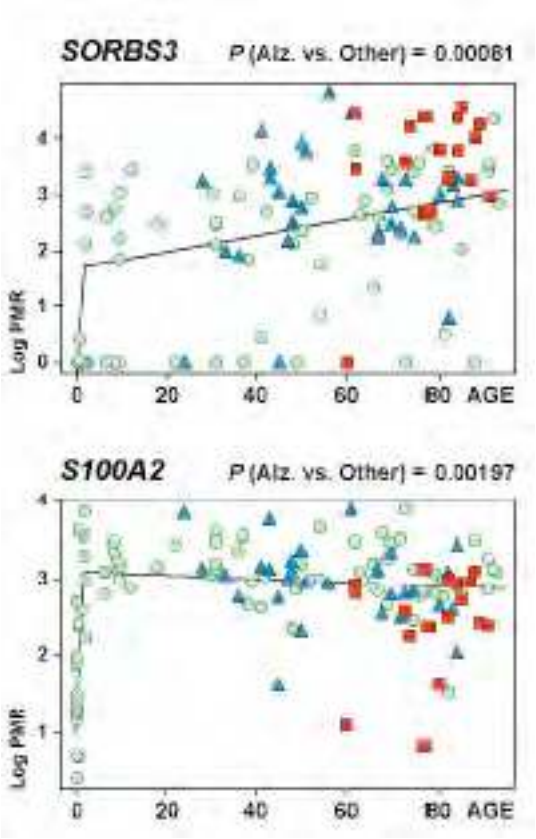

Figure 3: Acceleration of age-associated DNA methylation changes in Alzheimer's disease. Scatter plots showing age-associated methylation changes for *SORBS3* and *S100A2* across all ages. N = 125 subjects, including Alzheimer subjects (red squares), schizophrenics (blue triangles) and controls (green dots). P-values refer to T-tests for comparison of Alzheimer subjects versus all other subjects older than 60 years. One outlier (ID 2763, 104 years old, Suppl. Table 4) was omitted from the age-associated analyses.

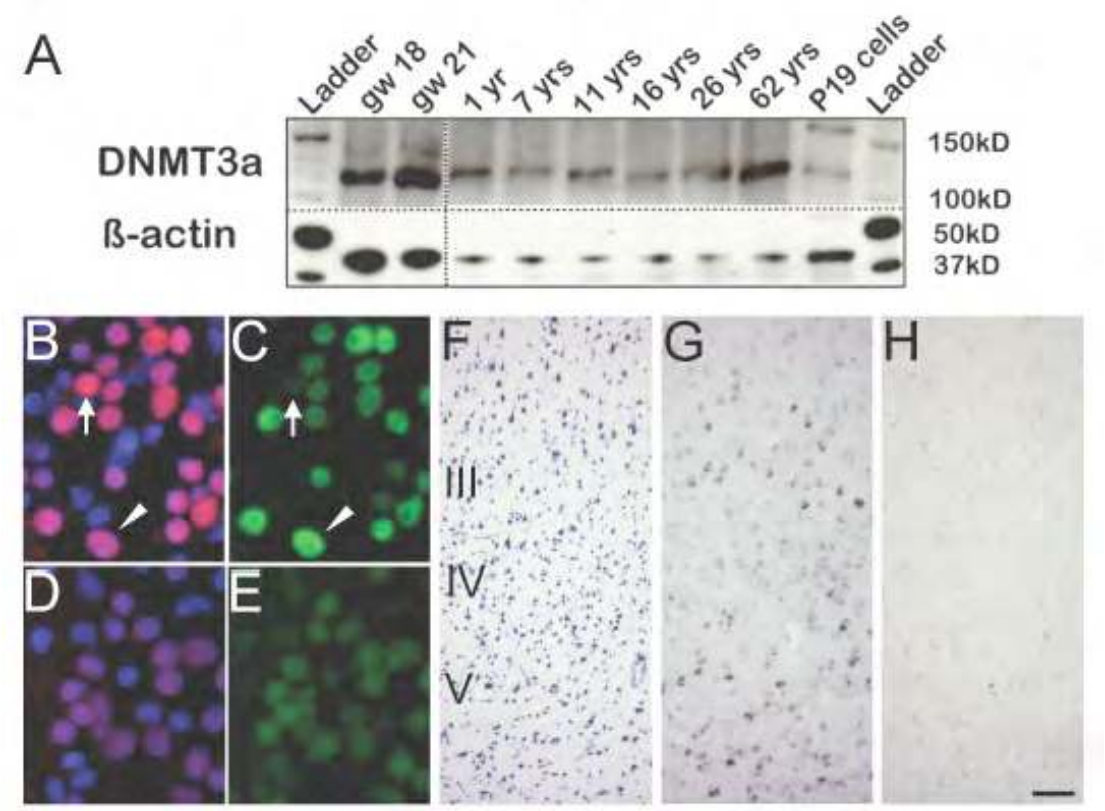

Figure 4: Developmental and cellular expression pattern of DNMT3a in the cerebral cortex. (**A**) Representative immunoblotting of temporal cortex homogenates with anti-DNMT3a antibody (top) and β-actin as loading control (bottom). Left, fetal samples (gw = gestational week); right, child and adult brains (yrs = years) and, as positive control, murine embryonic carcinoma, "P19" cells. Notice expression of DNMT3a—indicated by a ~ 120 kDa band—across all ages. (**B, C**) Digitized images of temporal cortex nuclei from 1 year old infant, processed for DNMT3a (red) and NeuN (green) immunoreactivity and counterstained with DAPI. Notice numerous neuronal nuclei expressing both markers, including representative example marked by arrowhead. Occasional non-neuronal DNMT3a+ nucleus is marked by arrow. (**D,E**) show weak background staining and formalin fixation-related autofluorescence in negative controls processed without primary antibodies. (**F-H**) Images from layers III, IV and V of parallel sections from adult temporal cortex, stained for Nissl (F) or hybridized with digoxigenin-labeled DNMT3a antisense (G) or sense riboprobe (H). Notice in (G) robust expression of DNMT3a mRNA in a subset of layer III and V neurons. Images in B-E taken at with 20x objective. Bar (F-H) in H = 100 μm.

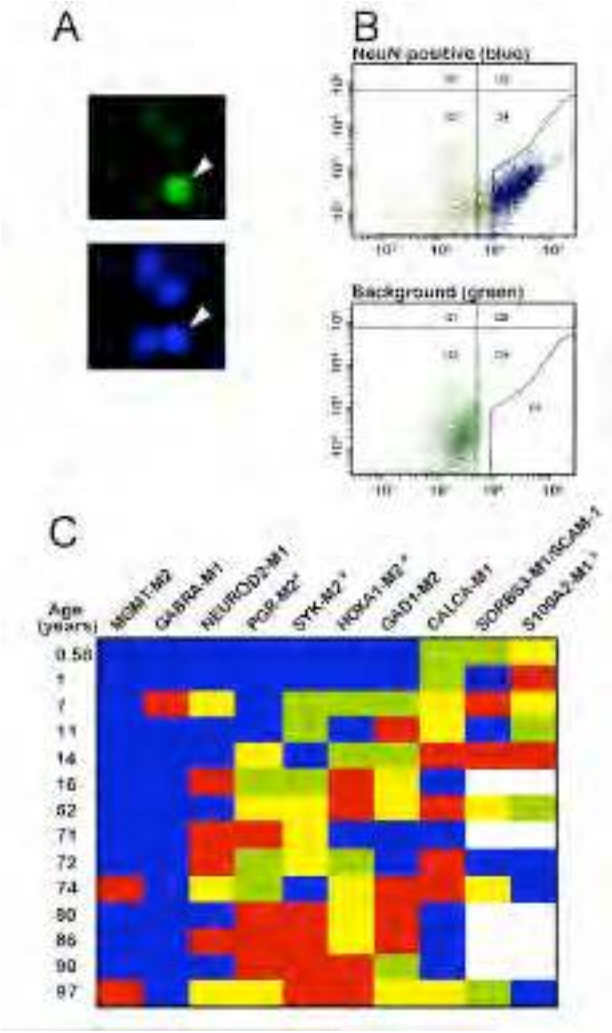

Figure 5: Age-related DNA methylation changes in differentiated neurons. (**A**) Examples of nuclei stained with anti-NeuN (green) and counterstained with DAPI; arrowhead marks double-labeled cell. Notice absence of detectable background and autofluorescence in these samples that were processed without prior fixation (**B**) Representative FACS of unfixed NeuN labeled material similar to the one shown in (A) (top) and of negative control (bottom); blue dots mark sorted neuronal nuclei (NeuN+). (**C**) Heatmap showing methylation levels of neuronal DNA isolates for 10 different genes across the lifespan (range: 0.6 – 97 years). Each gene is grouped into quartiles (blue = 1 low, green = 2 medium-low, yellow = 3 medium high, red = 4 high extent of methylation). The larger the number of samples with no detectable methylation, the fewer the number of observations coded green and yellow. White space = no data. * = $p < 0.05$, Mann-Whitney U

permutation based on comparison of immature/young (0.6 – 16 years) to old (62 + years) samples. Notice that neuronal DNA from advanced age group shows significant increase in DNA methylation for 3/10 gene loci (*PGR, SYK, HOXA1*), but decreased levels at *S100A2* locus.

REFERENCES:

1. Rodier, P.M., *The early origins of autism.* Sci Am, 2000. **282**(2): p. 56-63.
2. Trevarthen, C., *Autism as a neurodevelopmental disorder affecting communication and learning in early childhood: prenatal origins, post-natal course and effective educational support.* Prostaglandins Leukot Essent Fatty Acids, 2000. **63**(1-2): p. 41-6.
3. Folstein, S., Rutter M, *Infantile autism: a genetic study of 21 twin pairs.* J Child Psychol Psychiatry, 1977. **18**: p. 297-321.
4. Lemery-Chalfant, K., et al., *Wisconsin Twin Panel: current directions and findings.* Twin Res Hum Genet, 2006. **9**(6): p. 1030-7.
5. Cardno, A.G. and Gottesman, II, *Twin studies of schizophrenia: from bow-and-arrow concordances to star wars Mx and functional genomics.* Am J Med Genet, 2000. **97**(1): p. 12-7.
6. Davis, J.O., J.A. Phelps, and H.S. Bracha, *Prenatal development of monozygotic twins and concordance for schizophrenia.* Schizophr Bull, 1995. **21**(3): p. 357-66.
7. Hales, C.N. and D.J. Barker, *Type 2 (non-insulin-dependent) diabetes mellitus: the thrifty phenotype hypothesis.* Diabetologia, 1992. **35**(7): p. 595-601.
8. Barker, D.J., *The effect of nutrition of the fetus and neonate on cardiovascular disease in adult life.* Proc Nutr Soc, 1992. **51**(2): p. 135-44.
9. Bale, T.L., et al., *Early life programming and neurodevelopmental disorders.* Biol Psychiatry, 2010. **68**(4): p. 314-9.
10. Kouzarides, T., *Chromatin modifications and their function.* Cell, 2007. **128**(4): p. 693-705.
11. Peterson, C.L. and M.A. Laniel, *Histones and histone modifications.* Curr Biol, 2004. **14**(14): p. R546-51.
12. Barski, A., et al., *High-resolution profiling of histone methylations in the human genome.* Cell, 2007. **129**(4): p. 823-37.
13. Huang, H.S., et al., *Prefrontal dysfunction in schizophrenia involves mixed-lineage leukemia 1-regulated histone methylation at GABAergic gene promoters.* J Neurosci, 2007. **27**(42): p. 11254-62.
14. Abdolmaleky, H.M., et al., *Hypermethylation of the reelin (RELN) promoter in the brain of schizophrenic patients: a preliminary report.* Am J Med Genet B Neuropsychiatr Genet, 2005. **134B**(1): p. 60-6.
15. Grayson, D.R., et al., *Reelin promoter hypermethylation in schizophrenia.* Proc Natl Acad Sci U S A, 2005. **102**(26): p. 9341-6.
16. Sharma, R.P., D.R. Grayson, and D.P. Gavin, *Histone deactylase 1 expression is increased in the prefrontal cortex of schizophrenia subjects: analysis of the National Brain Databank microarray collection.* Schizophr Res, 2008. **98**(1-3): p. 111-7.

17. Veldic, M., et al., *In psychosis, cortical interneurons overexpress DNA-methyltransferase 1.* Proc Natl Acad Sci U S A, 2005. **102**(6): p. 2152-7.
18. Schanen, N.C., *Epigenetics of autism spectrum disorders.* Hum Mol Genet, 2006. **15 Spec No 2**: p. R138-50.
19. Williams, S.R., et al., *Haploinsufficiency of HDAC4 causes brachydactyly mental retardation syndrome, with brachydactyly type E, developmental delays, and behavioral problems.* Am J Hum Genet, 2010. **87**(2): p. 219-28.
20. Adegbola, A., et al., *A novel mutation in JARID1C/SMCX in a patient with autism spectrum disorder (ASD).* Am J Med Genet A, 2008. **146A**(4): p. 505-11.
21. Weaver, I.C., et al., *Epigenetic programming by maternal behavior.* Nat Neurosci, 2004. **7**(8): p. 847-54.
22. Weaver, I.C., et al., *Reversal of maternal programming of stress responses in adult offspring through methyl supplementation: altering epigenetic marking later in life.* J Neurosci, 2005. **25**(47): p. 11045-54.
23. Weaver, I.C., M.J. Meaney, and M. Szyf, *Maternal care effects on the hippocampal transcriptome and anxiety-mediated behaviors in the offspring that are reversible in adulthood.* Proc Natl Acad Sci U S A, 2006. **103**(9): p. 3480-5.
24. Zhang, T.Y., et al., *Maternal care and DNA methylation of a glutamic acid decarboxylase 1 promoter in rat hippocampus.* J Neurosci, 2010. **30**(39): p. 13130-7.
25. Murgatroyd, C., et al., *Dynamic DNA methylation programs persistent adverse effects of early-life stress.* Nat Neurosci, 2009. **12**(12): p. 1559-66.
26. Branchi, I., et al., *Epigenetic modifications induced by early enrichment are associated with changes in timing of induction of BDNF expression.* Neurosci Lett, 2011. **495**(3): p. 168-72.
27. Novikova, S.I., et al., *Maternal cocaine administration in mice alters DNA methylation and gene expression in hippocampal neurons of neonatal and prepubertal offspring.* PLoS One, 2008. **3**(4): p. e1919.
28. Ke, X., et al., *Intrauterine growth retardation affects expression and epigenetic characteristics of the rat hippocampal glucocorticoid receptor gene.* Physiol Genomics, 2010. **42**(2): p. 177-89.
29. McGowan, P.O., et al., *Epigenetic regulation of the glucocorticoid receptor in human brain associates with childhood abuse.* Nat Neurosci, 2009. **12**(3): p. 342-8.
30. Oberlander, T.F., et al., *Prenatal exposure to maternal depression, neonatal methylation of human glucocorticoid receptor gene (NR3C1) and infant cortisol stress responses.* Epigenetics, 2008. **3**(2): p. 97-106.
31. Mednick, S.A., et al., *Adult schizophrenia following prenatal exposure to an influenza epidemic.* Arch Gen Psychiatry, 1988. **45**(2): p. 189-92.
32. Brown, A.S., et al., *Serologic evidence of prenatal influenza in the etiology of schizophrenia.* Arch Gen Psychiatry, 2004. **61**(8): p. 774-80.

33. Brown, A.S. and P.H. Patterson, *Maternal infection and schizophrenia: implications for prevention.* Schizophr Bull, 2010. **37**(2): p. 284-90.
34. Desmond, N.M., Wilson GS, Blattner RJ, *Congenital rubella encephalitis. Course and early sequelae.* Journal of Pediatrics, 1967. **71**: p. 311-331.
35. Chess, S., *Follow-up report on autism in congenital rubella.* J Autism Child Schizophr, 1977. **7**: p. 69-81.
36. Atladottir, H.O., et al., *Association of hospitalization for infection in childhood with diagnosis of autism spectrum disorders: a Danish cohort study.* Arch Pediatr Adolesc Med, 2010. **164**(5): p. 470-7.
37. Clarke, M.C., et al., *Evidence for an interaction between familial liability and prenatal exposure to infection in the causation of schizophrenia.* Am J Psychiatry, 2009. **166**(9): p. 1025-30.
38. Prasad, K.M., et al., *Grey matter changes associated with host genetic variation and exposure to Herpes Simplex Virus 1 (HSV1) in first episode schizophrenia.* Schizophr Res, 2010. **118**(1-3): p. 232-9.
39. Van Lieshout, R.J. and L.P. Voruganti, *Diabetes mellitus during pregnancy and increased risk of schizophrenia in offspring: a review of the evidence and putative mechanisms.* J Psychiatry Neurosci, 2008. **33**(5): p. 395-404.
40. Challier, J.C., et al., *Obesity in pregnancy stimulates macrophage accumulation and inflammation in the placenta.* Placenta, 2008. **29**(3): p. 274-81.
41. Garver, D.L., R.L. Tamas, and J.A. Holcomb, *Elevated interleukin-6 in the cerebrospinal fluid of a previously delineated schizophrenia subtype.* Neuropsychopharmacology, 2003. **28**(8): p. 1515-20.
42. Potvin, S., et al., *Inflammatory cytokine alterations in schizophrenia: a systematic quantitative review.* Biol Psychiatry, 2008. **63**(8): p. 801-8.
43. Licinio, J., et al., *Elevated CSF levels of interleukin-2 in neuroleptic-free schizophrenic patients.* Am J Psychiatry, 1993. **150**(9): p. 1408-10.
44. Paterson, G.J., et al., *Selective increases in the cytokine, TNFalpha, in the prefrontal cortex of PCP-treated rats and human schizophrenic subjects: influence of antipsychotic drugs.* J Psychopharmacol, 2006. **20**(5): p. 636-42.
45. Li, X., et al., *Elevated immune response in the brain of autistic patients.* J Neuroimmunol, 2009. **207**(1-2): p. 111-6.
46. Vargas, D.L., et al., *Neuroglial activation and neuroinflammation in the brain of patients with autism.* Ann Neurol, 2005. **57**(1): p. 67-81.
47. Ashwood, P., et al., *Altered T cell responses in children with autism.* Brain Behav Immun, 2010.
48. McAllister, C.G., et al., *Increases in CSF levels of interleukin-2 in schizophrenia: effects of recurrence of psychosis and medication status.* Am J Psychiatry, 1995. **152**(9): p. 1291-7.
49. Martinez-Gras, I., et al., *The anti-inflammatory prostaglandin 15d-PGJ(2) and its nuclear receptor PPARgamma are decreased in schizophrenia.* Schizophr Res, 2011. **128**(1-3): p. 15-22.

50. Na, K.S. and Y.K. Kim, *Monocytic, Th1 and th2 cytokine alterations in the pathophysiology of schizophrenia.* Neuropsychobiology, 2007. **56**(2-3): p. 55-63.
51. Enstrom, A.M., et al., *Differential monocyte responses to TLR ligands in children with autism spectrum disorders.* Brain Behav Immun, 2010. **24**(1): p. 64-71.
52. Morgan, J.T., et al., *Microglial activation and increased microglial density observed in the dorsolateral prefrontal cortex in autism.* Biol Psychiatry, 2010. **68**(4): p. 368-76.
53. Arion, D., et al., *Molecular evidence for increased expression of genes related to immune and chaperone function in the prefrontal cortex in schizophrenia.* Biol Psychiatry, 2007. **62**(7): p. 711-21.
54. Saetre, P., et al., *Inflammation-related genes up-regulated in schizophrenia brains.* BMC Psychiatry, 2007. **7**: p. 46.
55. Narayan, S., et al., *Molecular profiles of schizophrenia in the CNS at different stages of illness.* Brain Res, 2008. **1239**: p. 235-48.
56. Garbett, K., et al., *Immune transcriptome alterations in the temporal cortex of subjects with autism.* Neurobiol Dis, 2008. **30**(3): p. 303-11.
57. Katila, H., K. Hanninen, and M. Hurme, *Polymorphisms of the interleukin-1 gene complex in schizophrenia.* Mol Psychiatry, 1999. **4**(2): p. 179-81.
58. Hanninen, K., et al., *Interleukin-1 beta gene polymorphism and its interactions with neuregulin-1 gene polymorphism are associated with schizophrenia.* Eur Arch Psychiatry Clin Neurosci, 2008. **258**(1): p. 10-5.
59. Napolioni, V., et al., *Family-based association study of ITGB3 in autism spectrum disorder and its endophenotypes.* Eur J Hum Genet, 2011. **19**(3): p. 353-9.
60. Akhondzadeh, S., et al., *Celecoxib as adjunctive therapy in schizophrenia: a double-blind, randomized and placebo-controlled trial.* Schizophr Res, 2007. **90**(1-3): p. 179-85.
61. Laan, W., et al., *Glucocorticosteroids associated with a decreased risk of psychosis.* J Clin Psychopharmacol, 2009. **29**(3): p. 288-90.
62. Boris, M., et al., *Effect of pioglitazone treatment on behavioral symptoms in autistic children.* J Neuroinflammation, 2007. **4**: p. 3.
63. Moots, R.J., et al., *Old drug, new tricks: haloperidol inhibits secretion of proinflammatory cytokines.* Ann Rheum Dis, 1999. **58**(9): p. 585-7.
64. Kato, T., et al., *Inhibitory effects of aripiprazole on interferon-gamma-induced microglial activation via intracellular Ca2+ regulation in vitro.* J Neurochem, 2008. **106**(2): p. 815-25.
65. Zheng, L.T., et al., *The antipsychotic spiperone attenuates inflammatory response in cultured microglia via the reduction of proinflammatory cytokine expression and nitric oxide production.* J Neurochem, 2008. **107**(5): p. 1225-35.

66. Bauer, S., B.J. Kerr, and P.H. Patterson, *The neuropoietic cytokine family in development, plasticity, disease and injury.* Nat Rev Neurosci, 2007. **8**(3): p. 221-32.
67. Boulanger, L.M., *Immune proteins in brain development and synaptic plasticity.* Neuron, 2009. **64**(1): p. 93-109.
68. Deverman, B.E. and P.H. Patterson, *Cytokines and CNS development.* Neuron, 2009. **64**(1): p. 61-78.
69. De Santa, F., et al., *The histone H3 lysine-27 demethylase Jmjd3 links inflammation to inhibition of polycomb-mediated gene silencing.* Cell, 2007. **130**(6): p. 1083-94.
70. Griffiths, D.S., et al., *LIF-independent JAK signalling to chromatin in embryonic stem cells uncovered from an adult stem cell disease.* Nat Cell Biol, 2011. **13**(1): p. 13-21.
71. Kuzumaki, N., et al., *Hippocampal epigenetic modification at the doublecortin gene is involved in the impairment of neurogenesis with aging.* Synapse, 2010. **64**(8): p. 611-6.
72. Brown, A.S., *Prenatal infection as a risk factor for schizophrenia.* Schizophr Bull, 2006. **32**(2): p. 200-2.
73. Hirano, T., et al., *Complementary DNA for a novel human interleukin (BSF-2) that induces B lymphocytes to produce immunoglobulin.* Nature, 1986. **324**(6092): p. 73-6.
74. Spooren, A., et al., *Interleukin-6, a mental cytokine.* Brain Res Rev, 2011.
75. Taga, T. and T. Kishimoto, *Gp130 and the interleukin-6 family of cytokines.* Annu Rev Immunol, 1997. **15**: p. 797-819.
76. Heinrich, P.C., et al., *Principles of interleukin (IL)-6-type cytokine signalling and its regulation.* Biochem J, 2003. **374**(Pt 1): p. 1-20.
77. Schobitz, B., et al., *Cellular localization of interleukin 6 mRNA and interleukin 6 receptor mRNA in rat brain.* Eur J Neurosci, 1993. **5**(11): p. 1426-35.
78. Gadient, R.A. and U. Otten, *Identification of interleukin-6 (IL-6)-expressing neurons in the cerebellum and hippocampus of normal adult rats.* Neurosci Lett, 1994. **182**(2): p. 243-6.
79. Gadient, R.A. and U. Otten, *Expression of interleukin-6 (IL-6) and interleukin-6 receptor (IL-6R) mRNAs in rat brain during postnatal development.* Brain Res, 1994. **637**(1-2): p. 10-4.
80. Dame, J.B. and S.E. Juul, *The distribution of receptors for the pro-inflammatory cytokines interleukin (IL)-6 and IL-8 in the developing human fetus.* Early Hum Dev, 2000. **58**(1): p. 25-39.
81. Ringheim, G.E., et al., *Enhancement of beta-amyloid precursor protein transcription and expression by the soluble interleukin-6 receptor/interleukin-6 complex.* Brain Res Mol Brain Res, 1998. **55**(1): p. 35-44.
82. Watanabe, D., et al., *Characteristic localization of gp130 (the signal-transducing receptor component used in common for IL-6/IL-11/CNTF/LIF/OSM) in the rat brain.* Eur J Neurosci, 1996. **8**(8): p. 1630-40.

83. Smith, S.E., et al., *Maternal immune activation alters fetal brain development through interleukin-6.* J Neurosci, 2007. **27**(40): p. 10695-702.
84. Parker-Athill, E., et al., *Flavonoids, a prenatal prophylaxis via targeting JAK2/STAT3 signaling to oppose IL-6/MIA associated autism.* J Neuroimmunol, 2009. **217**(1-2): p. 20-7.
85. Cheung, I., et al., *Developmental regulation and individual differences of neuronal H3K4me3 epigenomes in the prefrontal cortex.* Proc Natl Acad Sci U S A, 2010. **107**(19): p. 8824-9.
86. Huang, H.S. and S. Akbarian, *GAD1 mRNA expression and DNA methylation in prefrontal cortex of subjects with schizophrenia.* PLoS One, 2007. **2**(8): p. e809.
87. Lim, D.A., et al., *Chromatin remodelling factor Mll1 is essential for neurogenesis from postnatal neural stem cells.* Nature, 2009. **458**(7237): p. 529-33.
88. Kauffmann, A., R. Gentleman, and W. Huber, *arrayQualityMetrics--a bioconductor package for quality assessment of microarray data.* Bioinformatics, 2009. **25**(3): p. 415-6.
89. Langmead, B., et al., *Ultrafast and memory-efficient alignment of short DNA sequences to the human genome.* Genome Biol, 2009. **10**(3): p. R25.
90. Zhang, Y., et al., *Model-based analysis of ChIP-Seq (MACS).* Genome Biol, 2008. **9**(9): p. R137.
91. Anders, S. and W. Huber, *Differential expression analysis for sequence count data.* Genome Biol, 2010. **11**(10): p. R106.
92. Gentleman, R.C., et al., *Bioconductor: open software development for computational biology and bioinformatics.* Genome Biol, 2004. **5**(10): p. R80.
93. Bullard, J.H., et al., *Evaluation of statistical methods for normalization and differential expression in mRNA-Seq experiments.* BMC Bioinformatics, 2010. **11**: p. 94.
94. Siddiquee, K., et al., *Selective chemical probe inhibitor of Stat3, identified through structure-based virtual screening, induces antitumor activity.* Proc Natl Acad Sci U S A, 2007. **104**(18): p. 7391-6.
95. Devon, R.S., et al., *The genomic organisation of the metabotropic glutamate receptor subtype 5 gene, and its association with schizophrenia.* Mol Psychiatry, 2001. **6**(3): p. 311-4.
96. Hashimoto, T., et al., *Alterations in GABA-related transcriptome in the dorsolateral prefrontal cortex of subjects with schizophrenia.* Mol Psychiatry, 2008. **13**(2): p. 147-61.
97. Volk, D.W., et al., *Decreased glutamic acid decarboxylase67 messenger RNA expression in a subset of prefrontal cortical gamma-aminobutyric acid neurons in subjects with schizophrenia.* Arch Gen Psychiatry, 2000. **57**(3): p. 237-45.
98. Allen-Brady, K., et al., *A high-density SNP genome-wide linkage scan in a large autism extended pedigree.* Mol Psychiatry, 2009. **14**(6): p. 590-600.

99. Zaccaria, K.J., et al., *Resistance to change and vulnerability to stress: autistic-like features of GAP43-deficient mice.* Genes Brain Behav, 2010. **9**(8): p. 985-96.
100. Roginski, R.S., et al., *Assignment of an ionotropic glutamate receptor-like gene (GRINL1A) to human chromosome 15q22.1 by in situ hybridization.* Cytogenet Cell Genet, 2001. **93**(1-2): p. 143-4.
101. Buyske, S., et al., *Analysis of case-parent trios at a locus with a deletion allele: association of GSTM1 with autism.* BMC Genet, 2006. **7**: p. 8.
102. Harada, S., H. Tachikawa, and Y. Kawanishi, *Glutathione S-transferase M1 gene deletion may be associated with susceptibility to certain forms of schizophrenia.* Biochem Biophys Res Commun, 2001. **281**(2): p. 267-71.
103. Nafissi, S., et al., *Association between three genetic polymorphisms of glutathione S-transferase Z1 (GSTZ1) and susceptibility to schizophrenia.* Psychiatry Res, 2011. **187**(1-2): p. 314-5.
104. Pae, C.U., et al., *Glutathione S-transferase M1 polymorphism may contribute to schizophrenia in the Korean population.* Psychiatr Genet, 2004. **14**(3): p. 147-50.
105. Rodriguez-Santiago, B., et al., *Association of common copy number variants at the glutathione S-transferase genes and rare novel genomic changes with schizophrenia.* Mol Psychiatry, 2010. **15**(10): p. 1023-33.
106. Brown, A.S. and E.J. Derkits, *Prenatal infection and schizophrenia: a review of epidemiologic and translational studies.* Am J Psychiatry, 2010. **167**(3): p. 261-80.
107. Wulf, P. and U. Suter, *Embryonic expression of epithelial membrane protein 1 in early neurons.* Brain Res Dev Brain Res, 1999. **116**(2): p. 169-80.
108. Pei, Z., et al., *Homeobox genes Gsx1 and Gsx2 differentially regulate telencephalic progenitor maturation.* Proc Natl Acad Sci U S A, 2011. **108**(4): p. 1675-80.
109. Waclaw, R.R., et al., *Distinct temporal requirements for the homeobox gene Gsx2 in specifying striatal and olfactory bulb neuronal fates.* Neuron, 2009. **63**(4): p. 451-65.
110. Vanhove, B., et al., *Gem, a GTP-binding protein from mitogen-stimulated T cells, is induced in endothelial cells upon activation by inflammatory cytokines.* Endothelium, 1997. **5**(1): p. 51-61.
111. Youn, M.Y., et al., *hCTR9, a component of Paf1 complex, participates in the transcription of interleukin 6-responsive genes through regulation of STAT3-DNA interactions.* J Biol Chem, 2007. **282**(48): p. 34727-34.
112. Milne, T.A., et al., *Multiple interactions recruit MLL1 and MLL1 fusion proteins to the HOXA9 locus in leukemogenesis.* Mol Cell, 2010. **38**(6): p. 853-63.
113. Yang, J., et al., *Reversible methylation of promoter-bound STAT3 by histone-modifying enzymes.* Proc Natl Acad Sci U S A, 2010. **107**(50): p. 21499-504.

114. Fatemi, S.H., et al., *Defective corticogenesis and reduction in Reelin immunoreactivity in cortex and hippocampus of prenatally infected neonatal mice.* Mol Psychiatry, 1999. **4**(2): p. 145-54.
115. Fatemi, S.H., et al., *Differential expression of synaptosome-associated protein 25 kDa [SNAP-25] in hippocampi of neonatal mice following exposure to human influenza virus in utero.* Brain Res, 1998. **800**(1): p. 1-9.
116. Patterson, P.H., *Immune involvement in schizophrenia and autism: etiology, pathology and animal models.* Behav Brain Res, 2009. **204**(2): p. 313-21.
117. Shi, L., N. Tu, and P.H. Patterson, *Maternal influenza infection is likely to alter fetal brain development indirectly: the virus is not detected in the fetus.* Int J Dev Neurosci, 2005. **23**(2-3): p. 299-305.
118. Dahlgren, J., et al., *Interleukin-6 in the maternal circulation reaches the rat fetus in mid-gestation.* Pediatr Res, 2006. **60**(2): p. 147-51.
119. Meyer, U., et al., *The time of prenatal immune challenge determines the specificity of inflammation-mediated brain and behavioral pathology.* J Neurosci, 2006. **26**(18): p. 4752-62.
120. Ponzio, N.M., et al., *Cytokine levels during pregnancy influence immunological profiles and neurobehavioral patterns of the offspring.* Ann N Y Acad Sci, 2007. **1107**: p. 118-28.
121. Borrell, J., et al., *Prenatal immune challenge disrupts sensorimotor gating in adult rats. Implications for the etiopathogenesis of schizophrenia.* Neuropsychopharmacology, 2002. **26**(2): p. 204-15.
122. Meyer, U. and J. Feldon, *Neural basis of psychosis-related behaviour in the infection model of schizophrenia.* Behav Brain Res, 2009. **204**(2): p. 322-34.
123. Shi, L., et al., *Maternal influenza infection causes marked behavioral and pharmacological changes in the offspring.* J Neurosci, 2003. **23**(1): p. 297-302.
124. Zuckerman, L., et al., *Immune activation during pregnancy in rats leads to a postpubertal emergence of disrupted latent inhibition, dopaminergic hyperfunction, and altered limbic morphology in the offspring: a novel neurodevelopmental model of schizophrenia.* Neuropsychopharmacology, 2003. **28**(10): p. 1778-89.
125. Zuckerman, L. and I. Weiner, *Maternal immune activation leads to behavioral and pharmacological changes in the adult offspring.* J Psychiatr Res, 2005. **39**(3): p. 311-23.
126. Romero, E., et al., *Neurobehavioral and immunological consequences of prenatal immune activation in rats. Influence of antipsychotics.* Neuropsychopharmacology, 2007. **32**(8): p. 1791-804.
127. Fatemi, S.H., et al., *Prenatal viral infection leads to pyramidal cell atrophy and macrocephaly in adulthood: implications for genesis of autism and schizophrenia.* Cell Mol Neurobiol, 2002. **22**(1): p. 25-33.
128. Nyffeler, M., et al., *Maternal immune activation during pregnancy increases limbic GABAA receptor immunoreactivity in the adult offspring: implications for schizophrenia.* Neuroscience, 2006. **143**(1): p. 51-62.

129. Palmen, S.J., et al., *Neuropathological findings in autism.* Brain, 2004. **127**(Pt 12): p. 2572-83.
130. Cai, Z., et al., *Cytokine induction in fetal rat brains and brain injury in neonatal rats after maternal lipopolysaccharide administration.* Pediatr Res, 2000. **47**(1): p. 64-72.
131. Ozawa, K., et al., *Immune activation during pregnancy in mice leads to dopaminergic hyperfunction and cognitive impairment in the offspring: a neurodevelopmental animal model of schizophrenia.* Biol Psychiatry, 2006. **59**(6): p. 546-54.
132. Lalonde, R., et al., *Transgenic mice expressing the human C99 terminal fragment of betaAPP: effects on spatial learning, exploration, anxiety, and motor coordination.* Exp Gerontol, 2002. **37**(12): p. 1401-12.
133. Shi, G.L., B.S. Ku, and H.Y. Yao, *[Effects of jieyuwan on HPA axis and immune system in chronic stress models in rats].* Zhongguo Zhong Yao Za Zhi, 2007. **32**(15): p. 1551-4.
134. Abazyan, B., et al., *Prenatal interaction of mutant DISC1 and immune activation produces adult psychopathology.* Biol Psychiatry, 2010. **68**(12): p. 1172-81.
135. Bronson, S.L., et al., *Individual differences in maternal response to immune challenge predict offspring behavior: contribution of environmental factors.* Behav Brain Res, 2011. **220**(1): p. 55-64.
136. Deep-Soboslay, A., et al., *Psychiatric brain banking: three perspectives on current trends and future directions.* Biol Psychiatry, 2011. **69**(2): p. 104-12.
137. Susser, E.S., et al., *The design of the prenatal determinants of schizophrenia study.* Schizophr Bull, 2000. **26**(2): p. 257-73.
138. Brown, A.S., et al., *Maternal exposure to respiratory infections and adult schizophrenia spectrum disorders: a prospective birth cohort study.* Schizophr Bull, 2000. **26**(2): p. 287-95.
139. Sullivan, P.F., *The psychiatric GWAS consortium: big science comes to psychiatry.* Neuron, 2010. **68**(2): p. 182-6.
140. Bernstein, H.G., et al., *Strongly reduced number of parvalbumin-immunoreactive projection neurons in the mammillary bodies in schizophrenia: further evidence for limbic neuropathology.* Ann N Y Acad Sci, 2007. **1096**: p. 120-7.
141. Tweedie-Cullen, R.Y. and I.M. Mansuy, *Towards a better understanding of nuclear processes based on proteomics.* Amino Acids, 2010. **39**(5): p. 1117-30.
142. Connor, C.W. and S. Segal, *Accurate classification of difficult intubation by computerized facial analysis.* Anesth Analg, 2011. **112**(1): p. 84-93.
143. Lewis, D.A., T. Hashimoto, and D.W. Volk, *Cortical inhibitory neurons and schizophrenia.* Nat Rev Neurosci, 2005. **6**(4): p. 312-24.
144. Benes, F.M. and N. Lange, *Two-dimensional versus three-dimensional cell counting: a practical perspective.* Trends Neurosci, 2001. **24**(1): p. 11-7.

145. Ishikawa, M., et al., *GABAA receptor gamma subunits in the prefrontal cortex of patients with schizophrenia and bipolar disorder.* Neuroreport, 2004. **15**(11): p. 1809-12.
146. Martinowich, K., et al., *DNA methylation-related chromatin remodeling in activity-dependent BDNF gene regulation.* Science, 2003. **302**(5646): p. 890-3.
147. Uhlhaas, P.J. and W. Singer, *Abnormal neural oscillations and synchrony in schizophrenia.* Nat Rev Neurosci, 2010. **11**(2): p. 100-13.
148. Gandal, M.J., et al., *Validating gamma oscillations and delayed auditory responses as translational biomarkers of autism.* Biol Psychiatry, 2010. **68**(12): p. 1100-6.
149. Fan, G., et al., *DNA hypomethylation perturbs the function and survival of CNS neurons in postnatal animals.* J Neurosci, 2001. **21**(3): p. 788-97.
150. Chen, Q., et al., *Molecular imaging in patients with mood disorders: a review of PET findings.* Eur J Nucl Med Mol Imaging, 2011. **38**(7): p. 1367-80.
151. Urban, N. and A. Abi-Dargham, *Neurochemical imaging in schizophrenia.* Curr Top Behav Neurosci, 2010. **4**: p. 215-42.
152. Vallabhajosula, S., *Positron emission tomography radiopharmaceuticals for imaging brain Beta-amyloid.* Semin Nucl Med, 2011. **41**(4): p. 283-99.
153. Park, P.J., *ChIP-seq: advantages and challenges of a maturing technology.* Nat Rev Genet, 2009. **10**(10): p. 669-80.
154. Ruthenburg, A.J., C.D. Allis, and J. Wysocka, *Methylation of lysine 4 on histone H3: intricacy of writing and reading a single epigenetic mark.* Mol Cell, 2007. **25**(1): p. 15-30.
155. Li, B., M. Carey, and J.L. Workman, *The role of chromatin during transcription.* Cell, 2007. **128**(4): p. 707-19.
156. O'Neill, L.P. and B.M. Turner, *Immunoprecipitation of native chromatin: NChIP.* Methods, 2003. **31**(1): p. 76-82.
157. Zhang, Y., et al., *Model-based analysis of ChIP-Seq (MACS).* Genome Biol, 2008. **9**(9): p. R137.
158. Fu, Y., et al., *The insulator binding protein CTCF positions 20 nucleosomes around its binding sites across the human genome.* PLoS Genet, 2008. **4**(7): p. e1000138.
159. Adler, C.M., et al., *Evidence of white matter pathology in bipolar disorder adolescents experiencing their first episode of mania: a diffusion tensor imaging study.* Am J Psychiatry, 2006. **163**(2): p. 322-4.
160. Szeszko, P.R., et al., *White matter abnormalities in first-episode schizophrenia or schizoaffective disorder: a diffusion tensor imaging study.* Am J Psychiatry, 2005. **162**(3): p. 602-5.
161. Ho, B.C., et al., *Progressive structural brain abnormalities and their relationship to clinical outcome: a longitudinal magnetic resonance imaging study early in schizophrenia.* Arch Gen Psychiatry, 2003. **60**(6): p. 585-94.

162. Buchsbaum, M.S., et al., *Relative glucose metabolic rate higher in white matter in patients with schizophrenia.* Am J Psychiatry, 2007. **164**(7): p. 1072-81.
163. Shprintzen, R.J., *Velo-cardio-facial syndrome: 30 Years of study.* Dev Disabil Res Rev, 2008. **14**(1): p. 3-10.
164. Kiehl, T.R., et al., *Neuropathologic Features in Adults with 22q11.2 Deletion Syndrome.* Cereb Cortex, 2008.
165. Akbarian, S., et al., *Altered distribution of nicotinamide-adenine dinucleotide phosphate-diaphorase cells in frontal lobe of schizophrenics implies disturbances of cortical development.* Arch Gen Psychiatry, 1993. **50**(3): p. 169-77.
166. Akbarian, S., et al., *Maldistribution of interstitial neurons in prefrontal white matter of the brains of schizophrenic patients.* Arch Gen Psychiatry, 1996. **53**(5): p. 425-36.
167. Akbarian, S., et al., *Distorted distribution of nicotinamide-adenine dinucleotide phosphate-diaphorase neurons in temporal lobe of schizophrenics implies anomalous cortical development.* Arch Gen Psychiatry, 1993. **50**(3): p. 178-87.
168. Anderson, S.A., D.W. Volk, and D.A. Lewis, *Increased density of microtubule associated protein 2-immunoreactive neurons in the prefrontal white matter of schizophrenic subjects.* Schizophr Res, 1996. **19**(2-3): p. 111-9.
169. Beasley, C.L., D.R. Cotter, and I.P. Everall, *Density and distribution of white matter neurons in schizophrenia, bipolar disorder and major depressive disorder: no evidence for abnormalities of neuronal migration.* Mol Psychiatry, 2002. **7**(6): p. 564-70.
170. Bertram, I., et al., *Immunohistochemical evidence for impaired neuregulin-1 signaling in the prefrontal cortex in schizophrenia and in unipolar depression.* Ann N Y Acad Sci, 2007. **1096**: p. 147-56.
171. Eastwood, S.L. and P.J. Harrison, *Interstitial white matter neurons express less reelin and are abnormally distributed in schizophrenia: towards an integration of molecular and morphologic aspects of the neurodevelopmental hypothesis.* Mol Psychiatry, 2003. **8**(9): p. 769, 821-31.
172. Eastwood, S.L. and P.J. Harrison, *Interstitial white matter neuron density in the dorsolateral prefrontal cortex and parahippocampal gyrus in schizophrenia.* Schizophr Res, 2005. **79**(2-3): p. 181-8.
173. Kirkpatrick, B., et al., *Interstitial cells of the white matter in the inferior parietal cortex in schizophrenia: An unbiased cell-counting study.* Synapse, 1999. **34**(2): p. 95-102.
174. Kirkpatrick, B., et al., *Interstitial cells of the white matter in the dorsolateral prefrontal cortex in deficit and nondeficit schizophrenia.* J Nerv Ment Dis, 2003. **191**(9): p. 563-7.

175. Molnar, M., et al., *MRNA expression patterns and distribution of white matter neurons in dorsolateral prefrontal cortex of depressed patients differ from those in schizophrenia patients.* Biol Psychiatry, 2003. **53**(1): p. 39-47.
176. Nobuhara, K., et al., *Effects of electroconvulsive therapy on frontal white matter in late-life depression: a diffusion tensor imaging study.* Neuropsychobiology, 2004. **50**(1): p. 48-53.
177. Rioux, L., et al., *Distribution of microtubule-associated protein MAP2-immunoreactive interstitial neurons in the parahippocampal white matter in subjects with schizophrenia.* Am J Psychiatry, 2003. **160**(1): p. 149-55.
178. Ikeda, K., et al., *Distribution of neuropeptide Y interneurons in the dorsal prefrontal cortex of schizophrenia.* Prog Neuropsychopharmacol Biol Psychiatry, 2004. **28**(2): p. 379-83.
179. Kostovic, I. and M. Judas, *Transient patterns of cortical lamination during prenatal life: do they have implications for treatment?* Neurosci Biobehav Rev, 2007. **31**(8): p. 1157-68.
180. Kanold, P.O., *Transient microcircuits formed by subplate neurons and their role in functional development of thalamocortical connections.* Neuroreport, 2004. **15**(14): p. 2149-53.
181. Kostovic, I. and P. Rakic, *Developmental history of the transient subplate zone in the visual and somatosensory cortex of the macaque monkey and human brain.* J Comp Neurol, 1990. **297**(3): p. 441-70.
182. Ongur, D., W.C. Drevets, and J.L. Price, *Glial reduction in the subgenual prefrontal cortex in mood disorders.* Proc Natl Acad Sci U S A, 1998. **95**(22): p. 13290-5.
183. Woo, T.U., J.P. Walsh, and F.M. Benes, *Density of glutamic acid decarboxylase 67 messenger RNA-containing neurons that express the N-methyl-D-aspartate receptor subunit NR2A in the anterior cingulate cortex in schizophrenia and bipolar disorder.* Arch Gen Psychiatry, 2004. **61**(7): p. 649-57.
184. Sarnat, H.B., D. Nochlin, and D.E. Born, *Neuronal nuclear antigen (NeuN): a marker of neuronal maturation in early human fetal nervous system.* Brain Dev, 1998. **20**(2): p. 88-94.
185. Bernstein, H.G., et al., *Localization of neuregulin-1alpha (heregulin-alpha) and one of its receptors, ErbB-4 tyrosine kinase, in developing and adult human brain.* Brain Res Bull, 2006. **69**(5): p. 546-59.
186. Sei, Y., et al., *Neuregulin1-induced cell migration is impaired in schizophrenia: association with neuregulin1 and catechol-o-methyltransferase gene polymorphisms.* Mol Psychiatry, 2007. **12**(10): p. 946-57.
187. Lopez-Bendito, G., et al., *Tangential neuronal migration controls axon guidance: a role for neuregulin-1 in thalamocortical axon navigation.* Cell, 2006. **125**(1): p. 127-42.
188. Chang, A., et al., *Neurogenesis in the chronic lesions of multiple sclerosis.* Brain, 2008. **131**(Pt 9): p. 2366-75.

189. Ito, D., et al., *Microglia-specific localisation of a novel calcium binding protein, Iba1.* Brain Res Mol Brain Res, 1998. **57**(1): p. 1-9.
190. Vogt, B.A., et al., *Human cingulate cortex: surface features, flat maps, and cytoarchitecture.* J Comp Neurol, 1995. **359**(3): p. 490-506.
191. Mullen, R.J., C.R. Buck, and A.M. Smith, *NeuN, a neuronal specific nuclear protein in vertebrates.* Development, 1992. **116**(1): p. 201-11.
192. Wolf, H.K., et al., *NeuN: a useful neuronal marker for diagnostic histopathology.* J Histochem Cytochem, 1996. **44**(10): p. 1167-71.
193. Samuelsen, G.B., et al., *The changing number of cells in the human fetal forebrain and its subdivisions: a stereological analysis.* Cereb Cortex, 2003. **13**(2): p. 115-22.
194. Meyer, G., et al., *Morphology of neurons in the white matter of the adult human neocortex.* Exp Brain Res, 1992. **88**(1): p. 204-12.
195. Sanches, M., et al., *Neurodevelopmental basis of bipolar disorder: A critical appraisal.* Prog Neuropsychopharmacol Biol Psychiatry, 2008.
196. Jarskog, L.F., et al., *Apoptotic mechanisms in the pathophysiology of schizophrenia.* Prog Neuropsychopharmacol Biol Psychiatry, 2005. **29**(5): p. 846-58.
197. Spalding, K.L., et al., *Retrospective birth dating of cells in humans.* Cell, 2005. **122**(1): p. 133-43.
198. Kamiya, A., et al., *Recruitment of PCM1 to the centrosome by the cooperative action of DISC1 and BBS4: a candidate for psychiatric illnesses.* Arch Gen Psychiatry, 2008. **65**(9): p. 996-1006.
199. Corfas, G., K. Roy, and J.D. Buxbaum, *Neuregulin 1-erbB signaling and the molecular/cellular basis of schizophrenia.* Nat Neurosci, 2004. **7**(6): p. 575-80.
200. Torres-Reveron, J. and M.J. Friedlander, *Properties of persistent postnatal cortical subplate neurons.* J Neurosci, 2007. **27**(37): p. 9962-74.
201. Giguere, M. and P.S. Goldman-Rakic, *Mediodorsal nucleus: areal, laminar, and tangential distribution of afferents and efferents in the frontal lobe of rhesus monkeys.* J Comp Neurol, 1988. **277**(2): p. 195-213.
202. Kanold, P.O. and C.J. Shatz, *Subplate neurons regulate maturation of cortical inhibition and outcome of ocular dominance plasticity.* Neuron, 2006. **51**(5): p. 627-38.
203. Berretta, S., D.W. Munno, and F.M. Benes, *Amygdalar activation alters the hippocampal GABA system: "partial" modelling for postmortem changes in schizophrenia.* J Comp Neurol, 2001. **431**(2): p. 129-38.
204. Gonzalez-Burgos, G. and D.A. Lewis, *GABA neurons and the mechanisms of network oscillations: implications for understanding cortical dysfunction in schizophrenia.* Schizophr Bull, 2008. **34**(5): p. 944-61.
205. Jiang, Y., et al., *Isolation of neuronal chromatin from brain tissue.* BMC Neurosci, 2008. **9**: p. 42.

206. Dittrich, B., et al., *Molecular diagnosis of the Prader-Willi and Angelman syndromes by detection of parent-of-origin specific DNA methylation in 15q11-13.* Hum Genet, 1992. **90**(3): p. 313-5.
207. Driscoll, D.J., et al., *A DNA methylation imprint, determined by the sex of the parent, distinguishes the Angelman and Prader-Willi syndromes.* Genomics, 1992. **13**(4): p. 917-24.
208. Bell, M.V., et al., *Physical mapping across the fragile X: hypermethylation and clinical expression of the fragile X syndrome.* Cell, 1991. **64**(4): p. 861-6.
209. Oberle, I., et al., *Instability of a 550-base pair DNA segment and abnormal methylation in fragile X syndrome.* Science, 1991. **252**(5010): p. 1097-102.
210. Hansen, R.S., et al., *The DNMT3B DNA methyltransferase gene is mutated in the ICF immunodeficiency syndrome.* Proc Natl Acad Sci U S A, 1999. **96**(25): p. 14412-7.
211. Alaminos, M., et al., *EMP3, a myelin-related gene located in the critical 19q13.3 region, is epigenetically silenced and exhibits features of a candidate tumor suppressor in glioma and neuroblastoma.* Cancer Res, 2005. **65**(7): p. 2565-71.
212. Debinski, W., D. Gibo, and A. Mintz, *Epigenetics in high-grade astrocytomas: opportunities for prevention and detection of brain tumors.* Ann N Y Acad Sci, 2003. **983**: p. 232-42.
213. Felsberg, J., et al., *DNA methylation and allelic losses on chromosome arm 14q in oligodendroglial tumours.* Neuropathol Appl Neurobiol, 2006. **32**(5): p. 517-24.
214. Uhlmann, K., et al., *Distinct methylation profiles of glioma subtypes.* Int J Cancer, 2003. **106**(1): p. 52-9.
215. Inda, M.M. and J.S. Castresana, *RASSF1A promoter is highly methylated in primitive neuroectodermal tumors of the central nervous system.* Neuropathology, 2007. **27**(4): p. 341-6.
216. Lindsey, J.C., et al., *Epigenetic deregulation of multiple S100 gene family members by differential hypomethylation and hypermethylation events in medulloblastoma.* Br J Cancer, 2007. **97**(2): p. 267-74.
217. Harrison, P.J. and D.R. Weinberger, *Schizophrenia genes, gene expression, and neuropathology: on the matter of their convergence.* Mol Psychiatry, 2005. **10**(1): p. 40-68; image 5.
218. Newberg, A.R., et al., *Neurobiology of bipolar disorder.* Expert Rev Neurother, 2008. **8**(1): p. 93-110.
219. Kaminsky, Z., S.C. Wang, and A. Petronis, *Complex disease, gender and epigenetics.* Ann Med, 2006. **38**(8): p. 530-44.
220. Konradi, C., et al., *Molecular evidence for mitochondrial dysfunction in bipolar disorder.* Arch Gen Psychiatry, 2004. **61**(3): p. 300-8.
221. Akbarian, S., et al., *Chromatin alterations associated with down-regulated metabolic gene expression in the prefrontal cortex of subjects with schizophrenia.* Arch Gen Psychiatry, 2005. **62**(8): p. 829-40.

222. Middleton, F.A., et al., *Gene expression profiling reveals alterations of specific metabolic pathways in schizophrenia.* J Neurosci, 2002. **22**(7): p. 2718-29.
223. Karoutzou, G., H.M. Emrich, and D.E. Dietrich, *The myelin-pathogenesis puzzle in schizophrenia: a literature review.* Mol Psychiatry, 2008. **13**(3): p. 245-60.
224. Sokolov, B.P., *Oligodendroglial abnormalities in schizophrenia, mood disorders and substance abuse. Comorbidity, shared traits, or molecular phenocopies?* Int J Neuropsychopharmacol, 2007. **10**(4): p. 547-55.
225. Abdolmaleky, H.M., et al., *Hypermethylation of the reelin (RELN) promoter in the brain of schizophrenic patients: a preliminary report.* Am J Med Genet B Neuropsychiatr Genet, 2005. **134**(1): p. 60-6.
226. Tamura, Y., et al., *Epigenetic aberration of the human REELIN gene in psychiatric disorders.* Mol Psychiatry, 2007. **12**(6): p. 519, 593-600.
227. Tochigi, M., et al., *Methylation status of the reelin promoter region in the brain of schizophrenic patients.* Biol Psychiatry, 2008. **63**(5): p. 530-3.
228. Abdolmaleky, H.M., et al., *Hypomethylation of MB-COMT promoter is a major risk factor for schizophrenia and bipolar disorder.* Hum Mol Genet, 2006. **15**(21): p. 3132-45.
229. Dempster, E.L., et al., *The quantification of COMT mRNA in post mortem cerebellum tissue: diagnosis, genotype, methylation and expression.* BMC Med Genet, 2006. **7**: p. 10.
230. Murphy, B.C., R.L. O'Reilly, and S.M. Singh, *Site-specific cytosine methylation in S-COMT promoter in 31 brain regions with implications for studies involving schizophrenia.* Am J Med Genet B Neuropsychiatr Genet, 2005. **133**(1): p. 37-42.
231. Petronis, A., et al., *Monozygotic twins exhibit numerous epigenetic differences: clues to twin discordance?* Schizophr Bull, 2003. **29**(1): p. 169-78.
232. Iwamoto, K., et al., *DNA methylation status of SOX10 correlates with its downregulation and oligodendrocyte dysfunction in schizophrenia.* J Neurosci, 2005. **25**(22): p. 5376-81.
233. Mill, J., et al., *Epigenomic profiling reveals DNA-methylation changes associated with major psychosis.* Am J Hum Genet, 2008. **82**(3): p. 696-711.
234. Craddock, N. and M.J. Owen, *Rethinking psychosis: the disadvantages of a dichotomous classification now outweigh the advantages.* World Psychiatry, 2007. **6**(2): p. 84-91.
235. Pae, C.U., et al., *Effect of 5-haplotype of dysbindin gene (DTNBP1) polymorphisms for the susceptibility to bipolar I disorder.* Am J Med Genet B Neuropsychiatr Genet, 2007. **144**(5): p. 701-3.
236. Raybould, R., et al., *Bipolar disorder and polymorphisms in the dysbindin gene (DTNBP1).* Biol Psychiatry, 2005. **57**(7): p. 696-701.

237. Straub, R.E., et al., *Genetic variation in the 6p22.3 gene DTNBP1, the human ortholog of the mouse dysbindin gene, is associated with schizophrenia.* Am J Hum Genet, 2002. **71**(2): p. 337-48.
238. Polesskaya, O.O., C. Aston, and B.P. Sokolov, *Allele C-specific methylation of the 5-HT2A receptor gene: evidence for correlation with its expression and expression of DNA methylase DNMT1.* J Neurosci Res, 2006. **83**(3): p. 362-73.
239. Berman, K.F., et al., *Modulation of cognition-specific cortical activity by gonadal steroids: a positron-emission tomography study in women.* Proc Natl Acad Sci U S A, 1997. **94**(16): p. 8836-41.
240. Dreher, J.C., et al., *Menstrual cycle phase modulates reward-related neural function in women.* Proc Natl Acad Sci U S A, 2007. **104**(7): p. 2465-70.
241. Garcia-Bassets, I., et al., *Histone methylation-dependent mechanisms impose ligand dependency for gene activation by nuclear receptors.* Cell, 2007. **128**(3): p. 505-18.
242. Perillo, B., et al., *DNA oxidation as triggered by H3K9me2 demethylation drives estrogen-induced gene expression.* Science, 2008. **319**(5860): p. 202-6.
243. Inoue, H., et al., *Largest subunits of the human SWI/SNF chromatin-remodeling complex promote transcriptional activation by steroid hormone receptors.* J Biol Chem, 2002. **277**(44): p. 41674-85.
244. Klokk, T.I., et al., *Ligand-specific dynamics of the androgen receptor at its response element in living cells.* Mol Cell Biol, 2007. **27**(5): p. 1823-43.
245. Cheng, A.S., et al., *Combinatorial analysis of transcription factor partners reveals recruitment of c-MYC to estrogen receptor-alpha responsive promoters.* Mol Cell, 2006. **21**(3): p. 393-404.
246. Clark, S.J., et al., *DNA methylation: bisulphite modification and analysis.* Nat Protoc, 2006. **1**(5): p. 2353-64.
247. Beasley, C.L., et al., *Selective deficits in prefrontal cortical GABAergic neurons in schizophrenia defined by the presence of calcium-binding proteins.* Biol Psychiatry, 2002. **52**(7): p. 708-15.
248. Hashimoto, T., et al., *Gene expression deficits in a subclass of GABA neurons in the prefrontal cortex of subjects with schizophrenia.* J Neurosci, 2003. **23**(15): p. 6315-26.
249. Pantazopoulos, H., et al., *Parvalbumin neurons in the entorhinal cortex of subjects diagnosed with bipolar disorder or schizophrenia.* Biol Psychiatry, 2007. **61**(5): p. 640-52.
250. Zhang, Z.J. and G.P. Reynolds, *A selective decrease in the relative density of parvalbumin-immunoreactive neurons in the hippocampus in schizophrenia.* Schizophr Res, 2002. **55**(1-2): p. 1-10.
251. Hof, P.R., et al., *Loss and altered spatial distribution of oligodendrocytes in the superior frontal gyrus in schizophrenia.* Biol Psychiatry, 2003. **53**(12): p. 1075-85.
252. Tkachev, D., et al., *Oligodendrocyte dysfunction in schizophrenia and bipolar disorder.* Lancet, 2003. **362**(9386): p. 798-805.

253. Uranova, N.A., et al., *Oligodendroglial density in the prefrontal cortex in schizophrenia and mood disorders: a study from the Stanley Neuropathology Consortium.* Schizophr Res, 2004. **67**(2-3): p. 269-75.
254. Vostrikov, V.M., N.A. Uranova, and D.D. Orlovskaya, *Deficit of perineuronal oligodendrocytes in the prefrontal cortex in schizophrenia and mood disorders.* Schizophr Res, 2007. **94**(1-3): p. 273-80.
255. Rajkowska, G., et al., *Layer-specific reductions in GFAP-reactive astroglia in the dorsolateral prefrontal cortex in schizophrenia.* Schizophr Res, 2002. **57**(2-3): p. 127-38.
256. Webster, M.J., et al., *Glial fibrillary acidic protein mRNA levels in the cingulate cortex of individuals with depression, bipolar disorder and schizophrenia.* Neuroscience, 2005. **133**(2): p. 453-61.
257. O'Kusky, J. and M. Colonnier, *Postnatal changes in the number of astrocytes, oligodendrocytes, and microglia in the visual cortex (area 17) of the macaque monkey: a stereological analysis in normal and monocularly deprived animals.* J Comp Neurol, 1982. **210**(3): p. 307-15.
258. Siegmund, K.D., et al., *DNA methylation in the human cerebral cortex is dynamically regulated throughout the life span and involves differentiated neurons.* PLoS ONE, 2007. **2**(9): p. e895.
259. Kundakovic, M., et al., *DNA methyltransferase inhibitors coordinately induce expression of the human reelin and glutamic acid decarboxylase 67 genes.* Mol Pharmacol, 2007. **71**(3): p. 644-53.
260. Levenson, J.M., et al., *Evidence that DNA (cytosine-5) methyltransferase regulates synaptic plasticity in the hippocampus.* J Biol Chem, 2006. **281**(23): p. 15763-73.
261. Rampon, C., et al., *Effects of environmental enrichment on gene expression in the brain.* Proc Natl Acad Sci U S A, 2000. **97**(23): p. 12880-4.
262. Endres, M., et al., *DNA methyltransferase contributes to delayed ischemic brain injury.* J Neurosci, 2000. **20**(9): p. 3175-81.
263. Bollati, V., et al., *Changes in DNA methylation patterns in subjects exposed to low-dose benzene.* Cancer Res, 2007. **67**(3): p. 876-80.
264. Desaulniers, D., et al., *Comparisons of brain, uterus, and liver mRNA expression for cytochrome p450s, DNA methyltransferase-1, and catechol-o-methyltransferase in prepubertal female Sprague-Dawley rats exposed to a mixture of aryl hydrocarbon receptor agonists.* Toxicol Sci, 2005. **86**(1): p. 175-84.
265. Salnikow, K. and A. Zhitkovich, *Genetic and epigenetic mechanisms in metal carcinogenesis and cocarcinogenesis: nickel, arsenic, and chromium.* Chem Res Toxicol, 2008. **21**(1): p. 28-44.
266. Satta, R., et al., *Stimulation of brain nicotinic acetylcholine receptors (nAChRs) decreases DNA methyltransferase 1 (DNMT1) expression in cortical and hippocampal GABAergic neurons of Swiss albino mice.* Society for Neuroscience Abstract, 2007.

267. Marutha Ravindran, C.R. and M.K. Ticku, *Changes in methylation pattern of NMDA receptor NR2B gene in cortical neurons after chronic ethanol treatment in mice.* Brain Res Mol Brain Res, 2004. **121**(1-2): p. 19-27.
268. Numachi, Y., et al., *Methamphetamine alters expression of DNA methyltransferase 1 mRNA in rat brain.* Neurosci Lett, 2007. **414**(3): p. 213-7.
269. Numachi, Y., et al., *Psychostimulant alters expression of DNA methyltransferase mRNA in the rat brain.* Ann N Y Acad Sci, 2004. **1025**: p. 102-9.
270. Cheng, M.C., et al., *Chronic treatment with aripiprazole induces differential gene expression in the rat frontal cortex.* Int J Neuropsychopharmacol, 2008. **11**(2): p. 207-16.
271. Shimabukuro, M., et al., *Haloperidol treatment induces tissue- and sex-specific changes in DNA methylation: a control study using rats.* Behav Brain Funct, 2006. **2**: p. 37.
272. Fraga, M.F., et al., *Epigenetic differences arise during the lifetime of monozygotic twins.* Proc Natl Acad Sci U S A, 2005. **102**(30): p. 10604-9.
273. Richards, E.J., *Inherited epigenetic variation--revisiting soft inheritance.* Nat Rev Genet, 2006. **7**(5): p. 395-401.
274. Roth, T., et al., *The molecular scars of early stress: persisting changes in DNA methylation in a model of maternal maltreatment.* Society for Neuroscience Abstract, 2007.
275. Morgan, H.D., et al., *Epigenetic inheritance at the agouti locus in the mouse.* Nat Genet, 1999. **23**(3): p. 314-8.
276. Tsankova, N., et al., *Epigenetic regulation in psychiatric disorders.* Nat Rev Neurosci, 2007. **8**(5): p. 355-67.
277. Petronis, A., *Human morbid genetics revisited: relevance of epigenetics.* Trends Genet, 2001. **17**(3): p. 142-6.
278. Bird, A., *Perceptions of epigenetics.* Nature, 2007. **447**(7143): p. 396-8.
279. Reik, W., *Stability and flexibility of epigenetic gene regulation in mammalian development.* Nature, 2007. **447**(7143): p. 425-32.
280. Ausio, J., et al., *Syndromes of disordered chromatin remodeling.* Clin Genet, 2003. **64**(2): p. 83-95.
281. Xie, Z.H., et al., *Mutations in DNA methyltransferase DNMT3B in ICF syndrome affect its regulation by DNMT3L.* Hum Mol Genet, 2006. **15**(9): p. 1375-85.
282. Isles, A.R., W. Davies, and L.S. Wilkinson, *Genomic imprinting and the social brain.* Philos Trans R Soc Lond B Biol Sci, 2006. **361**(1476): p. 2229-37.
283. Miller, C.A. and J.D. Sweatt, *Covalent modification of DNA regulates memory formation.* Neuron, 2007. **53**(6): p. 857-69.
284. Scarpa, S., et al., *Presenilin 1 gene silencing by S-adenosylmethionine: a treatment for Alzheimer disease?* FEBS Lett, 2003. **541**(1-3): p. 145-8.

285. Nagarajan, R.P., et al., *Reduced MeCP2 expression is frequent in autism frontal cortex and correlates with aberrant MECP2 promoter methylation.* Epigenetics, 2006. **1**(4): p. 172-182.
286. Esteller, M., *Aberrant DNA methylation as a cancer-inducing mechanism.* Annu Rev Pharmacol Toxicol, 2005. **45**: p. 629-56.
287. Nguyen, S., et al., *Ablation of de novo DNA methyltransferase Dnmt3a in the nervous system leads to neuromuscular defects and shortened lifespan.* Dev Dyn, 2007. **236**(6): p. 1663-76.
288. Prabakaran, S., et al., *Mitochondrial dysfunction in schizophrenia: evidence for compromised brain metabolism and oxidative stress.* Mol Psychiatry, 2004. **9**(7): p. 684-97, 643.
289. Mirnics, K., et al., *Molecular characterization of schizophrenia viewed by microarray analysis of gene expression in prefrontal cortex.* Neuron, 2000. **28**(1): p. 53-67.
290. Hakak, Y., et al., *Genome-wide expression analysis reveals dysregulation of myelination-related genes in chronic schizophrenia.* Proc Natl Acad Sci U S A, 2001. **98**(8): p. 4746-51.
291. Trinh, B.N., T.I. Long, and P.W. Laird, *DNA methylation analysis by MethyLight technology.* Methods, 2001. **25**(4): p. 456-62.
292. Eads, C.A., et al., *MethyLight: a high-throughput assay to measure DNA methylation.* Nucleic Acids Res, 2000. **28**(8): p. E32.
293. Esteller, M., et al., *Inactivation of the DNA-repair gene MGMT and the clinical response of gliomas to alkylating agents.* N Engl J Med, 2000. **343**: p. 1350-1354.
294. Jellinger, K., *Glioblastoma multiforme: morphology and biology.* Acta Neurochir (Wien), 1978. **42**(1-2): p. 5-32.
295. Preusser, M., C. Haberler, and J.A. Hainfellner, *Malignant glioma: neuropathology and neurobiology.* Wien Med Wochenschr, 2006. **156**(11-12): p. 332-7.
296. Lipska, B.K., et al., *Critical factors in gene expression in postmortem human brain: Focus on studies in schizophrenia.* Biol Psychiatry, 2006. **60**(6): p. 650-8.
297. Ito, H., et al., *Phosphorylation by extracellular signal-regulated kinase of a multidomain adaptor protein, vinexin, at synapses.* J Neurochem, 2007. **100**(2): p. 545-54.
298. Hoyaux, D., et al., *S100 proteins in Corpora amylacea from normal human brain.* Brain Res, 2000. **867**: p. 280-288.
299. Selkoe, D.J. and M.B. Podlisny, *Deciphering the genetic basis of Alzheimer's disease.* Annu Rev Genomics Hum Genet, 2002. **3**: p. 67-99.
300. Flanagan, J.M., et al., *Intra- and interindividual epigenetic variation in human germ cells.* Am J Hum Genet, 2006. **79**(1): p. 67-84.
301. Song, D.L., et al., *Two Pax-binding sites are required for early embryonic brain expression of an Engrailed-2 transgene.* Development, 1996. **122**(2): p. 627-35.

302. Benjamini, Y. and Y. Hochberg, *Controlling the false discovery rate: a practical and powerful approach to multiple testing.* J R Statist Soc B, 1995. **57**: p. 289-300.
303. Reik, W., W. Dean, and J. Walter, *Epigenetic reprogramming in mammalian development.* Science, 2001. **293**(5532): p. 1089-93.
304. Okano, M., et al., *DNA methyltransferases Dnmt3a and Dnmt3b are essential for de novo methylation and mammalian development.* Cell, 1999. **99**(3): p. 247-57.
305. Feng, J., et al., *Dynamic expression of de novo DNA methyltransferases Dnmt3a and Dnmt3b in the central nervous system.* J Neurosci Res, 2005. **79**(6): p. 734-46.
306. Chen, T., et al., *A novel Dnmt3a isoform produced from an alternative promoter localizes to euchromatin and its expression correlates with active de novo methylation.* J Biol Chem, 2002. **277**(41): p. 38746-54.
307. Weisenberger, D.J., et al., *Identification and characterization of alternatively spliced variants of DNA methyltransferase 3a in mammalian cells.* Gene, 2002. **298**(1): p. 91-9.
308. Kornack, D.R. and P. Rakic, *Changes in cell-cycle kinetics during the development and evolution of primate neocortex.* Proc Natl Acad Sci U S A, 1998. **95**(3): p. 1242-6.
309. Jakovcevski, I. and N. Zecevic, *Sequence of oligodendrocyte development in the human fetal telencephalon.* Glia, 2005. **49**(4): p. 480-91.
310. Sauvageot, C.M. and C.D. Stiles, *Molecular mechanisms controlling cortical gliogenesis.* Curr Opin Neurobiol, 2002. **12**(3): p. 244-9.
311. Braus, D.F., et al., *Sensory information processing in neuroleptic-naive first-episode schizophrenic patients: a functional magnetic resonance imaging study.* Arch Gen Psychiatry, 2002. **59**(8): p. 696-701.
312. Weinberger, D.R., *From neuropathology to neurodevelopment.* Lancet, 1995. **346**(8974): p. 552-7.
313. Heckers, S., *Neuropathology of schizophrenia: cortex, thalamus, basal ganglia, and neurotransmitter-specific projection systems.* Schizophr Bull, 1997. **23**(3): p. 403-21.
314. Barreto, G., et al., *Gadd45a promotes epigenetic gene activation by repair-mediated DNA demethylation.* Nature, 2007. **445**(7128): p. 671-5.
315. Champagne, F.A., et al., *Maternal care associated with methylation of the estrogen receptor-alpha1b promoter and estrogen receptor-alpha expression in the medial preoptic area of female offspring.* Endocrinology, 2006. **147**(6): p. 2909-15.
316. Laird, P.W., et al., *Simplified mammalian DNA isolation procedure.* Nucleic Acids Res, 1991. **19**(15): p. 4293.
317. Weisenberger, D.J., et al., *Analysis of repetitive element DNA methylation by MethyLight.* Nucleic Acids Res, 2005. **33**(21): p. 6823-36.

318. Widschwendter, M., et al., *Association of breast cancer DNA methylation profiles with hormone receptor status and response to tamoxifen.* Cancer Res, 2004. **64**: p. 3807-3813.